The Hubble Space Telescope view of the nuclei of radio galaxies

CANDIDATE

Marco Chiaberge

SUPERVISORS

Dott. Annalisa Celotti

Dott. Alessandro Capetti

Thesis submitted for the degree of *"Doctor Philosophiæ"*.

Academic Year 1999/2000

Il presente lavoro costituisce la tesi presentata da Marco Chiaberge, sotto la direzione del Dott. Annalisa Celotti e del Dott. Alessandro Capetti, al fine di ottenere il diploma di *"Doctor Philosophiæ"* presso la Scuola Internazionale Superiore di Studi Avanzati, Settore di Astrofisica.

Ai sensi del Decreto del Ministro della Pubblica Istruzione n. 419 del 24 Aprile 1987, tale diploma di ricerca post-universitaria è equipollente al titolo di *"Dottore di Ricerca in Astronomia"*.

Abstract

The work presented in this thesis is a study of the optical nuclear properties of low redshift radio galaxies, mainly based on Hubble Space Telescope data. Thanks to the high resolution and sensitivity of HST, we are able to separate for the first time the "pure" AGN component from the underlying stellar emission. This allows us to explore the viability of AGN unification schemes by directly comparing the innermost nuclear structures of radio galaxies with their putative aligned sources.

First of all, we study the central unresolved components discovered in radio galaxies through the analysis of a complete sample of 33 FR I from the 3CR catalog. The emission from these optical nuclei show a striking linear correlation with the radio core one over four decades, both in flux and luminosity. This lead us to identify them with non-thermal synchrotron radiation from the inner jet. The high rate detection of optical cores suggests that a standard pc-scale, geometrically thick torus is not present in low luminosity radio galaxies. Thus the lack of broad lines in these sources cannot be adduced to obscuration. These optical nuclei also represent upper limits to any thermal/disc emission. For a $10^9 M_\odot$ black hole, typical of FR I sources, this limit translates into a fraction as small as $10^{-7} - 10^{-5}$ of the Eddington luminosity, suggesting that accretion might take place in a low efficiency radiative regime.

We then compare the optical nuclear properties of nearby $z < 0.1$ FR II to those of FR I of comparable redshift. FR II show a more complex behavior, which is however clearly related to their optical spectral classification. Broad Line Radio galaxies (BLRG) are located well above the FR I radio-optical core correlation, suggesting that a contribution from thermal (disc) emission is present. Three Narrow Line Radio Galaxies and one Weak line Radio Galaxy in which no nuclear source is seen, can be interpreted as the obscured counterparts of BLRG. We also discover a new class of FR II with FR I-like (synchrotron dom-

inated) nuclei, which do not fit in the usually adopted AGN unified scheme. These results imply that, at least at low redshifts, the FR II population is not homogeneous. Furthermore, the innermost nuclear properties of radio galaxies are not univocally connected with the extended radio morphology.

We also explore the viability of the unification of BL Lacs and FR I, taking advantage of the newly measured optical nuclear luminosity of FR I. We find that the bulk Lorentz factors required by the spread in the observed luminosity are significantly smaller than those implied by other independent methods. In order to reconcile the unification scenario, velocity structures in the jet are suggested, where a fast spine dominates the BL Lac emission, while a slower, but still relativistic, layer dominates the emission in the misaligned objects.

We then put together radio, near-IR and optical data from the HST, and X-ray data, re-analyzing archival ROSAT X-ray data of five FR I in which the nuclear component can be separated from any extended emission. Thus, we build for the first time the nuclear SED of FR I. We found that these are qualitatively similar to those of BL Lacs, thus supporting the identification of FRI sources as their mis-oriented counterparts.

We also consider the particular case of Centaurus A, for which we build the overall nuclear SED (from the radio to the gamma ray band). We model it in the frame of an homogeneous synchrotron-self Compton emission model, finding that the physical parameters for this source can be similar to those obtained in BL Lacs, except for a much lower beaming factor, which is not compatible with being originated by a fast misaligned blazar component. A possible solution is the presence of velocity structures in the jet, in analogy with what has been found in the comparison of complete samples of BL Lacs and radio galaxies.

Contents

List of Figures

List of Tables

Chapter 1

Introduction

Active Galactic Nuclei are sources in which very high luminosities (up to $10^{48} - 10^{49}$ erg s^{-1}) are produced in a very small volume ($d < 0.1$ pc), through physical processes which cannot be ascribed to stellar nuclear fusion. According to the most accepted scenario, the ultimate source of AGN luminosity resides in the gravitational potential of gas in the vicinity of a supermassive black hole, which looses angular momentum through viscous or turbulent processes and releases energy radiatively, giving rise to UV and soft X-ray emission. Strong IR, optical and UV broad emission lines are produced in the central region of the AGN ($d \lesssim 1$ pc), by photo-ionized clouds of gas rapidly moving ($v \sim 3000 - 10000$ Km s^{-1}) in the potential of the black hole (see Fig 1.1). These central regions are obscured to some line of sights by a dusty structure, usually represented as a torus. Outside the torus, in a region which can be as large as several kpc, slowly moving clouds produce the observed narrow emission lines ($v \sim 300 - 1000$ Km s^{-1}).

The AGN phenomenon manifest itself as a zoo of objects with different observed properties, and thus classified. Even if continuity among all their characteristic might exist, a certainly useful division is based on their radio-loudness, that is the relative importance of the radio observed flux with respect to the optical one[1]. The radio-loud objects

[1]The separation between radio-quiet and radio-loud objects is usually set at $F_5/F_B =$

represent the 15-20% of the AGN and their main distinguishing characteristic is the presence of powerful relativistic plasma jets outflowing from the nuclear regions. Such jets are believed to be the channels which continuously fuel the radio lobes observed on hundreds of kpc up to Mpc scales (Rees [124]). Historically, strong extragalactic radio sources have been divided into two classes: extended radio sources, which show a steep radio spectrum, and compact radio sources, showing a flat radio spectrum[2]. Originally it was thought that they were quite different objects, while it is now clear that they are essentially two different aspects of the same underlying phenomenon. Radio galaxies belong to the former class.

In the following section I will describe the main observed characteristics of the different classes of AGN, while the properties of radio galaxies are presented in Sect. 1.2. In Sect. 1.3 I will review the most accepted scenario for the AGN unification. In Sect. 1.4 I will summarize the most important discoveries about radio galaxies made with Hubble Space Telescope observations, and also describe the particular set of data we extensively use in this theses. Our questions on radio galaxies, and the plan of this theses are given in Sect. 1.5.

1.1 Classification of AGN

Active Galactic Nuclei can be classified on the basis of their radio-loudness and on the characteristics of their optical and UV spectra. The origin of the dicothomy between radio-quiet and radio-loud AGN might be related to the black hole spin (Blandford [13]), which might enable the formation of powerful relativistic jets in the latter sources. However, this idea has been questioned by the observation, made with ASCA X-ray satellite, of a strong and broad iron line in a Seyfert 1

10, where F_5 and F_B are the fluxes at 5 GHz and B band, respectively (Kellermann et al. [77]).

[2]The division between *steep* and *flat* spectra is somewhat subjective. In this case, the separation is usually set at $\alpha = 0.5$, for a flux density of $F_\nu \propto \nu^{-\alpha}$.

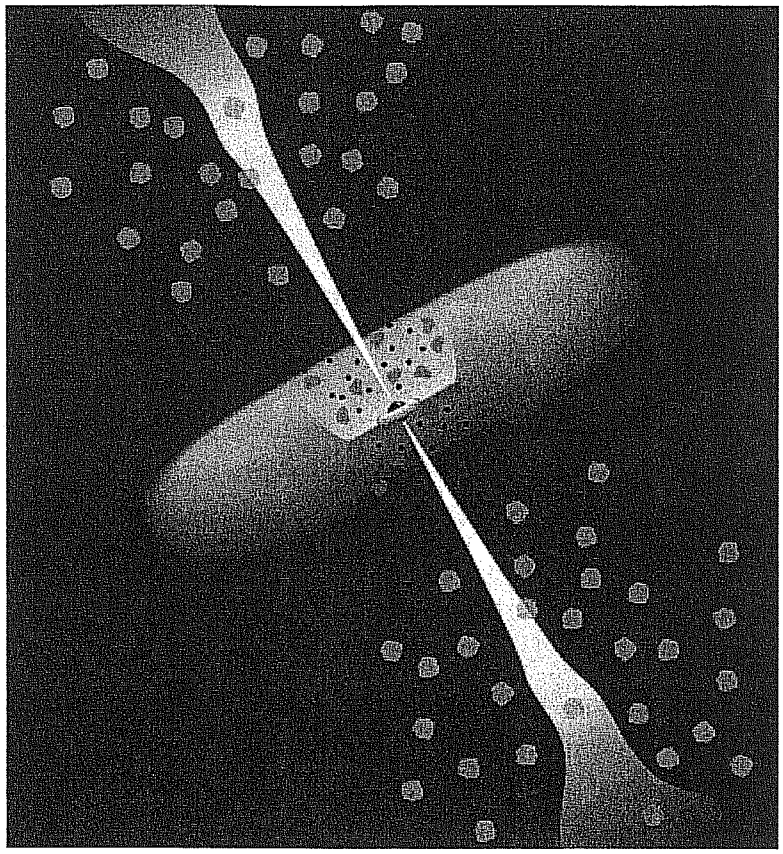

Figure 1.1: The basic scheme for radio loud AGN (from Urry & Padovani [152])

galaxy (MGC–6–30–15) whose shape might be well explained by emission from the inner regions of an accretion disc around a Kerr (maximally rotating) black hole (Iwasawa et al. [71]).

Although the AGN spectral classification is incomplete and sometimes misleading, it is certainly useful to impose some order in the chaos of the AGN.

- *Type I: Broad-Lined AGN*

This class of AGN shows bright continuum and broad emission lines

(FWHM $>$ 3000 Km s^{-1}), which are presumably produced by high velocity gas in the vicinity of the black hole. Variability time scales imply that the physical dimension of the broad line region (BLR) is $\lesssim 1pc$, although its size appear to depend strongly on the luminosity of the object. The radio-quiet *Type-I* group include **Seyfert 1** galaxies and their high luminosity (and high redshift) counterparts, the **radio-quiet quasars** (QSO). Recently, the unification of these two groups of AGN has been questioned by the discovery that most of QSO host galaxies are ellipticals, while Seyfert 1 are generally spirals (McLure et al. [103]). The radio-loud group is formed by low luminosity **Broad Line Radio Galaxies** (BLRG) and **radio-loud quasars**, which can be classified as Steep Spectrum or Flat Spectrum Radio Quasars (SSRQ and FSRQ, respectively), according to their spectral slopes in the radio band.

• *Type II: Narrow-Lined AGN*
Objects having weak continuum emission and *only* narrow emission lines are classified as *Type II* AGN. The radio quiet objects are **Seyfert 2** galaxies, while their high luminosity counterparts are still uncertain. The most likely candidate are the infrared-luminous galaxies (IRG). Radio-loud Type II objects are the **Narrow Line Radio Galaxies** (NLRG).

A further class of radio loud AGN which is not strictly included in the *Type II* group, is the sub-class of radio galaxies with only weak or absent emission lines in their optical spectrum. They are believed to be the low-luminosity counterparts of **NLRG**, and they can be classified as *Type 2* AGN as they do not show broad emission lines.

• *Blazars*
A small number of radio-loud AGN have unusual spectra, dominated by a strong non-thermal continuum emission at all wavelengths. Their main characteristics are:

- they are compact and core dominated flat spectrum radio sources;
- they show superluminal motions of VLBI components;
- they are strong emitters from the radio to the X-ray band; many of them are also gamma ray emitters;
- their fkux is strongly and rapidly variable (more than a factor of 2 on timescales of $\sim$ hours-days) in any observed band;
- they show strong and variable optical and radio polarization ($P >$ 3%).

In a $\log\nu - \log\nu F_\nu$ representation, these objects show an overall spectral energy distribution formed by two broad peaks. The lower energy one (situated between the IR and X-ray bands) is interpreted as due to synchrotron emission, while the high energy one (generally in the gamma-ray band) is adduced to inverse-Compton scattering. The seed photons for inverse-Compton emission might be either produced inside the emitting region (i.e. the synchrotron photons, e.g. Maraschi, Ghisellini & Celotti [96]), or outside the emitting region (e.g. from the accretion disc, from the BLR or from the dusty torus, Dermer & Schlickeiser [32], Sikora, Begelman, Rees [132], Ghisellini & Madau [51], Wagner et al. [156]). Their "extreme" properties imply that their emission is originated in the inner jet, and that they are strongly affected by relativistic beaming effects (Blandford & Rees [15]). Blazars have been historically classified on the basis of their optical spectrum: BL Lac objects have no or weak emission lines (Equivalent Width < 5 Å), while FSRQ, as already mentioned, have strong broad emission lines. Some BL Lac sometimes show faint broad lines, especially in the occurrence of low emission activity. Recently, continuity among blazars properties has been found, and there is evidence that they might form a single family of objects (Fossati et al. [48]). These authors have found that the SED of blazars is related to the observed luminosity. There is a rather well defined trend: the lowest luminosity BL Lacs peak at

the highest energies (HBL, High Energy Peaked BL Lacs, Padovani & Giommi [114]), while as the bolometric luminosity increases the peaks shift to lower frequencies (LBL Low Energy Peaked BL Lacs). FSRQ have the highest luminosities, the lowest peak energies, and a strong dominance of the Compton component with respect to the synchrotron one.

• *Other classes of AGN*
Not all AGN are included in the above classification. Other fonomenologies are included in the following classes:
LINERS are low luminosity AGN which are characterized by relatively strong emission lines of low ionization species, mainly originated by shocks.
Broad Absorption Lines QSO (BAL QSO) are quasars showing broad absorption features in their optical and UV spectra. The BAL phenomenon has been found among both radio-quiet and radio-loud objects (Becker et al. [8]).
Compact-Steep Spectrum and **GHz-Peaked Sources** (CSS and GPS) are intrinsically small AGN which are believed to be young and evolving radio sources that will become large-scale radio galaxies (Fanti et al. [44]).

1.2 Radio Galaxies

While weak radio emission ($L_r \sim 10^{37}$ erg s^{-1}) is observed in many "normal" galaxies, *Radio Galaxies* are powerful radio sources, with a total luminosity in the radio band of $L_r = 10^{41}$ up to 10^{46} erg s^{-1}. M 87 and NGC 5128 were the first two elliptical galaxies which have been identified as the optical counterparts of extragalactic radio sources (respectively Virgo A and Centaurus A; Bolton, Stanley & Slee [16]). This constituted the major evidence for the extragalactic nature of such objects. With the advent of interferometers, in the early '60s, many

other optical identifications were made, and now it is well established that radio galaxies are statistically associated with ellipticals.
The main structural components of radio galaxies are:

- **Cores**
  Radio cores are compact flat spectrum ($\alpha \sim 0$) stationary components associated with the power source in the nucleus of the radio galaxy. They are normally unresolved on the scale of VLBI observations, implying that their linear dimension is well less than ~ 0.1 pc in nearby objects. They are believed to be the optically thick base of the relativistic jet.

- **Jets**
  Radio jets are linear features linking the cores to the outer extended structures. They may be visible over all or only part of their path, they can be smooth or knotty, straight or curved, one or two-sided. The spectral index of radio jets is typically $\alpha = 0.6$.

- **Lobes**
  Lobes are a general term to describe the extended regions (hundreds of kpc from the core) of radio emitting plasma exhausted from the beams, showing steep radio spectra ($\alpha > 1$).

- **Hotspots**
  The hotspots are bright components located at the outer extremities of the lobes of powerful radio galaxies. Their linear dimensions are generally less than about 1 kpc. Hotspots spectra are in the range $\alpha \simeq 0.5 - 1$, and are somewhat flatter than the lobes. Hotspots are naturally interpreted as the "working surface", where the jet meets the ambient medium and creates a shock, which convert a significant fraction of the beam kinetic energy into relativistic particles.

Radio galaxies were originally classified into two classes, according to their radio morphology (Fanaroff & Riley [43]): Fanaroff-Riley class

I (FR I) were bright near their centers and slowly faded out further from the core (edge-darkened), while Fanaroff-Riley class II (FR II) were brightest at the extremities of the source and fainter close to their centers (edge-brightened). In more recent images, many FR I appear to possess twin, slowly broadening jets, while FR II have more collimated jets (generally one-sided) terminating in bright hot spots. Such simple morphological classification corresponds to a transition in the total radio power at 178 MHz, which formally occurs at $L_{178} = 2 \times 10^{26}$ W Hz^{-1}.

Owen & White ([112]) suggested that FR I and FR II were not only separated by a radio power division, but that this break depends strongly on the optical absolute magnitude of the host galaxy ($\propto L_{opt}^2$). A possible explanation for the origin of both this optical dependence and the different radio morphologies has been suggested by Bicknell ([9]). If the initial conditions are similar in FR I and FR II jets, the radio morphology might be related to environmental factors of the host galaxy interstellar medium, which might be in turn connected to the galaxy magnitude. In fact, the assumption of similar relativistic sub-parsec scale jets in both FR I and FR II seem to be supported by observations (see below). FR I jets should decelerate and become transonic (or subsonic) and midly relativistic on the kpc scale ($v \sim 0.6 - 0.7c$).

1.2.1 FR I and FR II radio jets: observed properties

The lower luminosity sources (FR I) tend to have prominent smooth continuous two-sided jets, running into large scale lobe structures. Most jets are one-sided (by 4:1 intensity ratio) close to the core, but become two-sided after a few kpc. Jets in FR I contribute over 10% to the total power of the extended structures. The magnetic field in the jets is generally aligned with the jet axis ($\mathbf{B}_{||}$) close to the core, at their very beginning, while it becomes perpendicular ($\mathbf{B}_{\perp}$) to the jet further out. A typical FR I jet structure is shown in Fig. 1.2. Although two-sided symmetry is typical of FR I, it should be noted that some objects

show significant asymmetries. Moreover, the FR I morphology is much less defined than FR II. In fact, it includes different sub-classes (twin jets, narrow angle tails, wide angle tails, fat doubles and many other sources which are difficult to classify uniquely) and sources showing intermediate characteristics between FR I and FR II are also present.

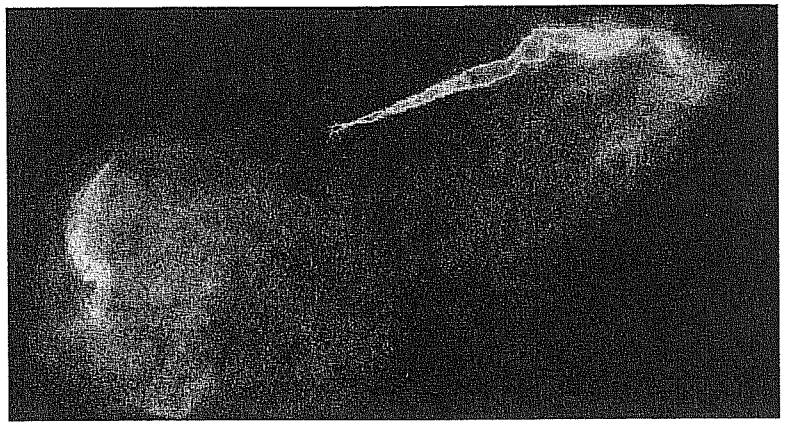

Figure 1.2: M 87 (3C 274) in the radio band, as seen from the VLA: an FR I with a one-sided jet. *National Radio Astronomy Observatory/National Science Foundation*

FR II radio jets are more difficult to be detected. When observed, they are generally not smooth, narrower, and one-sided. The magnetic field configuration is generally parallel to the jet direction, except in bright knots, in which $\mathbf{B}_\perp$ dominates. A typical FR II is shown in Fig. 1.3.

The most accepted scenario for the origin of the one-sidedness of some sources is the relativistic bulk motion of the emitting plasma. In fact, the radiation emitted by relativistically moving particles is beamed towards the direction of motion. Object observed at large angle between the jet axis and the line of sight will show more symmetric radio jets than sources observed at smaller angles. FR I jets are therefore not heavily affected by beaming on kpc scales. Conversely, if FR II jets (and the initial part of FR I ones) are intrinsically symmetric, the

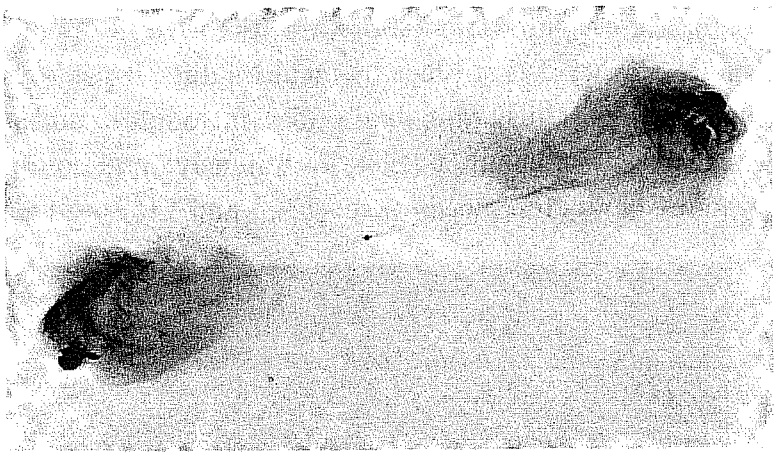

Figure 1.3: The radio galaxy Cygnus A, showing the typical FR II edge-brightened morphology and a one-sided jet. *Perley et al. ([118])*

jet–counterjet ratio is enhanced by relativistic beaming effects.

1.2.2 Optical properties of FR I and FR II

• Host Galaxies

It is now well established that the hosts of radio galaxies are essentially luminous ellipticals. However, elliptical galaxies are a somewhat vague class, as many objects which are "ellipticals" show different structural properties, when studied in details. The question is therefore to establish whether FR I and FR II are drawn from the same population of objects. Zirbel ([163]) have studied a large sample of radio galaxies with redshift up to $z = 0.5$, finding that FR I and FR II host galaxies are different in their magnitude distributions, colors, color gradient and, most importantly, in the galaxy structure. In particular, FR I's host galaxies are generally brighter than FR II's, they typically show a cD-like morphology (central dominant component of clusters, large ellipticals with a faint halo) or double-nuclei. Conversely, FR II are typically associated with N-galaxies (point-like nuclei and a steep brightness profile) or disturbed ellipticals, and avoid cD.

However, all present studies are based on ground based, relatively low-resolution observations. This could be a serious problem in the classification of some objects. In particular, the true nature of N-galaxies is somewhat unclear: the N morphology might in fact be originated by the dominance of the nuclear AGN component, and not related to the extended properties of the host galaxy. Clearly, future studied based on higher resolution images, in particular with the large database of the HST surveys, will establish more firmly the nature of the above differences, which are however certainly present.

Another important question is: are radio galaxies hosts different from normal (non-active) galaxies? Recent studies show that radio galaxies hosts are normal in most of their structural properties (e.g. ellipticity, isophote twisting), however they appear to be on average larger, brighter, bluer $(B - R)$ and with steeper color gradients with respect to normal ellipticals (Govoni et al. [60]). This means that the radio-loudness is only weakly related to the overall properties of the host galaxy.

• **Environment**

Another important difference between FR I and FR II is the environments they inhabit. First of all, FR I are predominantly found at low redshifts ($z \lesssim 0.3$) and they inhabit moderately rich clusters. On the contrary, FR II are either isolated or they are found in small groups. A detailed study on the environment of radio galaxies (up to $z = 0.5$) has been done by Zirbel ([162]). In this work, the author has evaluated the richness of the groups, counting the galaxies which surround each radio galaxy. The above indication is substantially confirmed, however it appears that FR II avoid rich groups at low redshifts, but they are present in rich groups at higher ($0.3 < z < 0.5$) redshifts. Since it has been established that such rich groups cannot evolve in the small low-redshift FR II groups, this means that the environments of FR II has changed with time, and the presence of the FR II morphology has a

different link with the environment, depending on redshift. Moreover, FR II appear to be more often involved with galaxy interactions with respect to FR I.

• **Emission lines**

Radio galaxies are often divided on the basis of their emission line properties. Strong emission lines are generally absent among FR I (although some exceptions are present), while FR II can be mainly divided into two classes: narrow line radio galaxies (NLRG), showing only narrow (FWHM $\lesssim 1000$ Km s^{-1}) permitted and forbidden emission lines; broad line radio galaxies (BLRG), showing broad permitted (FWHM $\gtrsim 3000$ Km s^{-1}) emission lines in addition to the narrow ones. Such spectral classification is analogous to that of Seyfert galaxies, and the characteristics of the emission line spectra are also similar. There is also a class of objects which, despite being associated with powerful FR II, they have only weak, low ionization emission lines (WLRG or LEG). We will assume for these sources the definition given by Jackson and Rawlings ([73]): they define a LEG a radio galaxy for which the equivalent width of the [OIII]λ5007 is less than 10Å, or [OII]/[OIII] > 1, or both. Conversely, both BLRG and NLRG are high-excitation galaxies (HEG). Notice that the difference between BLRG and quasars is somewhat subjective: historically, quasars were radio sources with a point-like optical counterpart, while in BLRG the host galaxy was clearly detected. But now the host galaxies of quasars can be detected up to high redshifts ($z \sim 2.5$, see e.g. Lehnert et al. [91]) in HST images. More physical distinctions are based either on the width of the broad lines (BLRG show smaller velocities than quasars, on average, McCarty [102]), or on the relative importance of the nuclear emission with respect to the underlying stellar component of the host (Jackson & Rawlings [73]).

• **The origin of the emission line spectra**
Which is the origin of the emission lines? Powerful radio emission is generally associated with optical emission lines. The radio-optical link is now quantified by several studies which show the existence of correlations between the emission line luminosity and the radio power (Baum & Heckman [7], Rawlings & Saunders [122], Morganti et al. [107], Zirbel et al. [164], Tadhunter et al. [142]). It is generally assumed that the emission line properties of radio galaxies can be explained in terms of a quasar illumination model. The emission line regions are assumed to be photoionezed by EUV photons from a central illuminating source. In this frame, the correlations between optical and radio properties are explained if the jet power is linked to the strength of the ionizing continuum by the physics of the central engine (e.g. Rawlings & Saunders [122]). Although this might be the dominant mechanism for the production of emission lines, the interaction of relativistic jets and the interstellar medium clearly plays a role. This has been recently stated through high resolution HST observations: similarly to what has been found in some Seyfert galaxies (e.g. Capetti et al. 1999) Feinstein et al. [45] have shown that the extended NLR in 3C 299 (an FR II radio galaxy at $z = 0.367$) is apparently associated with the radio structures. The observations are explained by a model in which the line emitting gas is shocked by the interaction with the jet plasma.

1.3 Unification of AGN

The unification of different classes of AGN is mainly based on their anisotropic emission. Intrinsically identical sources appear different to observers situated at different angles of sight. This anisotropy can arise for two different reasons:
i) obscuration of the central regions by a geometrically thick structure (for both radio-quiet and radio-loud);
ii) relativistic beaming of the radiation emitted by the inner jet (for

radio-loud sources).

The unification of *Type I* and *Type II* AGN requires the presence of obscuring material in the central regions. Such structure is generally represented as a geometrically thick, pc-to-tens-of-pc-scale dusty torus, although the real geometry has not yet been firmly established. Alternative representations are in fact possible, such as warped discs and clumpy structures. *Type I* objects are observed "pole-on", and the BRL inside the torus is directly visible, while *Type II* objects are seen "edge-on", thus the nucleus and BLR are obscured. Evidence for this unifying picture mainly comes from the following observations:
– detection of polarized (scattered) broad lines in Seyfert 2 and NLRG (e.g. NCG 1068, Antonucci & Miller [4]; 3C 234, Antonucci [2]);
– the weakness of the soft X-ray continuum in *Type II* AGN can be successfully modeled with typical *Type I* spectra absorbed by high column densities of cold gas towards the line of sight;
– infrared observations: since the optical depth decreases at wavelengths longer than the optical, infrared observations can probe the nuclear regions of obscured nuclei. Compact and bright IR cores are detected in some NLRG (e.g. Djorgovski et al. [35]) and in a few cases infrared spectroscopy has revealed broad wings on the Paα line, implying that high velocity gas is present in these sources, although completely obscured in the optical (e.g. 3C 184.1, 3C 219, 3C 223, Hill et al. [68]);
– observations of the bi-conical structure of both polarized radiation, and emission line regions in *Type II* objects (e.g. NGC 1068, NGC 5728, Capetti et al. [24], [25], Wilson et al. [158], Morganti et al. [108]).

The anisotropic emission from a relativistic jet is the basis for unification of *blazars* with other radio-loud AGN. Blazars are believed to be observed at small angles with the jet axis, and therefore the relativistically beamed radiation of the jet dominates the observed emission at all wavelengths. For larger angles of view, the same object should appear to the observer as a radio galaxy. At high luminosities, powerful FR II

are considered the "parent population" of radio-loud quasars, while low luminosity FR I are associated with BL Lac objects. Evidence for this unifying picture comes from:
– extended radio properties: the radio structure of blazars are compatible with being "aligned" radio galaxies, and their extended radio powers are similar (Padovani [115], Kollgaard et al. [79]);
– extended optical properties: although in blazars the nuclear emission generally outshines the host galaxy, the "resolved" blazars appear to be hosted in elliptical galaxies (e.g. McLure et al. [103], Urry et al. [150]), as it is for radio galaxies;
– the host galaxy magnitudes of FR I and FR II are comparable to those of BL Lacs and quasars, respectively (e.g. Urry et al. [150]);
– the luminosity distribution of the narrow [OII]λ5007 emission line in the spectra of NLRG and quasars, which is assumed to be emitted isotropically, completely overlap (Hes et al. [67]); only faint line emission (when present) is detected in both BL Lacs and FR I;
– statistical unification: a further test of the unified schemes can be made via the number statistics of complete samples of blazars and radio galaxies. The radio luminosity functions of radio galaxies, once beamed, are compatible with the observed blazars ones (Urry & Padovani [152]), although the inferred average bulk Lorentz factor of the jet are lower ($\Gamma \sim 7$) than those determined with other independent methods (see chapter 4).

1.4 The HST view of radio galaxies

Significant progresses in the understanding of the inner structure of radio galaxies have been obtained thanks to the high resolution and sensitivity of Hubble Space Telescope observations. Such high resolution ($\sim$ 0.1arcsec at optical wavelengths) is still $\sim$ 10 times better than what can be achieved by ground based telescopes. Most importantly, HST studies have revealed the presence of dusty or gaseous kpc-scale

discs in the inner regions of several FR I radio galaxies (Fig. 1.4). The study of the dynamics of such discs provides one of the strongest pieces of evidence of the presence of supermassive black holes associated to active nuclei. Spectroscopic studies of the central regions of radio galaxies have been performed with the HST for several objects, namely M 87, NGC 6251, NGC 4261, M 84 and NGC 7052 (Ferrarese et al. [46], Bower et al. [17], Van der Marel & Van der Bosh [154]), leading to the measurement of black hole masses in the range $2 - 8 \times 10^8 M_\odot$.

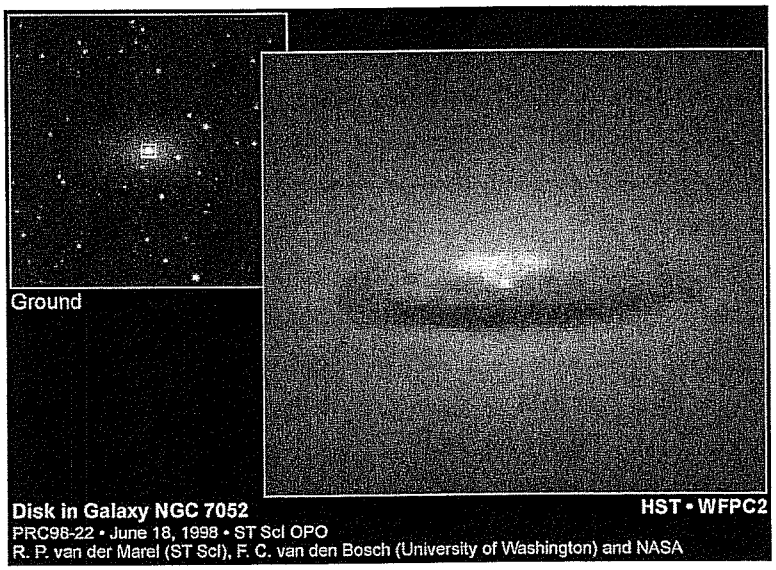

Figure 1.4: The kpc-scale disc discovered by the Hubble Space Telescope in the nucleus of the FR I radio galaxy NGC 7052 *(Jaffe et al. [74])*.

1.4.1 Two striking objects: M 87 and Centaurus A

M 87 is one of the closest powerful radio galaxies, thus it is an extraordinary laboratory for the study of the AGN activity. HST observations have revealed an ionized gas disc surrounding the nuclear regions, which is oriented approximatively perpendicularly to the jet (Fig. 1.5). Macchetto et al. [93]) studied the kinematics of such

disc through HST/FOC observations, observing the emission line of [OII]λ3727 at three different positions separated by 0.2 arcsec, with a spatial sampling of 0.03 arcsec (corresponding to $\sim 2pc$ at the distance of M 87). They measured the rotation curve of of the inner $\sim 1''$ of the disc, to a distance as close as $0.07''$ to the dynamical center. They found that these observations are consistent with a thin keplerian disc, rotating around a central mass of $(3.2 \pm 0.9) \times 10^9 M_\odot$. Such mass must be distributed in a sphere whose maximum radius is 3.5 pc, thus the most likely explanation is the presence of a supermassive black hole.

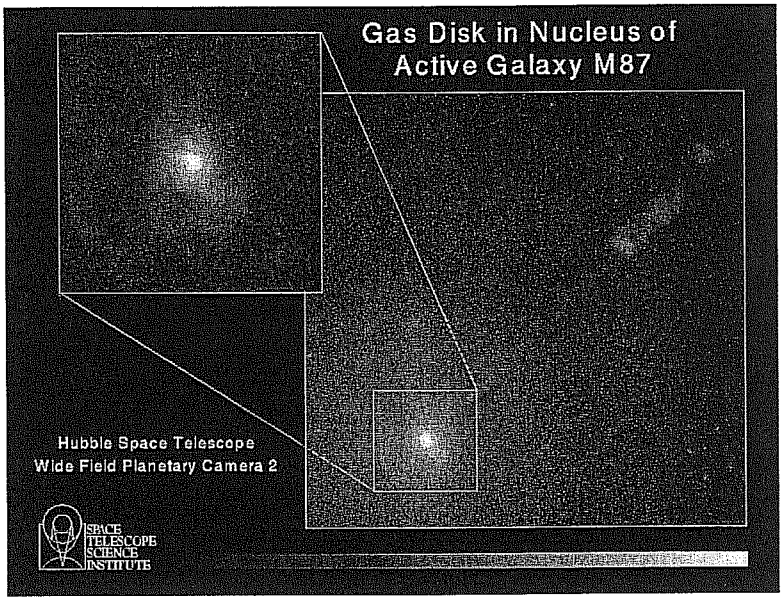

Figure 1.5: HST image of the ionized gas disc orbiting around a central black hole of $(3.2 \pm 0.9) \times 10^9 M_\odot$ *Ford et al., STScI.*

Also, an HST study of the famous optical jet in M 87 has been performed. Multiple observations made with the Faint Object Camera, taken between 1994 and 1998, led Biretta et al. ([10]) to the discovery of superluminal motions of several features within the first $6''$ of the jet, having apparent speeds of $4c - 6c$. Subluminal ($v \sim 0.63c - 0.84c$) components are found in the inner $1''$ of the jet. The discovery of such

apparent velocities, which imply bulk Lorentz factors of the order of $\Gamma \sim 6$ for a jet orientation of $\sim 20°$, strongly supports the BL Lac/FR I unification.

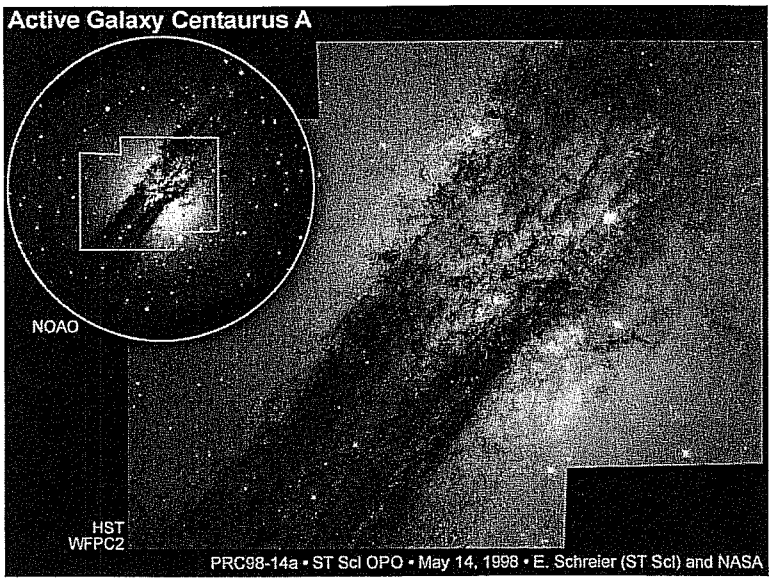

Figure 1.6: The central regions of Centaurus A as seen by the HST (Marconi et al. [97]), compared to a ground-based image.

The case of Centaurus A (NGC 5128) is also particularly interesting. This object is a low-luminosity FR I radio galaxy, being the closest radio-loud AGN ($d = 3.5$ Mpc, Hui et al. [72]). Therefore, it offers a unique opportunity to investigate the putative supermassive black hole, the associated accretion processes and the jet. However the study of its nuclear regions at optical through UV wavelenghts is strongly hampered by the presence of a prominent dust lane (Fig. 1.6). The dust lane can be modeled by a thin warped disc, and it is interpreted as the result of a relatively recent merger event with a small, gas rich, disc galaxy. Dust extinction is strongly reduced in the infrared band, and a bright nuclear component is clearly visible in such spectral region even through ground based observations (Bailey et al. [5]). Thanks to a

precise determination of the position of the IR nucleus made through recent HST/NICMOS observations (NICMOS is the HST near infrared camera), the faint optical counterpart has been found in the R and V bands, while it vanishes completely in the B band (Marconi et al. [97]). Moreover, HST images have shown the presence of a 20pc nuclear disc, which is detected in both Paα and [FeII]λ1.64 μm lines, with an ionization level typical of low-ionization Seyfert and LINERS. The large scale dust lane, a bar detected by ISO and SCUBA observations (Mirabel et al. [104]), and the inner Paα disc might all represent aspects of the feeding of the central blach hole.

1.4.2 The HST snapshot survey of the 3CR catalog

A large systematic survey of nearly all the extragalactic radio sources from the 3CR Catalog (Spinrad et al. [137]) in the V and R bands as well as through narrow-band filters[3] has been performed with the Wide Field and Planetary Camera 2 (WFPC2), the CCD imager on board HST. The 3CR Catalog is ideal for an HST snapshot survey seeking to explore the nature of radio galaxies. It is unbiased, it spans a wide range in redshift and radio power, and there is a vast suite of ground and space-based observations in nearly all wavelength regimes for comparison. Moreover, 3CR sources are selected at a low radio frequency (178 MHz), in a spectral region where the radiation from the extended components of radio sources (i.e. the lobe emission) dominates. Therefore, if the extended emission is not affected by relativistic beaming (as it is widely believed), 3CR sources are randomly oriented in the plane of the sky and this catalog is also ideal for testing the AGN unification models.

The R-band images are presented in a series of papers and are available to the scientific community in the public HST archive: (1) radio

[3]The HST broad band filters set is similar, but not equal, to the UBVRI Jonhson-Couisins photometric system. Details on the filters used in this thesis work will be given in the following chapters.

galaxies at low redshifts ($z < 0.1$), (2) radio galaxies at intermediate redshifts ($0.1 < z < 0.5$; de Koff et al. [33]), (3) radio galaxies at high redshifts ($z > 0.5$; McCarthy et al. [101]), (4) the QSOs (Lehnert et al. [91]). At the $0.1''$ resolution of the images, lots of details are visible. The first results of the analysis of such a large database of images concern the study of the host galaxies structure, the environment of these sources, the detection of optical jets, kpc-scale discs, extended dust lanes. A statistical study of all of these properties is currently in preparation.

1.4.3 Unresolved optical cores in FR I

Further features discovered in radio galaxies through HST observations, which we will concentrate on, are faint nuclear components, unresolved in HST images. These optical nuclei might represent the elusive emission associated with the AGN. In a pilot study of five objects in which both a gas disc and an unresolved optical nucleus have been detected, Capetti & Celotti ([23]) have shown that there is evidence for a correlation between disc inclination and the luminosity of the nuclear component. This behavior is quantitatively consistent with a scenario in which such nuclear emission is dominated by the radiation from a relativistic jet with Lorentz factor $\sim 5 - 10$ observed at large angles to the line of sight, thus supporting the basic features of the FR I/BL Lac unification. Further, independent support to this interpretation comes from the rapid variability of the central source of M 87, the only object for which multi epoch HST data are avaliable (Tsvetanov et al. [149]). Clearly, these results show that the analysis of such nuclear components might constitute a direct tool for testing the FR I - BL Lac unification scheme. However, the non-thermal origin of these nuclei has still to be proved. Several observational tests can be performed to confirm the above results: a spectral analysis of the central regions might be performed in order to establish their non-stellar nature, while multiple observations of single sources can prove the expected variability. How-

ever, the study of a much larger (and complete) sample of FR I can be performed even without indication of the source orientation. Thus the large database provided by the 3CR HST snapshot survey is a ideal for such an investigation, which constitutes, in fact, the starting point of the work presented in this theses.

1.5 Our questions about radio galaxies

HST studies have been proven to be a fundamental tool for the investigation of the nuclear regions of AGN. Our interests focus in particular on the inner structures of both FR I and FR II radio galaxies, which can be directly related to the AGN activity. Also we are interested in testing the radio galaxies/blazars unifying scheme with the information we obtain from the study of radio galaxies nuclei. Our main questions on radio galaxies, which we intend to investigate in this thesis, are summarized in the following.

1. What are the central components, unresolved in the HST images of FR I sources? The non-thermal, relativistically beamed emission from the jet, which in the frame of the FR I/BL Lac unification should dominate the BL Lac observed radiation, should be also present in the nuclei of radio galaxies, although unbeamed or strongly debeamed. The possibility of directly detecting this component in the optical band thanks to the HST capabilities, has been explored in the above cited work by Capetti & Celotti ([23]). They found that their properties are quantitatively consistent with a scenario in which such nuclear emission in is dominated by the radiation from a relativistic jet. Alternatively, these optical nuclei has been interpreted as the emission from a hot accretion disc (Jaffe et al. [74]). In order to understand the real nature of these sources, a much larger (complete and with objects randomly oriented in the plane of the sky) sample should be analyzed.

2. Are there obscuring tori in FR I? The role of obscuration in low luminosity FR I radio galaxies is still a matter of debate. In analogy with the unification scheme for Seyfert galaxies, it is believed that in radio galaxies the Broad Line Region (BLR) and the nuclear continuum source are hidden by an absorbing, edge-on torus. A combination of obscuration and beaming is essential for the unification of powerful radio sources (Barthel [6]). However, although circumnuclear tori appear to be commonly associated with active galactic nuclei, there is as yet no evidence in favour of nuclear obscuring material in FR I (and this is not strictly required by the FR I / BL Lac unified scheme, Urry & Padovani [152]). A search for H_2O megamasers (which have been successfully used to probe the dense molecular gas associated to the torus in Seyfert galaxies, Miyoshi et al. [100], Braatz et al. [18]) in a sample of FR I galaxies gave negative results (Henkel et al. [66]).

3. Which is the accretion rate in FR I radio galaxies? In spite of the presence of powerful relativistic jets, the absence of both strong emission lines and a prominent blue-bump in low luminosity radio-loud AGN lead to the hypothesis that radiatively inefficient accretion (advection-dominated flows, ADAF) might be present in such objects (Rees et al. [123]). Conversely, in luminous quasars, the accretion disc is directly observed, and the estimated radiative regimes are quite high, with luminosities close to the Eddington limit. Therefore, it is also very important to investigate the nuclear properties of FR I in order to establish if radiatively efficient, geometrically thin discs or, instead, ADAFs are the origin of their activity.

4. How the extended radio morphology is related to the innermost nuclear properties? The original classification of extended radio galaxies by Fanaroff & Riley ([43]) is based on a morphological criterion, i.e. edge darkened (FR I) vs edge brightened (FR II)

radio structure. Differences between the two classes are present in the structure of the host galaxy, environment and spectral properties (see Sect. 1.2). From the point of view of the unification schemes, FR I and FR II are believed to be the parent populations of BL Lacs and radio-loud quasars, respectively. However, this traditional dicothomy is probably inadequate, and several observational arguments argue in favour of a continuity between the two classes. Therefore, one of the most important questions is whether the FR I/FR II dichotomy is generated by two different manifestations of the same astrophysical phenomenon, and the transition between the two classes is indeed continuous, or instead it reflects fundamental differences in the innermost structure of the central engine.

5. What can we learn from the comparison of the optical nuclear emission of FR I and BL Lacs? The emission from relativistic jet should be strongly de-amplified in radio galaxies. While the direct comparison of the aligned and misaligned components is possible in the radio band, by comparing blazars to the radio core emission of radio galaxies, in the optical band this kind of study is hampered by the stellar emission from the host galaxy, which dominates in ground based observations. Thanks to the HST, such nuclear emission might be detected, and through the comparison of the beamed and unbeamed components could lead to important information on the jet structure and velocity.

6. One of the final goals of our research will be to build up, for the first time, the spectral energy distribution of radio galaxies using "pure" nuclear data. The interpretation and modeling of multi–wavelength observations of radio galaxies clearly represent an alternative and more detailed way to test the unification schemes, as their SED can be directly compared with those of blazars. Although this cannot be yet achieved for a large sam-

ple of sources, as a pilot study, we will put together HST data with radio-through-high energy nuclear data for a small number of FR I radio galaxies.

The following chapters of the thesis are self-consistent parts of the above research line. The work presented has been done in collaboration with several people: Annalisa Celotti and Alessandro Capetti (all chapters), Gabriele Ghisellini (chapter 4), Edoardo Trussoni, Luigina Feretti (chapter 5). This has led to the publication of the following papers:
Chiaberge M., Capetti A., Celotti A., 1999, A&A 349, 77
Chiaberge M., Capetti A., Celotti A., 2000 A&A, 355, 873;
Chiaberge M., Celotti A., Capetti A., Ghisellini, 2000, A&A 358, 104;
Capetti A., Trussoni E., Celotti A., Feretti L., Chiaberge M., 2000, MNRAS, in press
Chiaberge M., Capetti A., Celotti A., in preparation;
where the authorship order reflects my own relative contribution.

In chapter 2 we investigate the nature of the central unresolved components discovered in radio galaxies through the analysis of a complete sample of all FR I radio galaxies from the 3CR catalog. The emission from these optical nuclei is anisotropic, and show a striking linear correlation with the radio core one, which lead us to identify them with non-thermal synchrotron radiation from the inner jet. Thus, these also represent upper limits to any thermal/disc emission. For a $10^9 M_\odot$ black hole, typical of FR I sources, this limit translates into a fraction as small as $10^{-7} - 10^{-5}$ of the Eddington luminosity, suggesting that accretion might take place in a low efficiency radiative regime.
In chapter 3 we compare the optical nuclear properties of nearby $z < 0.1$ FR II to those of FR I of comparable redshift. FR II show a more complex behavior, which is however clearly related to their optical spectral classification. We also discover a new class of FR II with FR I-like (synchrotron dominated) nuclei, which do not fit in the usually adopted

AGN unified scheme. Our results imply that, at least at low redshifts, FR II are not a homogeneous population. Furthermore, the traditional FR I/FR II dicothomy is not univocally related to the innermost nuclear properties.

In chapter 4 we use the newly measured optical nuclear luminosity of FR I to explore the viability of the FR I/BL Lacs unification model. We find that the bulk Lorentz factors required by the spread in the observed luminosity are significantly smaller than those implied by other independent methods. In order to reconcile the unification scenario, velocity structures in the jet are suggested, where a fast spine dominates the BL Lac emission, while a slower, but still relativistic, layer dominates the emission in the misaligned objects.

In chapter 5 we re-analyze archival ROSAT X-ray data of five FR I in which the nuclear component can be separated from extended cluster emission. We put together X-ray, radio, near-IR and optical data, building for the first time the nuclear SED of FR I. We found that FR I SED are qualitatively similar to those of BL Lacs, thus supporting the identification of FRI sources as their mis-oriented counterparts. We will also consider the particular case of Centaurus A, for which we build the overall nuclear SED (from the radio to the gamma ray band). We model it in the frame of an homogeneous synchrotron-self Compton emission model, finding that the physical parameters for this source are similar to those obtained in BL Lacs, except for a much lower beaming factor.

Chapter 7 contains the conclusions, a summary of the thesis, and future perspectives.

$H_0 = 75$ km s^{-1} Mpc^{-1} and $q_0 = 0.5$ are adopted.

This research has made use of the NASA/IPAC Extragalactic Database (NED) which is operated by the Jet Propulsion Laboratory, California Institute of Technology, under contract with the National Aeronautics and Space Administration.

This thesis is based on observations with the NASA/ESA Hubble Space Telescope, obtained at the Space Telescope Science Institute, which is operated by AURA, Inc., under NASA contract NAS 5-26555 and by STScI grant GO-3594.01-91A

Chapter 2

The HST view of FR I radio galaxies nuclei

In this chapter we investigate the nature of the unresolved nuclear sources (to which we refer as Central Compact Cores, CCC) discovered by the HST in FR I radio galaxies. We consider a complete sample of 33 3CR radio galaxies, morphologically identified as FR I sources. For 32 of these, HST/WFPC2 images are available in the public archive. Most of the images were taken as part of the HST snapshot survey of the 3C radio source counterparts, and are already presented by Martel et al. ([98]) (objects with $z < 0.1$) and by De Koff et al. ([34]) (objects with $0.1 < z < 0.5$).

The selection of the sample is presented and discussed in Sect. 2.1, while in Sect. 2.2 we describe the HST observations. In Sect. 2.3 and Sect. 2.4 we focus on the detection and origin of the CCC component, respectively and in Sect. 2.5 we discuss some of the consequences of our results. Our findings are summarized in the final Sect. 2.6.

Table 2.1: Summary of radio and optical data of the sample.

Name	Other name	Redshift	F_c (5 GHz)	ref.	F_t (178 MHz)	L_t (178 MHz)
		z	mJy		Jy	W Hz^{-1}
3C 028		0.1952	<0.2	G88	16.3	26.94
3C 029	UGC 595	0.0448	93.0	M96	15.1	25.71
3C 031	NGC 383	0.0169	92.0	G88	16.8	24.93
3C 066B		0.0215	182.0	G88	24.6	25.30
3C 075		0.0232	39.0	M96	10.5	25.00
3C 76.1		0.0324	—		12.2	25.35
3C 078	NGC 1218	0.0288	964.0	M96	19.75	25.46
3C 083.1	NGC 1265	0.0251	21.0	R75	26.6	25.47
3C 084	NGC 1275	0.0176	42370.0	T96	40.5	25.32
3C 089		0.1386	49.0	Z95	20.2	26.76
3C 264	NGC 3862	0.0206	200.0	G88	26.0	25.29
3C 270	NGC 4261	0.0074	308.0	G88	55.45	24.73
3C 272.1	M 84	0.0037	180.0	G88	19.4	23.68
3C 274	M 87	0.0037	4000.0	G88	1050.0	25.42
3C 277.3	COMA A	0.0857	12.2	G88	9.0	26.03
3C 288		0.2460	30.0	G88	18.9	27.17
3C 293	UGC 8782	0.0452	100.0	G88	12.7	25.65
3C 296	NGC 5532	0.0237	77.0	G88	13.0	25.11
3C 305	IC 1065	0.0414	29.5	G88	15.7	25.66
3C 310		0.0540	80.0	G88	55.1	26.43
3C 314.1		0.1197	<1.0	G88	10.6	26.37
3C 315		0.1083	150.0	G88	17.8	26.51
3C 317	UGC 9799	0.0342	391.0	M96	47.3	25.98
3C 338	NGC 6166	0.0303	105.0	G88	46.9	25.87
3C 346		0.1620	220.0	G88	10.9	26.62
3C 348	Her A	0.1540	10.0	M96	350.0	28.09
3C 386		0.0170	14.	S78	23.9	25.09
3C 424		0.1270	18.	B92	14.0	26.54
3C 433		0.1016	5.	G88	56.2	26.96
3C 438		0.2900	17.0	Z95	46.3	27.68
3C 442	ARP 169	0.0262	2.0	G88	16.1	25.29
3C 449	UGC 12064	0.0181	37.0	G88	11.5	24.82
3C 465	NGC 7720	0.0301	270.0	G88	37.8	25.78

F_c and F_t are the core and total radio fluxes. In column 5 we report the references to the core fluxes. B92: Black et al. [12], G88: Giovannini et al. [56], L91: Leahy & Perley [90], M96: Morganti et al. [106], R75: Riley & Pooley [126], T96: Taylor et al. [145], Z95: Zirbel & Baum [166], S78: Strom et al. [139]. The radio core flux of 3C 424 has been estimated from the contour map (observations at 8.3 GHz).

2.1 The sample

Our sample comprises all radio galaxies belonging to the 3CR catalogue (Spinrad et al. [137]) and morphologically identified as FR I radio sources by Laing et al. ([87]) and/or Zirbel & Baum [164] (see Table 2.1).

However, the powerful but simple original morphological FR I/II classification has revealed to be often inadequate, as being somewhat subjective and sensibly depending on the quality, resolution and frequency of the available radio maps. Also, several radio sources show a complex morphology: for example signatures of FR I structures (such as extended plumes and tails) can be detected together with typical characteristics of FR II sources (narrow jets and hot spots) in sources which might represent transition FRI/II objects (see e.g. Parma et al. [116], Capetti et al. [26]). Furthermore, even among the edge darkened radio galaxies, a large variety of structures is present, including wide and narrow angle tails, fat doubles and twin jet sources. Although all these objects are classified as FR I and share the common characteristic of a low total radio luminosity, it is far from obvious that they represent a well defined class.

Therefore, in order to establish possible differences among the optical properties of the various subclasses of FR I galaxies and also directly re-assess their radio morphology against erroneous or doubtful identifications, we searched the literature for recent radio maps of each object of our sample. The radio structure of at least four sources is peculiar, there are several transition FR I/II objects and each of the FR I morphological 'types' described above is represented in the sample. In view of this ambiguity of the simple morphological classification, in the following we will also consider separately objects below and above a total radio luminosity of $L_{178} = 2 \times 10^{26}$ W Hz^{-1}, i.e. the fiducial radio power separation between FR I and FR II. Two thirds of the sources of our sample lie below this value.

Having only excluded 3C 231 (M 82) from the original list, as it is in fact a well known starburst galaxy, the remaining radio galaxies constitute a complete, flux limited sample of 33 FR I sources. In Table 2.1 we report redshifts, radio fluxes and total luminosities as taken from the literature: redshifts span the range $z = 0.0037 - 0.29$, with a median value of $z = 0.03$, and total radio luminosities at 178 MHz are between $10^{23.7}$ and $10^{28.1}$ W Hz^{-1}.

2.2 HST observations

HST observations are available in the public archive (up to July 1998) for 32 out of the 33 sources (only 3C 76.1 has not been observed). The HST images were taken using the Wide Field and Planetary Camera 2 (WFPC2). The pixel size of the Planetary Camera, in which the target is always located, is $0''.0455$ and the 800×800 pixels cover a field of view of $36'' \times 36''$. The whole sample was observed using the F702W filter as part of the HST snapshot survey of 3C radio galaxies (Martel et al. [98], De Koff et al. [34]). For about half of the sources, additional archival images taken through narrow and broad filters are also available. The HST observations log is reported in Table 2.2.

The data have been processed through the PODPS (Post Observation Data Processing System) pipeline for bias removal and flat fielding (Biretta et al. [11]). Individual exposures in each filter were combined to remove cosmic rays events.

In Figs. 2.1, 2.2 we present the final broad band images of the innermost regions ($1.5'' - 6\ ''$) of our 32 radio galaxies. The most interesting feature which is present in the great majority of them, is indeed an unresolved central source.

Table 2.2: Log of HST observations

Name	Filter	t_{exp} (s)	Date	Name	Filter	t_{exp} (s)	Date
3C 28	F702W	280	17/10/94	3C 277.3	F702W	560	16/03/94
3C 29	F702W	280	12/01/95		F555W	600	06/06/96
3C 31	F702W	280	19/01/95		FR680N	600	27/11/95
	FR680N	600	01/09/95	3C 288	F702W	280	30/04/95
3C 66B	F702W	280	18/03/94	3C 293	F702W	280	15/01/95
3C 75	F547M	900	10/03/97	3C 296	F702W	280	14/12/94
	F791W	750	10/03/97	3C 305	F702W	560	4/09/94
	F673N	2500	10/03/97	3C 310	F702W	280	12/09/94
3C 76.1	—	—	—	3C 314.1	F702W	280	22/12/94
3C 78	F702W	280	17/08/94	3C 315	F702W	280	29/11/94
	F673N	600	07/08/95	3C 317	F814W	6500	10/08/97
	F555W	600	16/09/96		F555W	6200	10/08/97
3C 83.1	F702W	280	22/07/94	3C 338	F702W	280	09/09/94
	F673N	600	22/10/95		F673N	600	27/11/95
3C 84	F702W	560	31/03/94	3C 346	F702W	280	01/08/94
	F450W	200	16/11/95	3C 348	F702W	280	09/05/94
3C 89	F702W	280	02/07/94	3C 386	F702W	280	1/04/ 95
3C 264	F547M	900	19/05/96	3C 424	F702W	280	05/09/94
	F673N	2500	19/05/96	3C 433	F702W	280	26/04/95
	F791W	750	19/05/96	3C 438	F702W	300	15/12/94
3C 270	F791W	800	13/12/94	3C 442	F791W	280	29/12/94
	F547M	800	13/12/94		F673N	2500	20/04/96
3C 272.1	F814W	520	04/03/96		F547M	900	20/04/96
	F547M	1200	04/03/96	3C 449	F702W	280	06/08/94
	F658N	2600	04/03/96		FR680N	600	24/08/95
3C 274	F814W	30	03/02/95	3C 465	F702W	280	23/01/95
	F547M	30	03/02/95		F673N	600	23/08/95

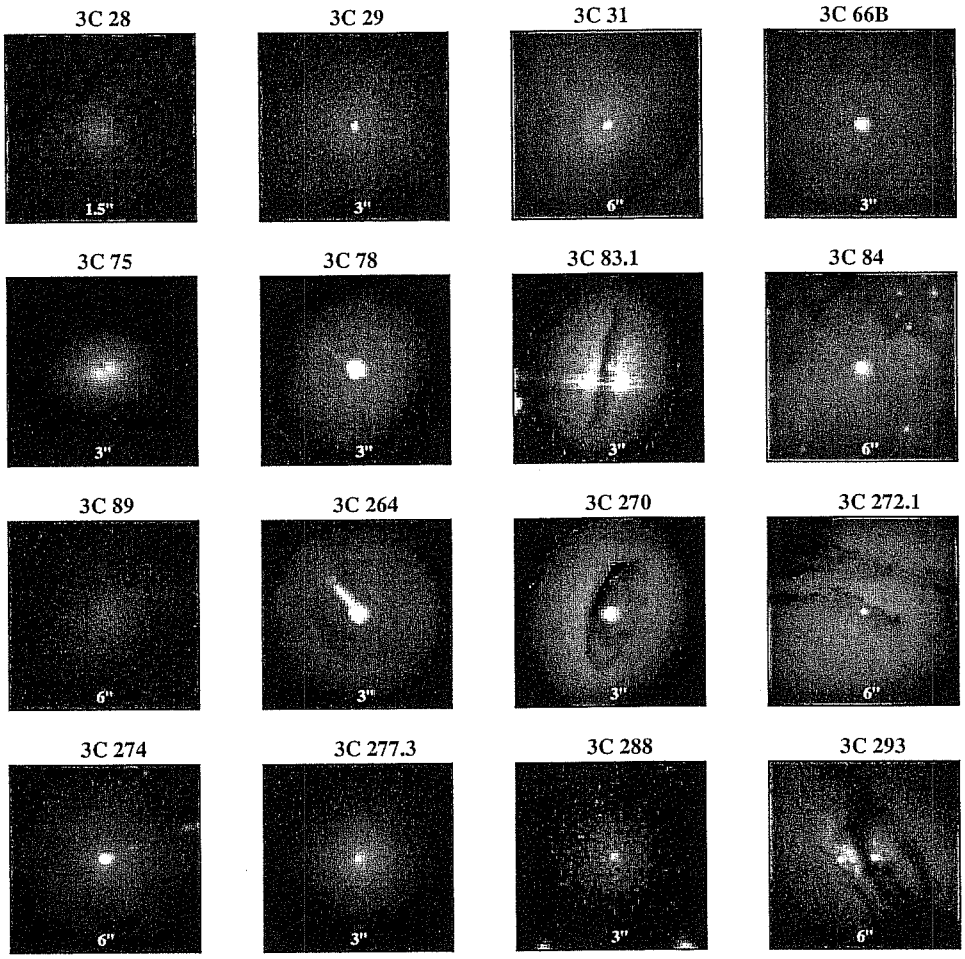

Figure 2.1: HST/WFPC2 broad band images of the FR I radio galaxies of the sample (a).

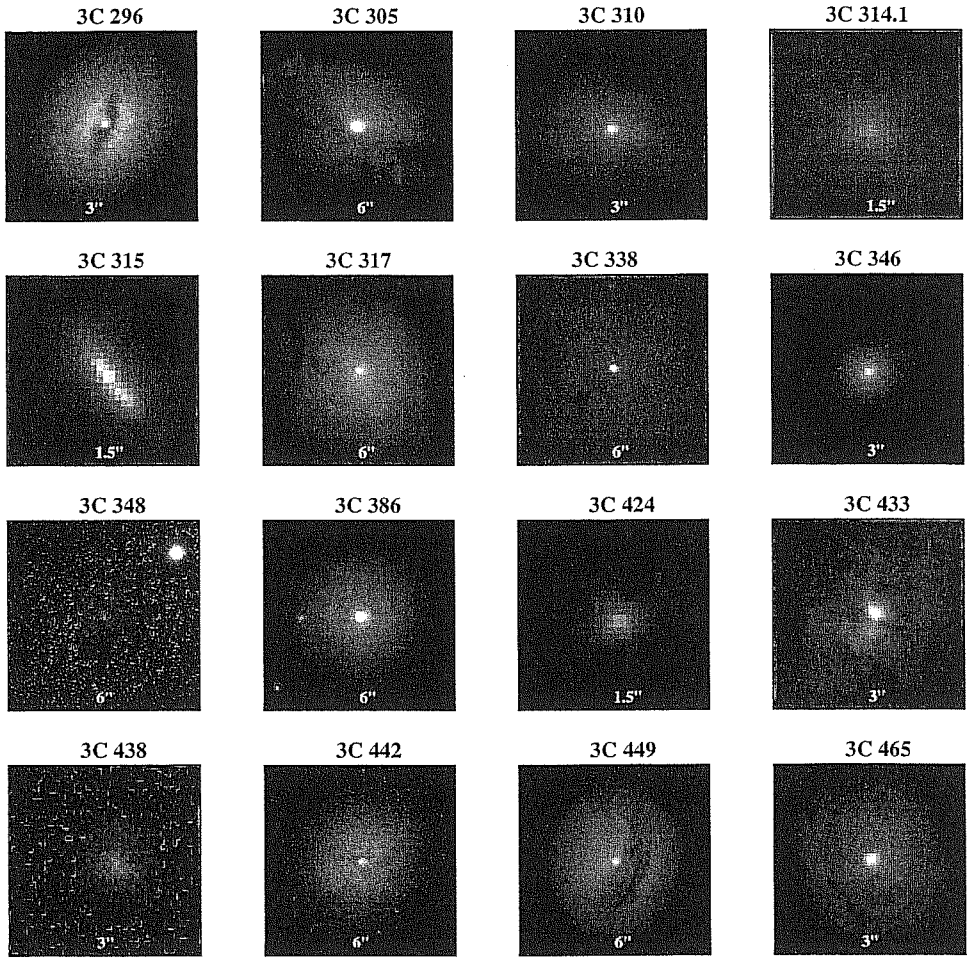

Figure 2.2: HST/WFPC2 broad band images of the FR I radio galaxies of the sample (b).

Table 2.3: Summary of the CCC photometry

Name	CCC flux, filter 1 erg $s^{-1}cm^{-2}Å^{-1}$	CCC flux, filter 2 erg s^{-1} cm^{-2} $Å^{-1}$	Name	CCC flux, filter 1	CCC flux, filter 2
3C 028	<3.2 E-19 [a]		3C 296	(3.4 ± 0.3) E-18 [a]	
3C 029	(5.8 ± 0.7) E-18 [a]		3C 305	——	
3C 031	(1.5 ± 0.4) E-17 [b]		3C 310	(3.5 ± 0.7) E-18 [a]	
3C 066B	(4.93 ± 0.07) E-17 [a]		3C 314.1	<9.5 E-19 [a]	
3C 075	——		3C 315	——	
3C 078	(2.38 ± 0.04) E-16 [b]	(3.09 ± 0.05) E-16 [e]	3C 317	(9.6 ± 1.0) E-18 [d]	(1.5 ± 0.2) E-17 [e]
3C 083.1	1.4 E-18:		3C 338	(1.0 ± 0.1) E-17 [b]	
3C 084	(1.5 ± 0.3) E-15 [b]	(1.43 ± 0.07) E-15 [g]	3C 346	(2.3 ± 0.3) E-17 [a]	
3C 089	< 2 E-19		3C 348	(8.0 ± 1.0) E-19 [a]	
3C 264	(1.14 ± 0.06) E-16 [c]	(1.54 ± 0.05) E-16 [f]	3C 386	(1.4 ± 0.1) E-15 [a]	
3C 270	(5.1 ± 0.1) E-18 [c]	(6.0 ± 2.0) E-18 [f]	3C 424	<1.5 E-18 [a]	
3C 272.1	(5.9 ± 0.2) E-17 [d]	(4.2 ± 0.1) E-17 [f]	3C 433	——	
3C 274	(3.9 ± 0.2) E-16 [d]	(6.5 ± 0.2) E-16 [f]	3C 438	<4.0 E-19 [a]	
3C 277.3	(1.5 ± 1.2) E-18 [b]	(3.5 ± 1.2) E-18 [e]	3C 442	(9.1 ± 3.3) E-19 [a]	(8.0 ± 2.0) E-19 [f]
3C 288	(7.0 ± 1.0) E-19 [a]		3C 449	(1.8 ± 0.1) E-17 [b]	
3C 293	——		3C 465	(1.9 ± 0.1) E-17 [b]	

HST filters coding: [a] F702W, [b] F702W line subtr., [c] F791W, [d] F814W, [e] F555W, [f] F547M, [g] F450W

2.3 The Central Compact Cores

2.3.1 Identification of CCCs

While it is straightforward to identify unresolved sources when they are isolated, the situation is more complex when these are located at the center of a galaxy, superposed to a brightness distribution with large gradients and whose behaviour in the innermost regions cannot be extrapolated from its large scale structure with any degree of confidence.

We therefore adopted a simple operative approach: we derived the radial brightness profiles of the nuclear regions of all galaxies using the IRAF *RADPROF* task and measured the FWHM setting the background level at the intensity measured at a distance of ∼5 pixels (∼0.23″) from the center. In 22 cases the measured FWHM is in the range 0.05″ – 0.08″, i.e. indicative of the presence of an unresolved source at the HST resolution.

In 5 cases, namely 3C 28, 3C 89, 3C 314.1, 3C 424 and 3C 438, the fitting procedure yields FWHM larger than 0.15″. The behaviour of these sources is radically different from those in which a CCC is detected and therefore we believe that, even with this operative definition, no ambiguity exists on whether or not a central unresolved source is present.

The remaining 5 sources have complex nuclear morphologies. The central regions of 3C 75, 3C 293, 3C 305 and 3C 433 are covered by dust lanes. Bright compact knots are seen, but they are completely resolved and offset from the center of the galaxy. Conversely 3C 315 has a peculiar highly elongated structure, contrasting with the typical roundness of FR I host galaxies, and no central source is seen.

2.3.2 CCC photometry

The F702W transmission curve covers the wavelength range 5900 - 8200 Å and thus, within our redshift range, includes the Hα and [N II] emission lines. To estimate the continuum emission of the CCC we therefore preferred, when possible, to use images obtained with the F814W or F791W filters which are relatively line-free spectral regions up to a redshift of 0.075.

We performed aperture photometry of the 22 CCCs, adopting the internal WFPC2 flux calibration, which is accurate to better than 5 per cent. However, the dominant photometric error is the determination of the background in regions of varying absorption and steep brightness gradients, especially for the faintest CCCs, resulting in a typical error of 10% to 20%. Narrow-band images were used, where available, to remove the line contamination from the F702W images. We found that the line contribution is typically 5 to 40 per cent of the total flux measured in the F702W filter, therefore even the uncorrected fluxes are (for our purposes) reliable estimates of the continuum level. Optical fluxes of the CCCs are given in Table 2.3.

HST images in two broad filters are available for 9 galaxies. How-

ever, only in 5 cases (3C 78, 3C 84, 3C 264, 3C 272.1, 3C 274) is the accuracy of the photometry sufficient to deduce reliable estimates of the optical slope. For the last three objects data were taken simultaneously in the two bands, which avoids uncertainties due to possible variability. Galactic extinction is significant (and we corrected for it) only in the case of 3C 84, for which $A_B = 0.7$. In 3C 272.1 we estimated, by comparing the F547M and the F814W images, that the extended nuclear dust lane produces an absorption of $1 - 2$ mag in the V band. The derived spectral indices (corrected for reddening) are in the range $\alpha_o = 0.7 - 1.3$.

For the galaxies only showing diffuse emission we set as upper limits the light excess of the central 3x3 pixels with respect to the surrounding galaxy background. For the complex sources no photometry was performed.

2.4 Origin of the Central Compact Cores

With the aim of investigating the origin of CCC emission we now explore possible (cor-)relations between the CCC flux/luminosity and other observed properties.

No trend is found between CCC luminosities and total radio power or absolute visual magnitude of the host galaxy. Conversely, the CCCs emission bears a clear connection with the radio core. In Fig. 2.3 we plot the optical flux of the CCCs F_o versus the core radio flux F_r (at 5 GHz): a clear trend is visible.

In order to quantify this relation let us consider separately the low and high luminosity sub–samples.

The 18 CCCs associated to the low luminosity sources show a tight correlation between F_o and F_r. Only one point, representing 3C 386, is well separated from the others. We perform a non-weighted least squares fit (excluding 3C 386): the correlation coefficient is $r = 0.88$ which gives a probability that the points are taken from a random

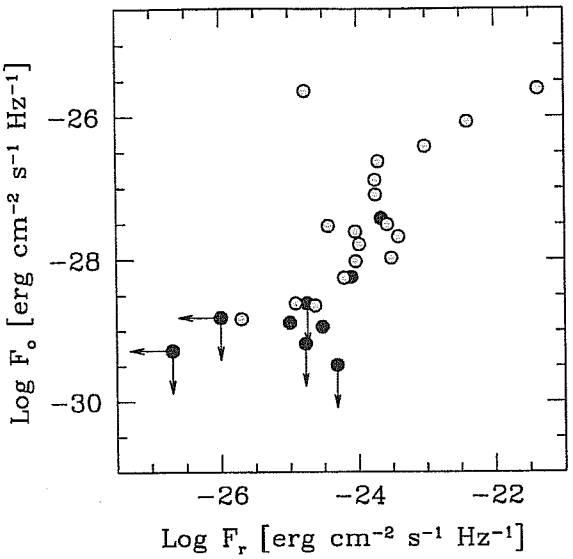

Figure 2.3: Optical flux of the CCC versus core radio (5 GHz) flux. Note the clear trend between the two quantities. Only the peculiar object 3C 386 is significantly offset (see text for discussion). Different symbols mark sources with total radio luminosity below (open circles) and above (filled circles) $L_{178} = 2 \times 10^{26}$ [W Hz^{-1}].

distribution of $P = 3.1 \times 10^{-6}$. The dotted lines in Fig. 2.4 are the fits to the data using each of the two fluxes as independent variables. The best fit is represented by the bisectrix of these two regressions (dashed line) and has a slope of 0.95 ± 0.10. The statistical parameters of the fits are reported in Table 2.4.

A similarly strong correlation ($P = 6.0 \times 10^{-6}$) is present also between radio core and CCC luminosities (Fig. 2.5). The fact that the correlation is found both in flux and luminosity gives us confidence that it is not induced by either selection effects or a common redshift dependence. Moreover the 3CR sample has been selected according to the total radio flux at low frequency which is only weakly correlated with the core properties entering in the correlations (e.g. Giovannini et al. [56]).

Let us then consider the case of 3C 386, which we excluded from the statistical analysis. While all points are closely clustered around the linear fit, with a dispersion of only ~ 0.4 dex, 3C 386 deviates by 3 orders of magnitude, clearly indicating that its optical/radio properties

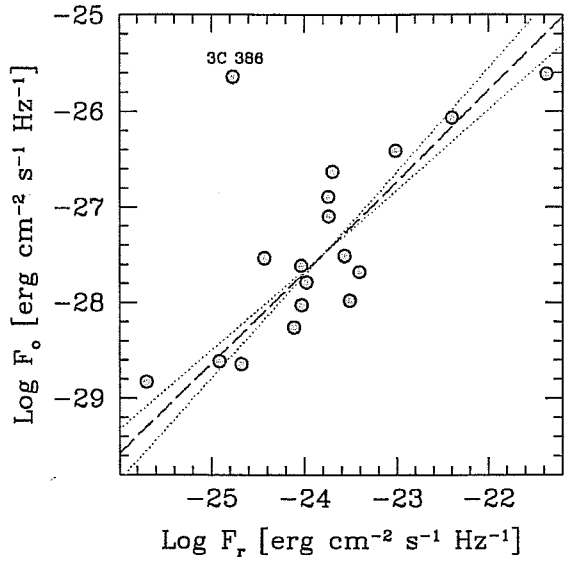

Figure 2.4: Optical CCC vs radio core fluxes at 5 GHz for the low power sub-sample (see text). Dotted lines are the fits to the data using each of the two fluxes as independent variables. Dashed lines represent the best fits. The peculiar object 3C 386 is excluded from the fitting procedure.

differ from the remaining of the sample. This suggestion is strengthened by the presence of a further peculiarity in the optical band of this object, i.e. the detection of a broad Hα line (Simpson et al. [133]), atypical of FR I radio galaxies. In any case, although the inclusion of 3C 386 in the analysis decreases the statistical significance of the correlation to $P = 2.6 \times 10^{-3}$, it would not affect our conclusions.

Turning now to the high luminosity sub-sample, five out of the nine points are upper limits, since no CCC is detected. This prevents us

Table 2.4: Linear fit parameters

r	0.88		
P	3.1×10^{-6}		
F_o vs F_r	$a = 0.84 \pm 0.12$	$b = -7.5 \pm 2.8$	rms = 0.42
F_r vs F_o	$a = 0.92 \pm 0.13$	$b = 1.7 \pm 3.5$	rms = 0.44

Statistical parameters for the correlation between radio core and optical CCC fluxes. The fitted linear relation is of the form $y = ax + b$.

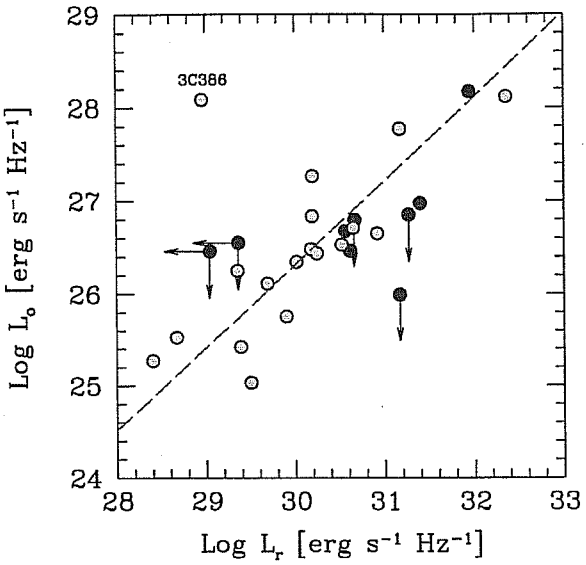

Figure 2.5: CCC luminosity versus radio (5 GHz) core luminosity for both the lower (open circles) and higher (filled circles) total radio luminosity. The dashed line is the best fit to the data of the low luminosity subsample, having excluded the peculiar object 3C 386.

from performing a meaningful statistical analysis. Note, however, that the four detected CCC fluxes lie along the same correlation defined by the lower luminosity objects (see Fig. 2.5).

We conclude that a striking linear correlation is present between the core radio and CCC fluxes (and luminosities): it extends over four orders of magnitude, has an extremely high statistical significance, a small dispersion and a slope consistent with unity. Since the radio core emission is certainly originated as synchrotron radiation the above tight link is a strong suggestion that also the optical CCC emission is produced by the same non–thermal process.

Independent support for this hypothesis comes from considering the spectral information relative to the CCCs, which can be compared with that of sources where synchrotron emission dominates in the optical as well as in the radio band (e.g. blazars, optical jets). First of all, we find that the radio–optical spectral indices of the CCC of our radio galaxies span the range $\alpha_{ro} \sim 0.6$–0.9, similar to those of optical jets (e.g. Sparks et al. [134]) and at the upper end of the spectral indeces

of blazars for which $\alpha_{ro} \sim 0.2$–0.9 (e.g. Fossati et al. [48]).

Furthermore, the CCC optical spectral indices (determined however for only five sources) are in the range $\alpha_o \sim 0.7 - 1.3$, also typical of the synchrotron-emitting sources mentioned above.

2.4.1 Alternative explanations

Even though synchrotron radiation provides a rather convincing interpretation of the nature of CCCs, in the following we consider and discuss other emission processes usually occurring in the nuclei of active galaxies. We should however note that none of these mechanisms seems to account naturally for the linear correlation between the radio and optical CCC luminosities and even less for its small dispersion, as radio cores are strongly affected by relativistic beaming while in all alternative scenarios the optical emission is essentially quasi–isotropic.

• Nuclear cusps or star clusters:
recent work has shown that stellar concentrations are often present in the nuclear regions of elliptical galaxies (e.g. Lauer et al. [88]). However, the CCCs optical spectral slopes are not compatible with the 'red' colors typical of old stellar populations.

• Nuclear starburst:
as CCCs are observed in the great majority of the galaxies of our sample, star formation should be maintained continuously for a timescale comparable to the lifetime of the radio sources, i.e. $\sim 10^{7-8}$ yr (Parma et al. [117]). Although some ad hoc mechanisms regulating the star formation rate might exist, this possibility appears implausible.

• Accretion discs:
the optical spectral information also contrasts with the emission expected at least in the simplest hypothesis of a Shakura-Sunyaev geometrically thin, optically thick disk, which generally predicts a harder spectral slope ($\alpha \lesssim -0.3$). A softer index is expected only at higher frequencies (UV–soft–X; e.g. Szuszkiewicz et al. [141]). No observational constraints are provided by more complex disc models (e.g. the

recently proposed case of low density radiatively inefficient accretion flows, ADAF, Rees et al. [123]; Narayan & Yi [110]; Chen et al. [29]) as they can reproduce widely different spectral slopes in the optical band.

• Emission line region:
as already pointed out, although line emission contributes from 5 to 40 per cent, continuum emission provides the bulk of the total CCC flux.

We conclude from this analysis that the most likely explanation for the origin of CCCs, except non–thermal synchrotron emission.

2.5 Discussion

2.5.1 Implications for unified models

For the first time, thanks to the high spatial resolution of HST, it has been possible to separate the contribution of the host galaxy from the genuine nuclear emission in FR I radio galaxies, which manifests itself as a Central Compact Core.

CCCs appear to be associated with non–thermal synchrotron emission. Three pieces of evidence also suggest that the CCC radiation is anisotropic due to relativistic beaming:

1. Capetti & Celotti ([23]) studied five radio galaxies in which HST images revealed the presence of extended nuclear discs, which appear to be useful indicators of the radio sources orientation. The FR I CCC luminosity shows a suggestive correlation with the orientation of the radio galaxies with respect to the line of sight;

2. Sparks et al. ([135]) argued that jets are detected in the optical band only when pointing towards the observer. This would explain why jets with optical counterparts are smaller (they are foreshortened), brighter and one-sided (they are relativistically beamed) with respect to typical radio jets. Five sources of our

sample (namely 3C 66B, 3C 78, 3C 264, 3C 274 and 3C 346) indeed show optical jets and these very same objects clearly stand out for being among the brightest CCC of their respective subsamples (see Fig. 2.6 where we report the CCC luminosity versus the total radio power). Sources with optical jets are also the only FR I galaxies detected in UV HST observations (Zirbel & Baum [165]);

3. as noted above, the radio core emission is certainly beamed and the corresponding orientation dependence is reflected in the large spread found when comparing the core to extended (quasi–isotropic) radio luminosities ($\sim$ 1 order of magnitude for both, Giovannini et al. [56], Zirbel & Baum 1995). Therefore if the optical emission were isotropic the F_o vs F_r correlation would show at least a similarly large scatter.

The beamed synchrotron scenario which emerges for the origin of the CCC is therefore strong evidence in favour of the idea that FR I are the misoriented counterparts of BL Lacs. The large spread (3 orders of magnitude) in CCC luminosity among objects of similar extended properties (see Fig. 2.6) can be ascribed to different orientations. An extensive and quantitative analysis of this issue and of the relationship between FR I and BL Lacs in the light of these results will be presented in Chapter 4.

2.5.2 Are there obscuring tori in FR I?

The observation of optical synchrotron emission has important consequences on the role/geometry of absorption structures in the nuclear regions of such objects. A very important result of our analysis is in fact the high fraction of galaxies in which the central source has been detected.

Limiting ourselves, for the moment, to the low luminosity subsample, we found a CCC in 85 % of the objects. The sources in which we

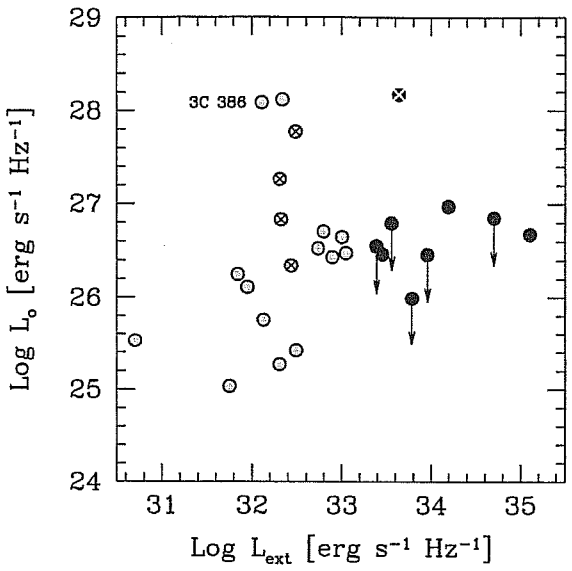

Figure 2.6: Optical CCC luminosity versus total radio luminosity. Different symbols mark sources with total radio luminosity below (open circles) and above (filled circles) $L_{178} = 2 \times 10^{26}$ [W Hz^{-1}]. Crossed symbols are for galaxies with known optical jets.

do not detect it (namely 3C 75, 3C 293 and 3C 305) are three out of the four cases in which the center of the galaxy is affected by obscuration from a large scale dust structure (the fourth galaxy is 3C 272.1 whose CCC, although reddened, shines through the dust lane). In order to estimate the optical depth of obscuring material in these sources, we derived their expected optical flux from the CCC vs radio core flux correlation. We found that an extinction of only a few magnitudes ($A_V \lesssim 6$ mag, corresponding to a column density of $N_H \lesssim 1.2\ 10^{22}$ cm^{-2}) is sufficient to hide the CCC optical emission. Therefore, even in these three cases the presence of an optically (Thomson) thick structure is not required (although it cannot be ruled out) and the CCC emission might be simply obscured by the foreground dust. Infrared observations can address this issue.

The behaviour of the 11 sources with higher total radio luminosity is probably different and certainly more complex:
– four of them have CCC fluxes and luminosities consistent with the correlations found for lower power FR I, and would simply lie on the

high luminosity part of the radio–optical correlation (see Fig. 2.5)
– two of them show complex (possibly absorbed) nuclei;
– in the last five objects no unresolved component is detected (upper limits in Figs. 2.3, 2.6, 2.5; see also Sect. 2.3). The upper limits derived could be in general agreement with the F_o vs F_r CCC correlation, except possibly in the case of 3C 89 (the lowest point in Fig. 2.3).

The smaller number of CCC found could be simply due to the fact that this subsample is on average at higher redshift. Clearly, we cannot exclude the alternative possibility, i.e. that these sources are indeed obscured, which might indicate that the degree of obscuration increases with the source power (a crucial test here is the inclusion in the sample of FR II radio galaxies, see Chapter 3).

The detection of CCCs indicates that we have a direct view of the innermost nuclear regions of FR I. Limits on the extension of CCC are implied by the variability of the nucleus of M 87 on time scales of two months (Tsvetanov et al. [149]). Furthermore, since the optical emission in relativistic jets is likely to be produced co-spatially or even closer to the black hole with respect to the radio emission, we can infer a further constraint on the CCC extension from VLBI observations. These in fact show that most of the radio emission comes from a source unresolved at mas resolution which can be as small as 0.01 pc, i.e. only $\sim$ 100 Schwarzschild radii for a $\sim 10^9$ $M_\odot$ black hole (e.g. Junor & Biretta [76]).

It therefore appears that a "standard", pc scale, geometrically thick torus is not present in low luminosity radio galaxies. Any absorbing material must be distributed in a geometrically thin structure (our CCC detection rate implies a thickness over size ratio $\lesssim 0.15$) or thick tori are present only in a minority of FR I. This result is particularly intriguing since dusty nuclear discs on kpc scales have been discovered in several FR I and they indeed are geometrically thin (Jaffe et al. [75]). In this sense, the lack of broad emission lines in FR I cannot be accounted for by obscuration.

2.5.3 Limits on thermal disc emission and AGN efficiency

Except for blazars, whose overall spectral energy distributions are almost always dominated by the non–thermal emission from a relativistic jet, the nuclear emission of AGNs from the optical to the soft-X band is generally interpreted as thermal emission from accreting material. Conversely, we find that in FR I a non–thermal synchrotron component dominates the emission in all sources. In fact, a sufficiently bright isotropic optical component would produce a flattening in the radio/optical CCC correlation, due to the presence of an additional source of optical flux (with no radio counterpart), which we do not observe (see Figs. 2.4 and 2.5). This is surprising if one considers that, in a complete sample, a substantial fraction of the objects are observed at large angles from the line of sight and thus the emission from their jets is expected to be strongly de-beamed, favouring the detection of any isotropic (disc) emission.

The CCC fluxes thus set upper limits to the disc emission, which in turn imply extremely low radiative efficiency of the accretion process. Note, in fact, that the observed CCC emission corresponds to $\lesssim 10^{-7}$–10^{-5} of the Eddington luminosity of a $10^9 M_\odot$ black hole, which appears to be typical for these radio galaxies. While these values argue against the presence of a radiatively efficient accretion phase, they are still compatible with the expected radiative cooling rate of low density and high temperature accreting plasma in which the electron–ion coupling is ineffective and most of the thermal energy is thus advected inwards and not radiated (Rees et al. [123]; also ADAF, e.g. Narayan & Yi [110], Chen et al. [29] and ADIOS, Blandford & Begelman [14]). This latter possibility has been indeed proposed to account for the paucity of emission in radio galaxies harbouring supermassive black holes (Fabian & Rees 1995). The HST observations of CCC set consistent but independent constraints relative to the optical emission in these systems.

This low efficiency in producing thermal emission might also account for the lack of broad lines in FR I spectra, which could be at-

tributed just to the lack of those ionizing photons which, in the other classes of active nuclei, illuminate the dense clouds forming the Broad Line Region. Indeed Zirbel et al. ([166]) have suggested the possibility that FR I sources produce far less UV radiation than FR II on the basis of the comparison between emission line and radio luminosities of radio galaxies. Intriguingly, the only object in which a broad line has been detected is 3C 386, whose CCC presents a much larger optical luminosity with respect to the sources with similar radio core power, possibly indicative of a thermal contribution.

2.6 Conclusions

HST images of a complete sample of 33 FR I radio galaxies belonging to the 3CR catalogue have revealed that an unresolved nuclear source (Central Compact Core, CCC) is present in the great majority of these objects.

- The CCC emission is found to be strongly connected with the radio core emission and anisotropic. We propose that the CCC emission can be identified with optical synchrotron radiation produced in the inner regions of a relativistic jet. Support for this possibility comes also from spectral information. These results are qualitatively consistent with the unifying model in which FR I radio galaxies are misoriented BL Lac objects.

- The identification of the CCC radiation with misoriented BL Lac emission opens the possibility of studying this class of AGNs from a different line of sight. This can be particularly useful in understanding the jet structure and the level of the activity occurring near the central object whose emission in blazars is swamped by the highly beamed component. Further information on the nature of CCC can be inferred by simultaneous studies of radio cores and CCC optical variability which could establish whether their

emission is indeed produced in the same region.

- The detection of CCC indicates that we have a direct view of the innermost regions of the AGN ($\lesssim 100 R_S$). If we restrict the analysis to objects with a total radio power of $< 2 \times 10^{26}$ W Hz^{-1}, a CCC is found in all galaxies except three, where absorption from extended dust structures clearly plays a role. This casts serious doubts on the presence of obscuring thick tori in FR I as a whole.

- Given the dominance of non-thermal emission, the CCC luminosity represents a firm upper limit to any thermal component, which translates into an optical luminosity of only $\lesssim 10^{-5} - 10^{-7}$ times the Eddington one (for a $10^9 M_\odot$ black hole). This limit on the radiative output of accreting matter is independent but consistent with those inferred in X–rays for large elliptical galaxies, thus suggesting that accretion might take place in a low efficiency radiative regime (Fabian & Rees 1995).

The picture which emerges is that the innermost structure of FR I radio galaxies differs in many crucial aspects from that of the other classes of AGN; they lack the substantial BLR, tori and thermal disc emission, which are usually associated with active nuclei.

Similar studies of higher luminosity radio galaxies are clearly crucial to determine if either a continuity between low an high luminosity sources exists or, alternatively, they represent substantially different manifestations of the accretion process onto a supermassive black hole. We will investigate this issue in Chapter 3.

Chapter 3

The HST view of the FR I/FR II dicothomy

The analysis of the previous chapter lead to the conclusion that low luminosity FR I radiogalaxies have essentially unobscured nuclei, lack radiatively efficient accretion discs and broad emission line region. As already pointed out, while such components are not strictly required for FR I in the frame of the unification scheme with BL Lacs, they must be present in the FR II class. In order to explore how the differences in radio morphology are related to the optical nuclear properties, in this chapter we study the HST images of a sample of low redshift FR II radio galaxies, and compare them to the FR I class. In particular, one of the most important questions is whether the FR I/FR II dichotomy is generated by two different manifestations of the same astrophysical phenomenon, and the transition between the two classes is indeed continuous, or instead it reflects fundamental differences in the innermost structure of the central engine.

The selection of the sample is presented and discussed in Sect. 3.1, while in Sect. 3.2 we describe the HST observations. In Sect. 3.3 we focus on the detection and photometry of the optical cores. Finally, in Sect. 3.4 we discuss our findings.

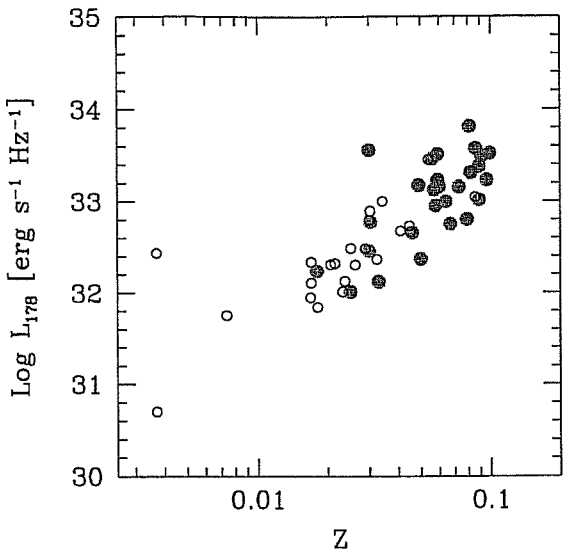

Figure 3.1: Total radio luminosity (at 178 MHz) vs redshift diagram for the FR I (empty circles) and FR II (filled circles) samples.

3.1 The sample

The sample considered here comprises all radio galaxies belonging to the 3CR catalogue (Spinrad [137]) with redshift $z < 0.1$, morphologically classified as FR II. We directly checked their classification for erroneous or doubtful identifications by searching the literature for the most recent radio maps. The final list (see Table 3.1) constitutes a complete, flux and redshift limited sample of 26 FR II radio galaxies.

We searched for optical spectral classification and/or optical spectra, in order to differentiate our sources on the basis of the presence of broad or narrow emission lines. For only one source (namely 3C 136.1) we could not find spectral information in the literature. All spectral types usually associated with FR II galaxies are represented in the sample: five objects are BLRG, fifteen are classified as NLRG, while four show only weak lines in their optical spectrum (WLRG). The remaining source, namely 3C 371, has been classified as a BL Lac object. In Table 3.1 redshifts and radio data are reported, as taken from the

Table 3.1: Summary of FR II radio and optical data.

Name	Redshift z	Spectral class.	Log L_{178} erg s^{-1} Hz^{-1}	Log L_r (5GHz) erg s^{-1} Hz^{-1}	F_o (7000 Å) erg s^{-1} cm^{-2} Hz^{-1}	Log L_o (7000 Å) erg s^{-1} Hz^{-1}
3C15	0.073	NLRG	33.16	31.54	<-28.12	<26.85
3C33	0.059	NLRG	33.51	30.27	no HST observations	
3C35	0.067	NLRG	32.75	30.27	<-28.47	<26.42
3C40	0.018	WLRG	32.24	30.60	–	–
3C88	0.030	WLRG	32.46	30.50	-27.64	26.57
3C98	0.030	NLRG	32.78	29.25	<-28.58	<25.64
3C105	0.089	NLRG	33.38	30.36	no HST observations	
3C111	0.049	BLRG	33.18	31.69	-26.51	28.12
3C136.1	0.064	-	33.00	–	–	–
3C192	0.060	NLRG	33.16	29.73	<-27.86	<26.94
3C198	0.082	NLRG	33.31	–	-27.10	27.96
3C227	0.086	BLRG	33.57	30.48	-26.27	28.83
3C236	0.099	WLRG	33.52	31.51	<-28.26	<26.95
3C285	0.079	NLRG	32.80	29.93	-29.44	25.58
3C318.1	0.046	NLRG	32.66	–	-28.94	25.63
3C321	0.096	NLRG	33.23	30.78	–	–
3C326	0.089	NLRG	33.02	30.34	<-28.11	<27.02
3C353	0.030	NLRG	33.56	30.54	<-28.71	<25.51
3C371	0.050	BL Lac	32.37	31.89	-25.56	29.09
3C382*	0.058	BLRG	32.95	31.13	-25.11*	29.66*
3C388	0.091	WLRG	33.49	31.04	-27.96	27.18
3C390.3*	0.056	BLRG	33.46	31.38	-25.91*	28.83*
3C402	0.025	NLRG	32.01	29.73	-27.49	26.57
3C403	0.059	NLRG	33.23	29.87	-28.19	26.60
3C445*	0.057	BLRG	33.13	31.34	-25.56*	29.20*
3C452	0.081	NLRG	33.81	31.24	<-28.22	<26.83

L_{178} and L_r are the total (at 178 MHz) and core radio luminosities, taken from the literature. F_o is the flux of the optical core. Total radio luminosities are calculated from Kühr et al. ([82]) or Gower et al. ([61]). Radio core luminosities are taken from Zirbel & Baum ([164]). "<" indicate upper limits, i.e. not detected optical cores, "*" indicate objects in which the optical core saturates, "–" in the F_o and L_o colums mark objects with complex nuclear morphologies for which we do not estimate the core flux and "–" in the L_r column indicate unavailable radio core data in the literature.

literature, together with the optical spectral classifications.

In Fig. 3.1 we show the redshift vs total radio luminosity diagram for the sample of FR II galaxies, together with the sample of FR I discussed in Chapter 2, but limited to sources with $z < 0.1$ for coherence with the FR II sample. FR II have a median redshift $z = 0.06$, and total radio luminosities at 178 MHz are between 10^{32} and 10^{34} erg s^{-1} Hz^{-1}. Notice that whereas the two samples are selected at the same limits of redshift and flux, FR II are, on average, more luminous and distant than FR I.

3.2 HST observations

HST observations of the FR II sources are available in the public archive (up to April 1999) for 25 out of the 26 sources (only 3C 33 and 3C 105 have not been observed). The HST images were taken using the Wide Field and Planetary Camera 2 (WFPC2). The whole sample was observed using the F702W filter as part of the HST snapshot survey of 3C radio galaxies (Martel et al. [98], De Koff et al. [34]). For 3C 192 we used a F555W image, as this source was not observed with the F702W filter. Exposure times are in the range 140–300 s.

3.3 Optical cores in FR II

We have searched for unresolved nuclear components using the method outlined in Sect. 2.3.1. As in the case of FR I sources, the FWHM fall into two very distinct regimes: in 11 cases we measured a FWHM = 0.05″ – 0.08″, i.e. indicative of the presence of an unresolved source at the HST resolution, while in 8 cases we found widths larger than 0.2″. We therefore believe that no ambiguity exists on whether or not a central unresolved source is present.

In three sources (3C 382, 3C 390.3 and 3C 445) the central regions are saturated. While, on the one hand, this prevents us from deriving

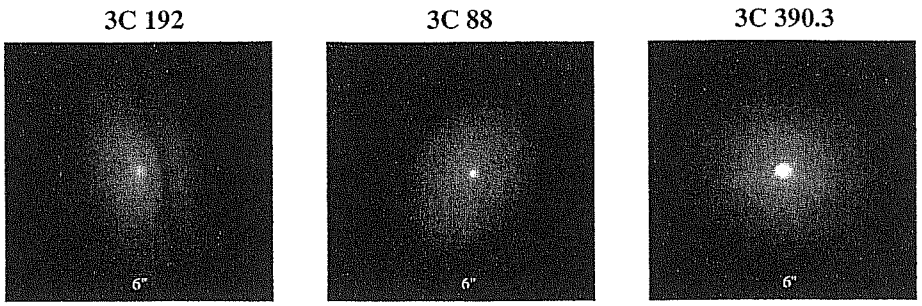

Figure 3.2: HST/WFPC2 broad band images of three FR II: 3C 192 is a NLRG showing a diffuse nucleus; 3C 388 is a NLRG with an optical core; 3C 390.3 is a BLRG.

their brightness profile, on the other is by itself a clear indication of a point-like source. In fact diffuse emission would produce saturation with our instrument configuration and exposure times only for surface brightness < 13 mag arcsec^{-2} in the R band, much larger than typically observed in the central regions of radio-galaxies at this redshift. Furthermore in all these sources we observe diffraction rings and spikes, the characteristic hallmarks of the HST Point Spread Function.

We performed aperture photometry of these components. using the same method described in chapter 2. For the saturated cores we evaluated their fluxes by comparing the PSF wings with those of several bright stars seen in archival HST images taken with the same filter. This method leads to a somewhat larger uncertainties, 25 % as estimated from the scatter of measures obtained with different reference stars, which arise from the time dependent structure of the HST PSF. In Table 3.1 we report fluxes and luminosities of the optical cores.

All of the images were taken using broad band filters, which include emission lines. In particular, the F702W transmission curve covers the wavelength range $5900 - 8200$ Å and thus within our redshift range includes the Hα and [N II] emission lines. Unfortunately, no HST narrow band images are available for the NLRG and WLRG, however, we expect the line contamination to be small, due to the wide spectral region covered by the filters used ($\sim$ 2000 Å) with respect to typical

lines equivalent width. We correct the broad band fluxes only in the case of BLRG, where the emission of broad lines is probably co-spatial to the optical core, using ground-based data taken from the literature (Zirbel & Baum [164]). The resulting emission line contribution is typically $25 - 30\%$ of the total flux measured in the F702W filter.

In 8 cases the nuclear regions only show diffuse emission: for such galaxies we estimate upper limits to a possible central component evaluating the light excess of the central 3x3 pixels with respect to the surrounding galaxy background. The remaining 3 sources show complex morphologies, e.g. with dust lanes obscuring the central regions, and no photometry was performed.

3.3.1 Results

FR II cores span a wide range of optical luminosities L_o (from $10^{25.5}$ up to 10^{30} erg s^{-1} Hz^{-1}). In Fig. 3.3 we report the optical core versus radio (5 GHz) core luminosity for the FR II sample, superimposed to the data (as from chapter 2) for FR I galaxies limiting ourselves, for consistency, to those with redshift $z < 0.1$. FR II show a complex behavior, which however seems to be related to their optical spectral classification.

Let us firstly consider the blazar, 3C 371. As one might expect, since its emission is dominated by beamed synchrotron radiation, it is among the brightest source both in the radio and in the optical band (see Fig. 3.3).

The second group of sources is represented by the BLRG (3C 111, 3C 227, 3C 382, 3C 390.3 and 3C 445): all of them have very luminous optical cores ($L_o > 10^{28}$ erg s^{-1} Hz^{-1}) being – together with 3C 371 – the most powerful objects of the sample and clearly separating from the other FR II in the diagram. Notice that they have an optical excess (or radio deficiency) of up to 2 orders of magnitude with respect to the radio-optical core luminosity correlation found for FR I.

In 5 WLRG and NLRG, namely 3C 88, 3C 285, 3C 388, 3C 402 and

3C 403, we detected optical cores which share the same region in the luminosity plane as FR I sources with luminosities between $L_o = 10^{25.5}$ up to more than $10^{27.5}$ erg s^{-1} Hz^{-1}.

The 8 upper limits, all associated with WLRG or NLRG, are also plotted. Four objects (3C 35, 3C 98, 3C 192 and 3C 326) lie close to the correlation defined by FR I. Conversely, 3C 15, 3C 353, 3C 452 and 3C 236 present an optical luminosity deficit of one to two orders of magnitude given their radio core emission with respect to FR I.

No radio core data have been found in the literature for 3C 136.1, 3C 198 and 3C 318.1.

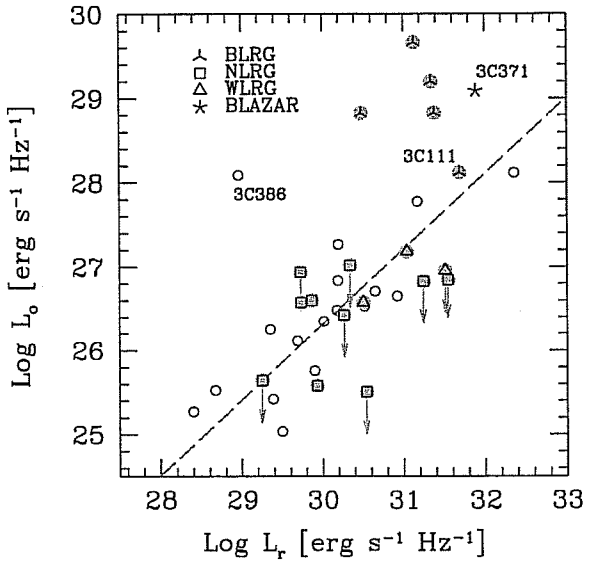

Figure 3.3: Optical nuclear luminosity versus radio (5 GHz) core luminosity for both the FR I (open circles) and FR II (filled circles) samples. Different symbols are used to identify different spectral classifications. The dashed line is the correlation found in the case of FR I galaxies (see chapter 2).

3.4 The nature of optical cores in FR II radio galaxies

In the 24 nearby FR II radio galaxies (out of a complete sample of 26) studied in this chapter, 13 show an unresolved optical core, in 8

cases we can only set an upper limit to their luminosity, while 3 sources present a complex nuclear morphology.

The optical core detection rate implies that the covering fraction of any obscuring material is less than ~ 0.54, or equivalently, the torus has an opening angle of $\sim 63°$. This can be even larger if at least some of the upper limits are actually just below the detection threshold. Notice that our determination of this critical angle is inconsistent with the division between higher redshift ($0.5 < z < 1$) 3CR quasars and radio galaxies, which has been found to be $\theta \sim 45°$ (Barthel [6]). This might be a problem, however the low redshift selection of our sources does not allow to derive any firm conclusion.

The location in the optical-radio core luminosity plane is clearly connected to the optical spectral classification. Conversely, cores in FR I radio galaxies show a linear correlation between their radio and optical luminosity, which strongly argues for a common non-thermal origin. The presence of such correlation provides a useful benchmark to investigate the origin of optical cores in FR II.

In the following we consider each FR II group separately.

3.4.1 Broad Line Radio Galaxies

Let us first focus on BLRG. These sources present, overall, a strong optical excess (or radio deficit) of up to two orders of magnitude, with respect to the correlation defined by the FR I cores (see Fig. 3.3). We are confident that this is not a "radio deficit", as in the plane defined by L_r versus total radio power BLRG do not show particular radio-core deficit. Note that in the sample of nearby FR I, the only source lying well above the radio-optical correlation is 3C 386, which also shows a broad Hα line.

BLRG are objects in which the innermost nuclear regions are thought to be unobscured along our line of sight (Barthel [6]). We therefore expect the presence of a thermal/disc component: indeed this might dominate over any synchrotron jet radiation and thus be responsible for

the observed emission. The idea that we see directly an accretion disc is supported by several observations: in the case of 3C 390.3, a bump in the spectral energy distribution has been interpreted as radiation emitted by a disc component with intermediate inclination (Edelson & Malkan [37]). Furthermore, the broad and double peaked Hβ line observed in this source as well as in other BLRG (see e.g. Eracleous & Halpern [40]), can be accounted for within a relativistic accretion disc model (Perez et al. [120]).

The location of 3C 111 is puzzling, as it lies along the correlation. However, several pieces of evidence point to the idea that beamed radiation from the relativistic jet significantly contributes in this source: it has the largest core dominance among the BLRG of our sample; superluminal motions with apparent speed $v \sim 3.4c$ have been revealed in the inner jet (Vermeulen & Cohen [155]), implying that the angle between the line of sight and the jet axis is smaller than $\sim 30°$; the radio core is strongly variable and polarized (Leahy et al. [89]). Furthermore a broad Kα iron line is detected in the X–ray band, but with a relatively small equivalent width which can be explained if the continuum emission is diluted by a beamed component (Reynolds et al. [125]). However, its total radio extent of ~ 250 kpc argues against a viewing angle typical of blazars. Thus 3C 111 appears to be a transition source between radio-galaxies and blazars, seen at an angle sufficiently small that the jet beaming already affects its nuclear properties.

3.4.2 WLRG and NLRG with optical cores

Let us now concentrate on the NLRG and WLRG in which we detected optical cores. These objects (2 WLRG and 3 NLRG), all with FR II radio morphology, have cores with radio and optical emission properties that are *completely consistent with those found in FR I.* This suggests that in these sources the nuclear emission is similarly dominated by synchrotron radiation from the inner jet. For this reason, in the following we will refer to such sources as "FR I–like".

In the case of FR I, based on the high fraction of detected nuclei, we suggested that any obscuring material must be geometrically thin and thus the absence of broad lines and the relative weakness of any thermal (disc) component with respect to the synchrotron emission cannot be ascribed to extinction.

For FR II with FR I–like nuclei – of which we do not have enough statistics – there is an alternative possibility, namely that the optical core (jet) emission is produced outside the obscuring torus (and thus outside the BLR). In this sense they would represent transition objects seen at an intermediate angle between the completely obscured and unobscured ones. However, VLBI observations show that radio cores are unresolved on scale of $\sim$ 0.1 pc in nearby radio galaxies and this suggests that their optical counter–parts have a similar extent, as already discussed in chapter 2. Furthermore, a symmetric jet-counter jet structure has been observed in several radio sources, implying that they lie essentially in the plane of the sky (Giovannini et al. [55]). If the core emission is indeed produced outside the torus, at a distance of, say, $\sim$1 pc from the central black hole, a clear separation between the two sides of the jet (and no stationary core) should be observed in these highly misoriented objects (although, at present, symmetric jets have been found only in FR I). This ad hoc geometrical model does not seem to be viable, but a conclusive test requires spectropolarimetry looking for polarized scattered broad lines. A further indication could be obtained from the comparison of the nuclear infrared (reprocessed?) luminosity of FR Is and FR IIs with FR I–like nuclei of similar optical luminosity.

We conclude that these FR II are intrinsically narrow-lined objects which are in every aspect, except their extended radio-morphology, similar to FR I. Note that the presence of an FR I-like nucleus in a FR II does not seem to be connected with the total (radio) luminosity or redshift of the galaxy. In fact, the total power of such sources spans the range $L_{178} = 10^{32}-10^{33.5}$ erg s^{-1} Hz^{-1} and the redshifts are between

$z = 0.025 - 0.091$, completely overlapping with the entire sample and not limited, as one might expect, to the low luminosity end.

Conversely, it appears that a possible relationship exists between the occurrence of FR I-like nuclei in FR II and the environment, as all these 5 galaxies reside in clusters. This result can be particularly important, as it is known that FR I and FR II inhabit different environments, with FR II generally avoiding rich groups, especially at low redshifts (Zirbel [162]), while FR I are usually located in rich clusters. However, before any firm conclusion can be drawn about this issue, a larger sample of objects has to be considered.

3.4.3 WLRG and NLRG without optical cores

In 8 galaxies, all WLRG or NLRG, we do not detect the presence of an unresolved nuclear component. Four sources are located above or very close to the FR I correlation. They are consistent with being objects in which an optical counter–part to the radio core is present, but it is too faint to be seen against the bright background of the host galaxy.

The remaining 4 objects (3 NLRG and 1 WLRG) are certainly more interesting, since they lie 1 - 2 orders of magnitude below the correlation. Therefore they lack not only of a BLR, but also of the expected optical counterpart of the radio core. However, note that these sources have radio core luminosities which cover the same range of BLRG. According to the prescriptions of the unification schemes, they can well be the obscured counter–parts of BLRG. Noticeably, excluding the blazar 3C 371, BLRG and these obscured sources clearly distinguish themselves for having the brightest radio cores among FR II.

Clearly, as noted above, this analysis is limited to low-redshift sources, which share the same range of total power as FR I. In particular, it is very important to extend the sample towards higher luminosities, in order to establish if the presence of a third class of FR II with synchrotron-dominated optical nuclei is confirmed, and to assess any dependence of the obscuring structure on luminosity. We are currently

studying a sample of 3CR FR II sources with $z < 0.3$, and in the next section we show some very preliminary results.

3.5 First results on $z < 0.3$ sources

In order to establish if the above results are confirmed for higher redshift and higher luminosity sources, we have selected a sample composed by all 60 FR II radio galaxies from the 3CR catalog, with $z < 0.3$. With respect to their spectral classification, they are divided as follows: 4 QSO, 10 WQ, 25 HEG, 16 LEG. For 5 sources we did not found any spectral classification in the literature.

We have found that 33 objects have an optical core. In Fig. 3.4 we show the results of the photometry of optical cores, in the plane defined by L_o vs L_r. Although their behavior appears to be complex, what is observed at low redshifts is qualitatively confirmed. All QSO and BLRG have an optical core, but analogously to what we have found in the low redshift sample, a significant number (18) of NLRG and WLRG have an optical core which lies on the correlation defined by FR I. The third class of unobscured, synchrotron-dominated FR II nuclei appears to persist, although a small number of "transition" objects fill in the the gap between broad line and narrow and weak-lined sources (which occurs at ($L_o \sim 10^{28}$ erg s^{-1} Hz^{-1}).

Notice that these results are consistent with what has been found by Willott et al. [157]: they calculated the quasar fraction in the 7C, 6C and 3CRR samples, finding that it decreases at low luminosities. Indeed they propose, as a possible explanation for this, the existence of a population of FR II which lack a well-fed quasar nucleus and thick obscuring torus.

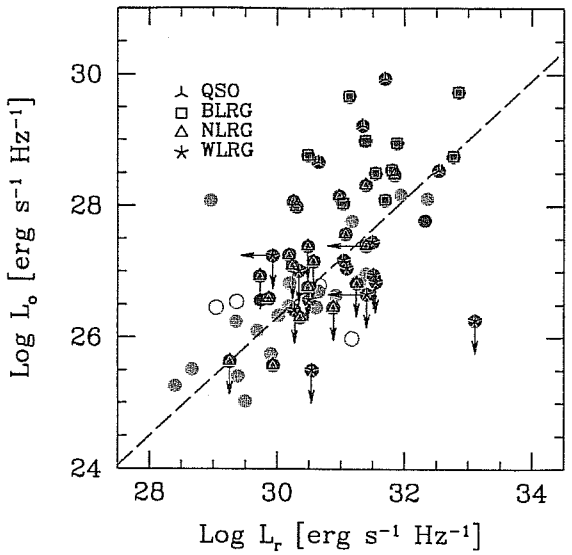

Figure 3.4: Optical nuclear luminosity versus radio (5 GHz) core luminosity for the FR I (yellow circles) and FR II up to $z = 0.1$ (blue circles) and for $0.1 < z < 0.3$ (red circles). Different symbols are used to identify different spectral classifications. Yellow empty circles are the FR I upper limits (optical and/or radio), and the dashed line is the FR I radio-optical correlation (see chapter 2).

3.6 Conclusions

In order to explore how the differences in radio morphology are related to the optical nuclear properties, we analyzed HST images of 24 extended radio-galaxies morphologically classified as FR II, belonging to the 3C catalog and with $z < 0.1$. We detected optical cores in 13 sources, which implies a dividing angle of $\sim 63°$, between broad and narrow line objects, inconsistent with the division between higher redshift 3CR quasars and radio galaxies.

Our results suggest that the radio morphology is not univocally connected with the optical properties of the innermost structure of radio galaxies. In fact, at least at low redshifts, there is not a single homogeneous population of FR II: unlike FR I, they show a complex behavior, which is however clearly related to their optical spectral classification.

In BLRG optical nuclei are likely to be dominated by thermal (disc) emission. As discussed above, line emission contamination cannot account for this excess. In agreement with the current unification scheme

of radio loud AGNs, we also identify their possible obscured counter–parts. It seems that broad lines and obscuring tori are closely linked and both might be present only in association with radiatively efficient accretion.

We also find five FR II sources, spectrally identified as narrow lined objects, which harbor nuclei essentially indistinguishable from those seen in FR I. By analogy with FR I, we argue that their optical nuclear emission is produced primarily by synchrotron radiation, they are not obscured to our line of sight and therefore intrinsically lack a BLR.

Clearly, a classification based on the optical nuclear properties, as seen in these HST images, is more likely to reflect true similarities (or differences) on the nature of the central engine (such as, e.g., the rate of radiative dissipation in the accretion disc) than the traditional dichotomy of radio morphology.

From our data and within the limits of the available statistics, we find no evidence of a continuous transition between the two classes (FR I and FR II), as they are well separated in the L_r vs L_o plane. At this stage we only point out that sources with cores below $L_o < 10^{27.5}$ erg s^{-1} Hz^{-1} (or equivalently $L_r < 10^{31}$ erg s^{-1} Hz^{-1}) have FR I like nuclei, while BLRG and "obscured" FR II start above this threshold.

It is of particular interest that a significant fraction of FR II (at least 20%, but can be as large as 40% depending on the nature of the sources without detected optical nuclei) have FR I–like nuclei. The fact that all of these are located in clusters, an environment typical of FR I, might represent an important hint on the origin of the different flavours of radio galaxies, worth exploring through the study of a larger sample of objects.

These results have also interesting bearings from the point of view of the unified models. In fact, this picture argues against the idea that all FR II radio galaxies constitute the parent population of radio-loud quasars. We propose instead that galaxies with FR II morphology and an FR I-like core are possibly mis-aligned counter–parts of BL Lac

objects. This can account for the observation that some radio-selected-type BL Lacs show radio morphologies more consistent with FR II than with FR I (e.g. Kollgaard et al. [80]).

To conclude, we note that all of the galaxies included in our sample are low redshift objects with total radio powers not exceeding $L_{178} \sim 10^{27}$ erg s^{-1} Hz^{-1}: thus a crucial observational issue is to understand whether these results hold to higher power/redshift samples or they are limited to low luminosities FR II. A preliminary analysis of a higher redshift sample of sources (up to $z < 0.3$) seem to confirm the above findings.

Chapter 4

Does the unification of BL Lac and FR I radio galaxies require jet velocity structures?

In the previous chapters we have reported the discovery of the optical cores of radio galaxies. In the case of FR I, we have shown that there is strong evidence for these components to be produced in the inner regions of the relativistic jet, therefore the detection of optical nuclei offer a new possibility of directly verifying the unification scheme. Our aim is now to compare their properties with BL Lacs, their putative aligned (beamed) counterparts, in order to infer information on the amount of relativistc beaming which affect the radiation emitted by these objects.

This chapter is structured as follows. The (complete) samples of BL Lacs and radio galaxies are presented in Sect. 4.1. In Sect. 4.2 we compare separately the core radio and optical emission of beamed and unbeamed objects with similar extended radio power. From this we infer the Lorentz factors requested by the unification scheme within

the simplest scenario in which the radiation is emitted by a single uniform region of the relativistic jet. In Sect. 4.3 the radio and optical data are considered together and, starting from the observed SED of BL Lacs, we derive the expected properties of the nuclear emission of FR I, by taking into account the spectral dependence of the relativistic transformations. As the single–region picture does not account for the observed properties, in Sect. 4.4 we explore a (simple) alternative scenario and test it also against the X-ray information.

4.1 The samples

4.1.1 FR I radio galaxies

Our complete sample of FR I radio galaxies belonging to the 3CR catalogue has been described in chapter 2. The total radio luminosities at 1.4 GHz are between $10^{30.2}$ and $10^{34.2}$ erg s^{-1} Hz^{-1}. We exclude from the original sample the peculiar object 3C 386, as discussed in Chapter 2. The optical and radio data are those reported in Chapter 2, while the X-ray ones are taken from Hardcastle & Worral ([62]). The optical data are extrapolated to the V band using a spectral index $\alpha_o = 1$.

4.1.2 Radio and X-ray selected BL Lacs samples

We consider both the complete sample of 34 radio selected BL Lacs derived from the 1Jy catalog (Stickel et al. [138], Kühr et al. [82]), and the BL Lac sample selected from the *Einstein* Slew survey (Elvis et al. [39], Perlman et al. [119]), which comprises 48 objects, and it is nearly complete. The extended radio power (at 1.4 GHz) $L_{\rm ext}$ [erg s^{-1} Hz^{-1}] spans the ranges $10^{30.1} - 10^{33.8}$ (1Jy BL Lacs, Kollgaard et al. [79]) and $10^{29.1} - 10^{33.4}$ (Slew survey BL Lacs, Kollgaard et al. [79], Perlman et al. [119]); the redshifts are between 0.049 and 1.048 (median $z = 0.501$) and between 0.031 and 0.513 (median $z = 0.188$) for the two samples, respectively (the redshifts of the Slew BL Lacs are

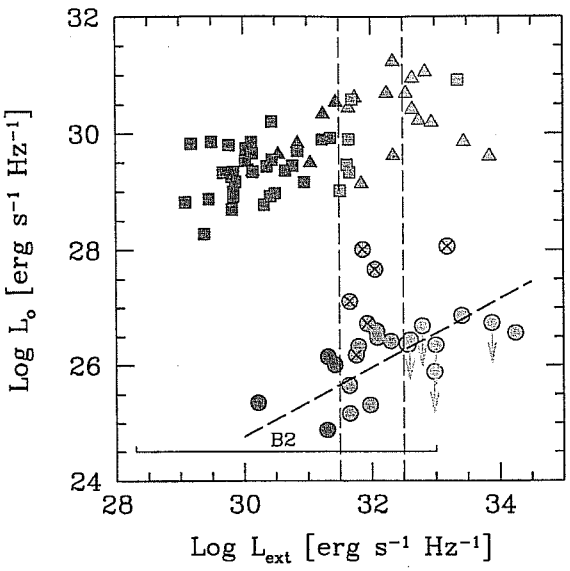

Figure 4.1: Optical core luminosity (V band) versus radio extended luminosity at 1.4 GHz for FR I (circles), HBLs (squares) and LBLs (triangles). The grey scale refers to the three bins of extended radio power. The dashed line represents the linear fit to the FR I sample, having excluded the most aligned sources, here marked with crosses (see text). The range of extended power covered by the B2 sample of radio galaxies is also indicated.

taken from the data collected by Fossati et al. [48]).

Instead of classifying BL Lacs according to their selection spectral band, in the following we adopt the definitions of high and low energy peaked BL Lacs (HBL and LBL respectively), which are based on the position of the (synchrotron) emission peak in the spectrum and therefore more indicative of the physical characteristics of the objects (Giommi & Padovani [53], Fossati et al. [48]). Of the 34 objects belonging to the 1 Jy sample, 32 are classified as LBL and 2 as HBL, while of the 48 X-ray selected BL Lacs, 40 are HBL and 8 are LBL.

The spectral data for both samples of BL Lacs are taken from Fossati et al. [48].

4.2 Core versus extended luminosity

According to the unification models the beamed and unbeamed populations must cover the same range of extended luminosity, as this is considered to be isotropic. On the contrary, emission from the

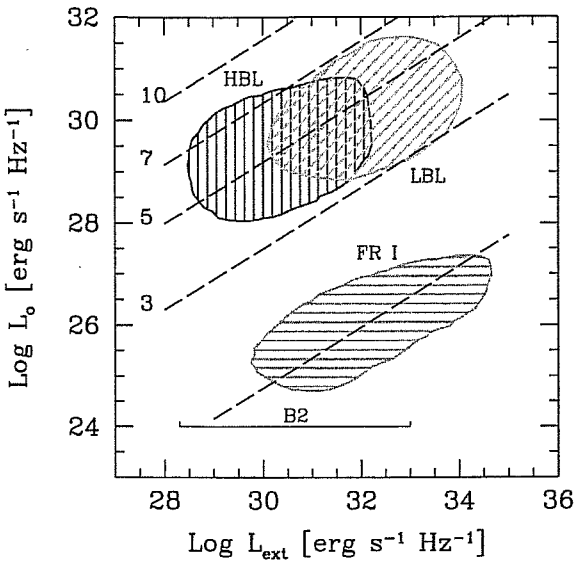

Figure 4.2: The regions occupied by the three samples in the optical luminosity versus extended radio luminosity plane, as for Fig. 4.1. The dashed lines indicate the correlation found between these two quantities when shifted by beaming effects for the values of the bulk Lorentz factor marked on the left.

core is affected by beaming: radio galaxies should have a fainter central component, whose intensity would depend on the Doppler factor $\delta = [\Gamma(1 - \beta\cos\theta)]^{-1}$, where $\Gamma = (1-\beta^2)^{-1/2}$, βc is the bulk velocity of the emitting plasma and θ the angle between the direction of the jet and the line of sight. The transformation law for the specific flux density is in fact $F_\nu = \delta^{p+\alpha} F'_\nu$, where the primed quantity refers to the comoving frame, α is the local spectral index, $p = 2$ for a continuous jet and $p = 3$ for a moving sphere.

Therefore the comparison of the core emission of beamed objects and their parent population with similar extended emission provides a direct estimate of the Lorentz factor of the radiating plasma, if the typical observing angles are known. With this aim and similarly to what has been done in the radio band (e.g. Kollgaard et al. [79]), we plot the optical V band luminosity (L_o) vs the extended radio luminosity at 1.4 GHz ($L_{\rm ext}$) for the three samples (Fig. 4.1).

First we should note that the HBL objects do not fully share the range of extended radio power of the 3CR radio galaxies (the HBL

total luminosities are in fact more similar to the objects belonging to the B2 sample of low power radio galaxies). Conversely, $L_{\rm ext}$ of LBL well match those FR I of the 3CR catalog.

Also notice that the regions occupied by the two samples of BL Lacs appear to be continuously connected, the lower radio power BL Lacs (which are HBLs) and the higher radio power ones (LBLs) having an optical luminosity which weakly increases for increasing extended luminosity. Because of this trend, in order to compare sources with the same $L_{\rm ext}$ we have sub-divided the samples into three bins, namely: $\log L_{\rm ext}$ [erg s^{-1} Hz^{-1}] < 31.5, $\log L_{\rm ext}$ between 31.5 and 32.5, and $\log L_{\rm ext} > 32.5$.

We thus calculate the median values of the observed nuclear luminosity of FR I and BL Lacs in each interval of extended power. BL Lacs are on average 4 orders of magnitude brighter than FR I cores. We can assume that BL Lacs are observed [1] at $\theta \sim 1/\Gamma$ and FR Is at $\theta = 60°$: in fact, for an isotropic distribution of objects, $\theta = 60°$ corresponds to the median angle if, as it is in the case of FR I, the scatter in the optical luminosity is dominated by relativistic beaming. Bulk Lorentz factors $\Gamma \sim 4$ for the case of an emitting sphere and ~ 6 for a continuous jet are required in order to account for the different core luminosities of FR I and BL Lacs in each bin of extended power. An optical spectral index $\alpha_o = 1$ is assumed for all sources (independent of beaming).

An alternative method to estimate Γ relies on the fact that, for a randomly oriented sample, the best fit regression line of a luminosity distribution corresponds to the behavior of sources observed at $\sim 60°$, once the most core dominated objects are excluded (Kollgaard et al. [79]). We thus determine the best fit regression of FR I in the $L_{\rm ext} - L_{\rm o}$ plane, after excluding from the sample the 5 objects in which optical jets are detected. In fact, as already noted in chapter 2, these sources have the most luminous optical cores, are among the most core

[1] At the particular angle $\theta \sim 1/\Gamma$, one obtains $\delta = \Gamma$.

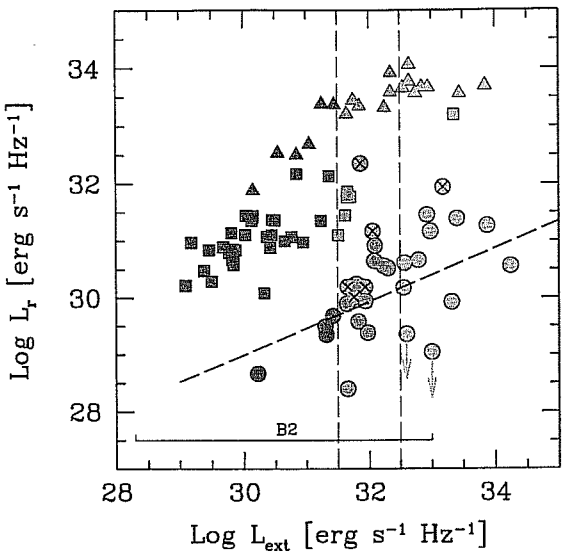

Figure 4.3: Radio core luminosity (at 5 GHz) versus radio extended luminosity at 1.4 GHz for FR I (circles), X-ray selected (squares) and radio-selected BL Lacs (triangles). The dashed line is the correlation between these two quantities found for a larger sample of galaxies by Giovannini et al. ([56]) and converted to 1.4 GHz using $\alpha_r = 0.7$.

dominated objects in the radio band, and their radio jets are shorter, indicating that they are pointing towards the observer (Sparks et al. [135]). Interestingly, we obtain that there is a remarkable correlation ($P > 99.9\%$) between $\log L_{\rm ext}$ and $\log L_o$, among the remaining 20 "highly misoriented" objects, although with a slope (~ 0.6) marginally steeper than the correlation between $L_{\rm ext}$ and core radio luminosity (L_r) found by Giovannini et al. ([56]) for a larger sample of radio galaxies. In Fig. 4.2 we show the regions in which the three samples are located in the $L_{\rm ext} - L_o$ plane, and the dashed lines represent the "beamed" FR I population as observed under an angle $\sim 1/\Gamma$ in the case of $p = 3$. Also with this method $\Gamma \sim 5$ (~ 7) are required to displace the FR I to the regions occupied by both HBL and LBL for $p = 3$ ($p = 2$).

Let us now consider L_r (at 5 GHz) versus $L_{\rm ext}$ (Fig. 4.3), analogously to what is shown by Kollgaard et al. ([79]) for a larger sample of radio galaxies (which also includes our objects). The typical radio core luminosities of HBL and LBL are significantly different, the latter

objects being on average about one order of magnitude more luminous than the former ones. Conversely, as we have already pointed out, no substantial difference between the two classes is found in the case of L_o.

These results have been initially attributed to a different amount of beaming for X-ray and radio-selected BL Lacs (i.e. different angle of sight and/or different jet velocities[2]) while more recently a consistent picture has emerged where this diversity can be accounted for by the different shape of their intrinsic SED (e.g. Padovani [115], Ghisellini & Maraschi [52], Giommi & Padovani [53], Fossati et al. [48]). The role of these two scenarios will be further explored in the next section, through the comparison of the SED of both types of BL Lacs with their parents.

We conclude that the Lorentz factors inferred from the comparison of the radio, but also optical emission of FR I and BL Lacs, are consistent with those previously estimated from the statistics of these sources within the unifying scheme. However, as already mentioned, such values are significantly and systematically lower than those required by other independent means, such as superluminal motions and high energy spectral constraints (fit to the overall SED and time–lags) in both LBLs and HBLs. (Maraschi et al. [96], Sikora et al. [132], Celotti et al. [28], Tavecchio et al. [144]). These latter methods require a value of the Doppler factor δ in the range 15–20 for the region emitting most of the radiation in both HBLs and LBLs. The need for high degrees of beaming will constitute a crucial point in the following.

4.3 FR I and BL Lac in the L_o and L_r plane

Since for the first time multifrequency data are available also for the nucleus of radio galaxies, we can now directly compare the spectral

[2]If so the inferred Lorentz factors, relative to our sample, are $\Gamma = 4$ (3) for HBL $\Gamma = 10$ (5) for LBL, in the case of p=2 (p=3)

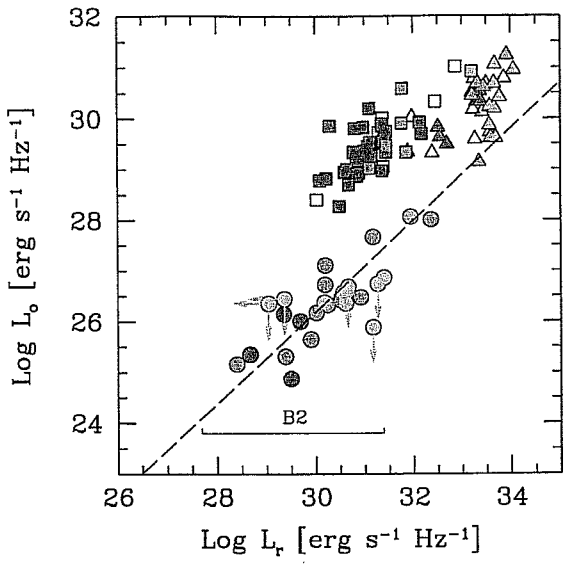

Figure 4.4: BL Lacs and FR I radio galaxies in the $L_r - L_o$ plane. Empty symbols are objects with no data on their extended radio power, filled symbols and grey scale are as in Fig. 4.1. The dashed line is the radio-optical core correlation (Paper I). The range of core luminosity of the B2 radio galaxies is also reported. Notice that the B2 cores could at most extend this correlation by ~ 1 order of magnitude towards lower luminosities.

properties of beamed objects and their parent population: this new approach can thus combine information from the SED of BL Lacs with those inferred from their relation with FR I. In particular in Chapters 2 and 3 we showed how the location of sources in the L_o and L_r plane represents a very useful tool to discuss their nuclear properties. In Fig. 4.4 we show the optical vs radio core luminosity for the three samples. The dashed line represents the (almost linear) correlation found between these two quantities among the FR I sources (Paper I). Radio galaxies, HBL and LBL occupy different regions of this plane: LBLs are located only marginally above the continuation of this correlation, while HBL are $\sim$ 2 order of magnitude brighter in the optical with respect to other objects for a given radio luminosity.

In order to determine how beaming affects the observed luminosities and thus how objects could be connected in this plane, we consider the SED of BL Lacs, observationally much better determined, and calculate the observed spectrum of the misaligned objects, by taking into account relativistic transformations.

In fact, an important point, previously neglected, is that these transformations depend on the spectral index in the band considered, which in itself might change as a function of the degree of beaming. Therefore, in order to correctly de–beam the SED of BL Lacs, a continuous representation of it and an estimate of the bulk Lorentz factor of the emitting region are needed (it is again assumed $\theta = 1/\Gamma$). While any continuous description of the SED and typical Lorentz factors can be used, we derive both of them by adopting a homogeneous synchrotron self–Compton emission model to reproduce the observed SEDs (e.g. Chiaberge & Ghisellini [30], Ghisellini et al. [49], Mastichiadis & Kirk [99]). This approach has the advantage of considering both the emission and dynamical (Γ) properties self–consistently. [3] The bulk velocities obtained in this way are fully compatible with those inferred from the already mentioned constraints (Sect. 4.2).

Let us firstly consider single objects for which the SED is well sampled, namely Mkn 421 (a typical HBL) and PKS 0735+178 (a typical LBL). We model the observed SED as explained, derive the value of $\Gamma(=\delta)$ for the two sources and then calculate their corresponding observed SEDs for different orientations. Clearly the net effect of debeaming is a "shift" of the SED towards lower luminosities and energies (see Fig. 4.5).

Notice that, as the model is appropriate for the optically thin part of the spectrum, in order to account for the radio emission, which necessarily has to be produced on larger scales, we linearly extrapolate the fit from the infrared-mm spectral region. However, at an angle of $\theta = 60°$ and for the Lorentz factors derived from the model, $\Gamma \sim 15-20$, the observed (debeamed) radiation at 5 GHz corresponds to what is seen in BL Lacs at far infrared frequencies (respectively $\sim 500-300\mu m$, see Fig. 4.5) and therefore the debeamed points in Fig. 4.6 represent

[3] These models, in fact, satisfy time variability constraints, assume continuous injection of particles, radiative and adiabatic cooling, γ–γ collisions and pair production. The continuous curves shown in Fig. 4.5 are then not only interpolating curves, but physically possible fits to the data.

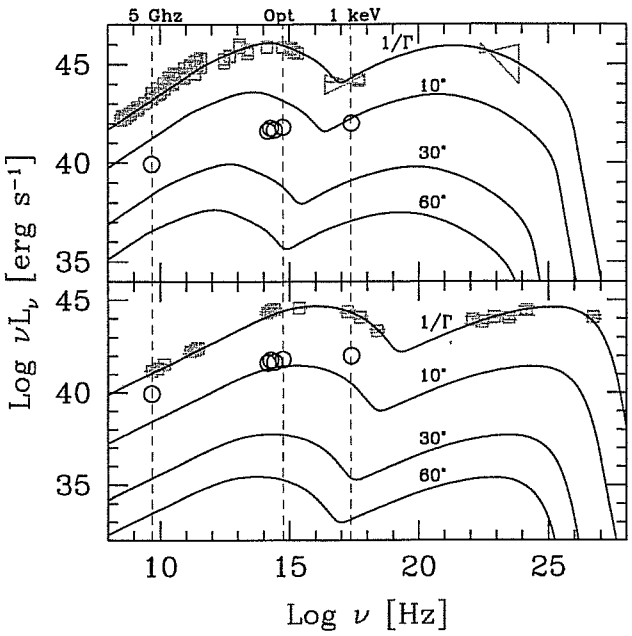

Figure 4.5: Spectral energy distributions of Mkn 421 (lower panel) and PKS 0735+178 (top panel) and debeamed SED for different viewing angles in the case of a single emitting component. The Lorentz factors inferred for the two sources are $\Gamma = 20$ and $\Gamma = 16$, respectively. For comparison, we report (empty circles) the radio, IR and optical (HST) and X-ray (ROSAT) data for 3C 264 (see chapter 5). The (non-simultaneous) data for PKS 0735+178 are taken from the literature (NED). The (quasi-simultaneous) data for Mkn 421 are from Macomb et al. ([95]).

the correct predicted luminosities of the BL Lac component at 5 GHz.

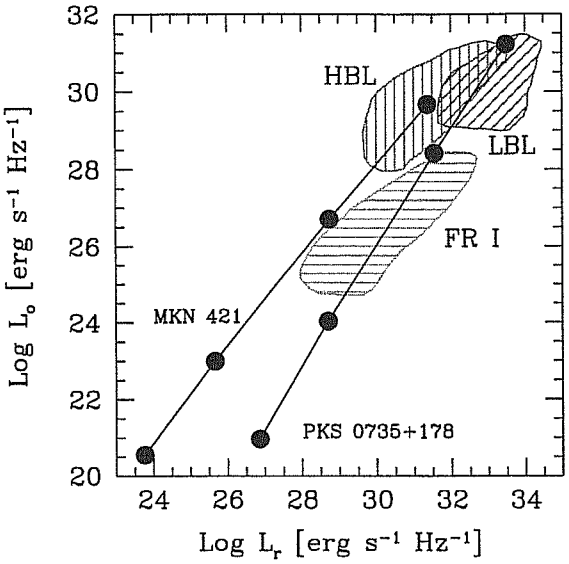

Figure 4.6: Debeaming trails in the radio-optical luminosity plane for Mkn 421 and PKS 0735+178, in the frame of a single emitting region model. The filled circles correspond to the predicted luminosities of objects at different viewing angles. Top to bottom: $\theta = 1/\Gamma$, 10°, 30° and 60°.

The resulting debeamed optical and radio luminosities are reproduced in Fig. 4.6. The lines represent "debeaming trails" and the filled circles the calculated debeamed luminosities for $\theta = 1/\Gamma$ (i.e. the BL Lac itself), 10°, 30° and 60°. Most noticeably, for $\theta = 60°$ – which is the mean angle of sight for the misaligned population – the BL Lac component is about four orders of magnitude below the radio galaxy region in the optical, and two/four in the radio band.

While equivalently incompatible with the FR I population, the HBL and LBL move on different trails. This is due to the different shape of their SED (see Fig. 4.5), and in particular to the position of the synchrotron peak frequency: if – for increasing values of θ – in the rest frame the peak overcomes the optical band, the spectral index steepens and the optical flux drops more rapidly than the radio one.

Another remarkable result is that the debeaming trail of the HBL does not even cross the region occupied by radio galaxies in the $L_r - L_o$ plane. As this might be a serious problem for the unified scheme, we

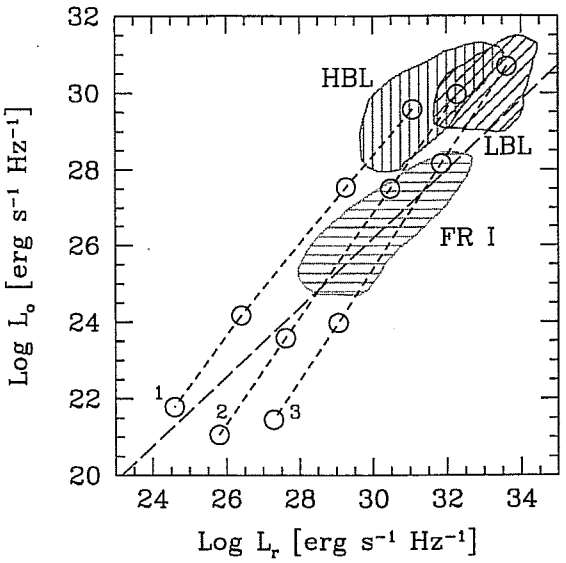

Figure 4.7: Debeaming trails in the radio-optical luminosity plane for average BL Lacs SED, in the frame of a single emitting component model. The filled circles correspond to the predicted optical-radio luminosity for different angles of sight (top to bottom: $\theta = 1/\Gamma$, 10°, 30° and 60°).

further examine this issue. In particular we closely examine the effect of the spectral shape and its relation with the intrinsic luminosity by considering three different SED, which represent the whole family of BL Lacs, from HBLs to LBLs. [4] In Fig. 4.7 we plot the resulting trails: once again, as in the cases of Mkn 421 and PKS 0735+178, the expected nuclear luminosity is 10-10^4 times fainter than what observed in FR I and the debeaming trail for the lower luminosity object (a typical HBL) does not even cross the FR I region. Note that if the luminosity is indeed related to the shape of the SED, this discrepancy would exacerbate for even fainter BL Lacs. In fact for HBL the radio and optical spectral slopes can be considered constant as the viewing angle increases, resulting in a linear (one to one) debeaming trail, parallel to the FR I correlation.

Summarizing: the radio and optical luminosities of BL Lacs and

[4] The three SED correspond to different bins of radio luminosity (at 5 GHz) – which appears correlated with the bolometric luminosity and the position of the peak frequency (Fossati et al. [48], Ghisellini et al. [49]).

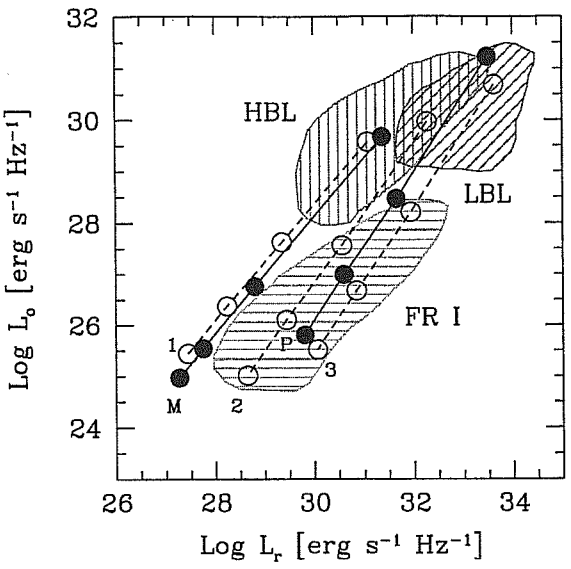

Figure 4.8: Debeaming trails in the radio-optical luminosity plane, for the case of the two-velocity jet. The five curves correspond to average SED (1,2 and 3), Mkn 421 (M) and PKS 0735+178 (P). For the average SEDs $\Gamma_{spine} = 15$ and $\Gamma_{layer} = 2$; for Mkn 421 $\Gamma_{spine} = 20$ and $\Gamma_{layer} = 1.2$; for PKS 0735+178 $\Gamma_{spine} = 16$ and $\Gamma_{layer} = 1.5$. Circles correspond to the predicted optical-radio luminosity for different angles of sight (top to bottom: $\theta = 1/\Gamma$, 10°, 30° and 60°).

FR I are not consistent with the simplest predictions of the unifying scheme, if a single emitting region is responsible for the different broad band spectral properties of the beamed and parent populations. More specifically: i) Lorentz factors ~ 15, as derived from the high energy spectral properties, underestimate the predicted emission from the parent population; ii) the relative ratio of radio to optical luminosity of HBL is inconsistent with the observed FR I spectra. In the next section we discuss and test a possible solution to these discrepancies.

4.4 A jet velocity structure

We have shown that the high bulk Lorentz factors required by the emission models of BL Lacs imply that if such objects are observed at 60° the resulting spectral properties are not compatible with what is observed in the nuclei of radio galaxies. And indeed the previous comparison of the core emission of FR I and BL Lacs (see Sect. 4.2)

led to lower values of Γ. How can these results be reconciled within the unifying scenario? A possible and plausible effect, which could account for this discrepancy, is provided by the existence of a distribution in the bulk velocity of the flow, with the emission from plasma moving at different speeds dominating the flux observed at different viewing angles.

Let us consider this hypothesis in the frame of the unification scheme and examine the simplest case, i.e. a model with two axisymmetric components having the same intrinsic luminosity and spectra. In other words, the only difference between the center and the layer of the jet is the bulk Lorentz factor which is determined for the *spine* ($\Gamma_{\rm spine}$) by modeling the BL Lac SED, while for the *layer* ($\Gamma_{\rm layer}$) by requiring that the debeamed BL Lac match the FR I distributions in the $L_{\rm ext} - L_o$ and $L_r - L_o$ planes.

The monochromatic intensity emitted by the jet is therefore calculated as

$$I(\nu,\theta) = \delta^3_{\rm spine}(\theta) I'(\nu/\delta_{\rm spine}) + \delta^3_{\rm layer}(\theta) I'(\nu/\delta_{\rm layer}),$$

where I' is the comoving intensity.

The predicted luminosity trails for the two specific BL Lacs are shown in Fig. 4.8. Values of $\Gamma_{\rm layer}$ are set to 1.2 and 1.5 for Mkn 421 and PKS 0735+178 respectively, so that the point of each trail corresponding to the angle $\theta = 60°$ falls approximatively onto the median of the FR I optical core luminosity in each $L_{\rm ext}$ bin (Fig. 4.9).

By using the same value of $\Gamma_{\rm layer}$ this two-velocity model satisfactorily predicts the properties of the debeamed counterparts of LBL and in particular it reproduces the FR I location in the $L_r - L_o$ plane.

Conversely this picture can not account for the observed optical–radio properties of debeamed HBL. The luminosity of objects seen at $\theta = 60°$ is close to the lower limit of the FR I region in the optical, but still one order of magnitude fainter in the radio. We must stress however that the extended radio powers of HBLs correspond more closely

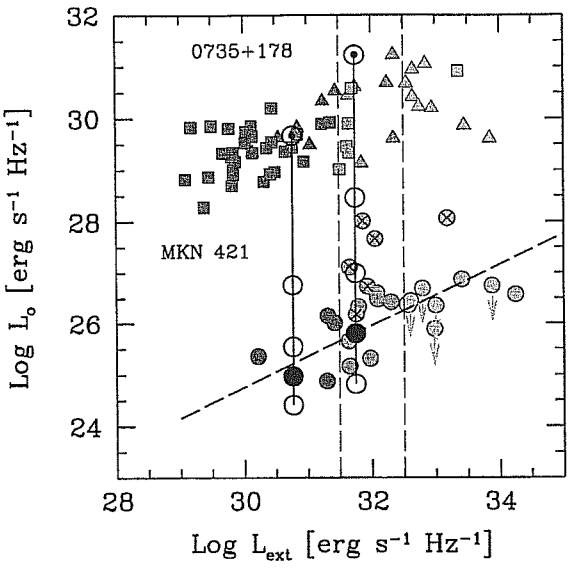

Figure 4.9: Debeaming trails for the optical emission of Mkn 421 and PKS 0735+178 in the two-velocity jet scenario. The circles connected by the vertical lines correspond to the sources observed at angles of (top to bottom) $1/\Gamma$, 10°, 30°, 60° (filled black circles) and 90°. The values of $\Gamma_{\rm layer}$ (1.2 for and 1.5 for Mkn 421 and PKS 0735+178, respectively) are chosen in order for the luminosity at 60° to correspond to the median value for each bin of extended radio power.

to the range covered by the B2 radio galaxies. Clearly, any firm statement on this issue must await for the analysis of the nuclear properties of the B2 sample, but the extrapolation of the 3CR radio-optical correlation does not match the debeamed predicted luminosities of HBL. This result does not depend on the specific value of $\Gamma_{\rm layer}$ adopted since, as already discussed in Sect. 4.3, the HBL trails run almost parallel to the radio-galaxies locus.

A further modification of this model is thus required for the HBL unification. Without altering the comoving spectra of the two components, the simplest change is to assume a lower Doppler factor for *spine* in the radio emitting region, as might be the case if the flow slows down between the optical and the radio emitting sites. This would increase the initial slope of the debeaming trail which would rapidly reach the FR I region.

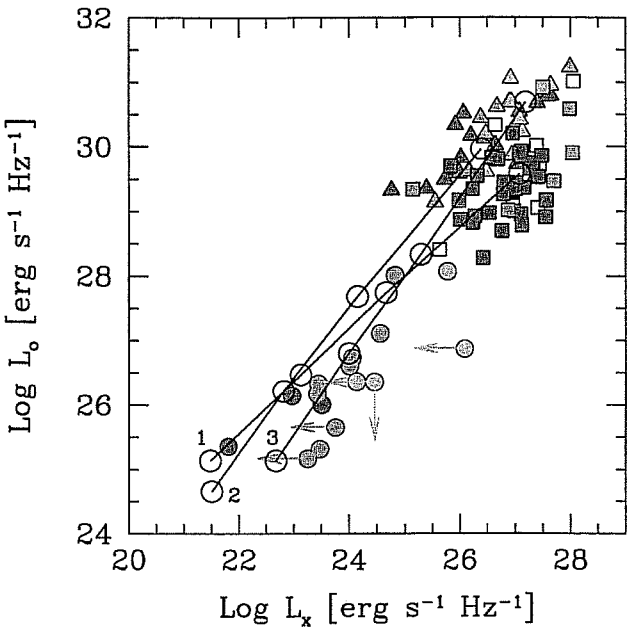

Figure 4.10: Debeaming trails in the optical-X-ray luminosity plane for the average BL Lacs SED. Two-velocity jet with $\Gamma_{\rm spine} = 15$ and $\Gamma_{\rm layer} = 2$ for all SED. Circles are FR I, squares and triangles represent X-ray and radio selected BL Lacs, respectively. Grey scales correspond to bins of extended radio luminosity, as for Fig. 4.1. Open triangles and squares are sources without measurement of their extended radio power. Open circles correspond to the predicted optical-X-ray luminosity for different angles of sight (top to bottom: $\theta = 1/\Gamma$, 10°, 30° and 60°).

4.4.1 Constraints from the X–ray observations

The limited angular resolution makes the analysis of X-ray observations of FR I sources less straightforward than in the radio and optical bands. In particular it is necessary to disentangle any non thermal nuclear radiation from the often dominant emission of the hot gas associated with the galactic corona and/or galaxy cluster. Nonetheless they provide useful constraints to high energy nuclear emission of these radio-galaxies.

We can test the validity of the two-velocity jet scenario by considering also this X-ray emission. In Fig. 4.10 we report the debeaming trails in the $L_X - L_o$ plane for the average SEDs assuming the same jet parameters as before: the predicted powers in both bands appear to be consistent with the observed properties of radio galaxies, supporting the presence of a less beamed plasma component (layer) dominating the emission in the parent population also in the X-ray band. Conversely, there is no need for a different amount of beaming in these two bands. This is somehow reassuring, as optical and X–ray are believed to originate co–spatially.

In addition, X–ray data can be used to define the location of radio–galaxies also in the broad band spectral indices plane. The spectral characteristics of blazars are often represented in the plane defined by $\alpha_{\rm ro}$ (5GHz-5500Å) and $\alpha_{\rm ox}$(5500Å-1 keV). It is therefore worthwhile to determine how relativistic beaming affects the position of the objects also in this plane. While an approximated relation between the BL Lacs and FR I broad band spectral slopes is derived in A in the case of constant local spectral indices, changes in the local spectral slopes are properly taken into account.

In this plane (Fig. 4.11), as already well established, HBL and LBL occupy the left (i.e. flatter $\alpha_{\rm ro}$) and the top-center (i.e. steeper $\alpha_{\rm ox}$) regions, respectively and their different position is accounted for by their different SEDs (e.g. Fossati et al. [48]), i.e. reflects the position of the peak of the emission. The FR I region is instead well defined at

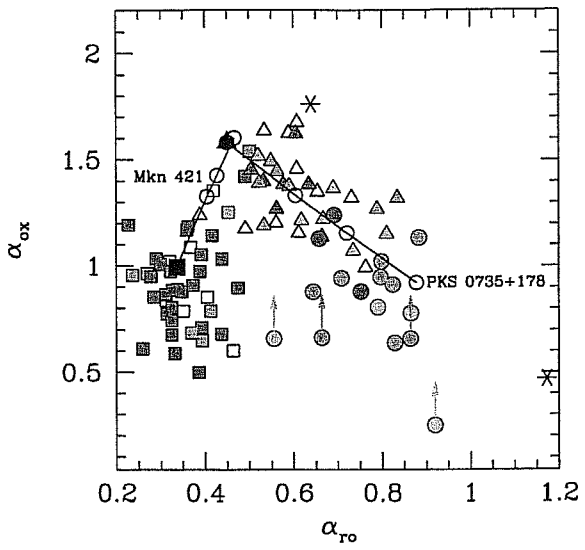

Figure 4.11: Debeaming trails in the $\alpha_{ro} - \alpha_{ox}$ plane for Mkn 421 and PKS 0735+178. The jet parameters are the same as in Fig. 4.8. The black filled symbols correspond to the observed BL Lac ($\theta = 1/\Gamma$), while the empty circles represent the predicted position for different angles of sight ($\theta = 10°$, $30°$ and $60°$) in the frame of a two-velocity jet model. The two asterisks indicate sources observed at $\theta = 60°$ in the case of a single emitting component.

the center of the diagram. The debeaming trails for Mkn 421 and PKS 0735+178 are also shown [5]: the empty circles correspond to $\theta = 1/\Gamma$, $10°$ $30°$, $60°$ in the case of the two components model, while the two asterisks represent each source as observed at $60°$ in the case of a single emitting region. PKS 0735+178 falls in the radio galaxy region for $\Gamma_{layer} = 3$ or less, while Mkn 421 does not intersect this area either in the single or in two component models, confirming the results of the analysis presented above.

[5]Note that again the two trails differ because of the different SEDs: for Mkn 421 the peak of the synchrotron component is between the optical and the X-ray bands and therefore the effect of debeaming is, initially (i.e. for increasing θ) to steepen both α_{ro} and α_{ox}; when the Compton peak enters the X-ray band, α_{ox} flattens. Instead, for PKS 0735+178 the synchrotron peaks between the radio and the optical, and the 1 keV flux is due to Compton and, for the range of angles of sight considered here, the change in the spectral indices turns out to be monotonous.

4.5 Conclusions

With the aim of exploring the viability of the unification scenario between (HBL, LBL) BL Lacs and FR I radio galaxies we have compared their nuclear emission in the radio, optical and X–ray bands.

We have firstly considered these spectral regions separately, comparing the nuclear emission of the two classes of objects for similar extended radio power. As the core radiation of BL Lacs is enhanced by relativistic beaming, we derived the bulk Lorentz factors requested to account for the observed distribution. The values of Γ thus inferred are not compatible with the higher bulk velocities requested by theoretical arguments, such as the pair production opacity and the spectral modeling of the SED of BL Lacs.

We then examined the core emission of three samples in the $L_r - L_o$ plane. In the frame of the simplest one-zone emission model, we calculated debeaming trails of the BL Lac broad band emission as predicted by the relativistic transformation for an increasing angle of sight. We found that the model does not account for the observed spectral properties of FR I, as expected from the above inconsistency of the Lorentz factors.

The simplest and rather plausible hypothesis to account for this discrepancy within the unification scenario is to assume a structure in the jet velocity field, in which a fast spine is surrounded by a slow layer. Note however that the slower jet component must be relativistic in order to explain the anisotropic radiation of radio galaxy cores (e.g. Capetti & Celotti [23]). The observed flux is dominated by the emission from either the spine or the slower layer, in the case of aligned and misaligned objects, respectively.

Interestingly, the existence of velocity structures in the jet has been suggested by various authors (Komissarov [83], Laing [86]) in order to explain some observed properties of FR I (and FR II) jets, such as the structure of the magnetic field in FR I which appears to be

longitudinal close to the jet axis and transverse at the edges. Swain et al. [140] obtained VLA images of 3C 353 (an FR II with straight jets), finding that a model consisting in a fast relativistic spine ($\beta > 0.8$) plus a slower outer layer ($\beta < 0.5$, but still relativistic in order to produce the observed jet-counterjet intensity asymmetry) could account for the apparently lower emissivity near the jet axis. Similar behaviours have been inferred for the two low luminosity radio galaxies M 87 (Owen et al. [113]) and B2 1144+35 (Giovannini et al. [54]). Furthermore, Laing et al. ([85]) showed that the jet asymmetries in FR I can be explained by means of a two-speed model. As a consequence, they argued that the lower velocity component dominates in the cores of the edge-on sources, while the fast spine emission dominates the end-on ones. This possibility might be also supported by recent numerical simulations of relativistic jets (Aloy et al. [1]). The same indication has been found through different approaches. Capetti & Celotti [23] reveal a trend in the radio galaxy/BL Lac relative powers with the line of sight, which is consistent with a slower (less beamed) component dominating at the largest angles.

We found that Lorentz factors of the layer $\Gamma_{\rm layer} \sim 2$ can account for the unification of FR I (of the 3CR) with LBL and intermediate luminosity BL Lacs. Instead the debeaming trails for the lowest luminosity HBL do not cross the FR I region in the $L_r - L_o$ plane. While the HBL behavior should be compared with that of radio galaxies with which they share the extended radio power (e.g. those of the B2 catalogue), our simple two-component jet model could not account for the observed properties if the cores of such low-power FR I radio galaxies lied on the extrapolation of the 3CR radio-optical correlation. The properties of such weak sources can be instead reproduced if their radio emitting region is less beamed than the optical one, as could be expected if the jet decelerates after the higher energy emitting zone.

Finally, the presence of velocity structures in jets of course affects the number counts of beamed and unbeamed sources: for example, the

lack of BL Lacs in clusters (Owen et al. [111]) could be attributed to values of typical bulk Lorentz factors higher than those derived from statistical arguments (Urry et al. [153]). Intriguingly, the very latter authors had to require a wide distribution of Lorentz factors to account for the number densities of FR I and BL Lacs in the radio band.

Much has still to be understood on the dynamics and emitting properties of relativistic jets. Multifrequency studies of the nuclear properties of beamed sources and their parent populations and their comparison – according to unification scenarios which are well supported by other independent indications – constitute a new and powerful tool to achieve that, both for well studied individual sources as well as complete samples. However, these studies are strongly hampered by the presence of bright extended components (the galaxy in the optical and IR, the emission from the cluster and the galactic halo in the X-ray band). In the next Chapter we will try to build, for the first time, the nuclear SED of five radio galaxies for which radio, near IR observations (NICMOS, HST), optical and X-ray (ROSAT) data are available.

Chapter 5

Spectral energy distributions of FR I nuclei and the FR I/BL Lac unifying model

Multi–wavelengths observations of FR I radio galaxies clearly represent a powerful way to test the unification model, as their SED can be directly compared with those of BL Lacs. SED of radio-galaxies and in particular of FR I have been derived by several authors (e.g. Impey & Gregorini, [70]; Ho [69]). However, the comparison with those of BL Lacs is hampered by the large aperture from which data have been obtained, which often includes a dominant contribution from the host galaxy. We therefore gathered archival observations of FR I from which it is possible to separate the nuclear from the extended emission, in particular ROSAT data and HST/NICMOS infrared images. These can be combined with our analysis of the HST optical images already presented in Chapter 2 and radio core measurements from the literature. Clearly, data in the infrared/optical and X–ray bands could also provide an independent test for the role of absorption from thick material (torus) in this unifying scheme. As the orientation of the radio galaxies is a crucial parameter, in this paper we focus on the sample of

Table 5.1: Main optical parameters

Source	Alt. name	z	$M^{a}_{B_{T_o}}$	Envir.	Orient.[a]
3C 31	NGC 383	0.0169	-21.19	Arp 331	35°
3C 264	NGC 3862	0.0216	-21.15	A 1367	15°
3C 270	NGC 4261	0.0074	-21.02	Group	65°
3C 465	NGC 7720	0.0291	-22.30	A 2634	45°
NGC 7052	B2 2116+26	0.0164	-21.41	Pair	72°

[a] Radio source orientation taken from CC99.

5 objects studied in Capetti & Celotti [23] (hereafter CC99), for which we have such information (see Table 5.1).

ROSAT archival pointed observations of 4 out of 5 galaxies are available and are presented in Section 5.1. HST/NICMOS infrared images have been obtained for 3 of the selected objects and are described in Section 5.2. In Section 5.3 we discuss the role of absorption with respect to the inferred nuclear SED, which we assemble in Section 5.4. The comparison with the SED of BL Lacs and the implications for the FR I/BL Lac unified scheme are discussed in Section 5.5.

5.1 The ROSAT observations

ROSAT HRI and PSPC data are available for 3 of the selected sources, namely 3C 31, 3C 270 and 3C 465, while for 3C 264 only PSPC data exist. In Table 5.2 we list the available pointed observations. The X–ray properties of these targets have been already discussed by different authors (see last column of the table) but we decided to re-analyze the data to follow a more homogeneous approach.

For the analysis we have used the EXSAS package (release of Jan. 1996; Zimmermann et al. [161]) and the data have been corrected for vignetting and dead time. In the PSPC observations only the energy range 0.15 - 2.1 keV has been considered and the spectra have been

rebinned according to the source count rate [1].

All targets are members of clusters or groups of galaxies, and this implies that any central non–thermal X–ray emission must be disentangled from that of a hot intergalactic medium, with temperatures $\sim 3-8$ keV (Sarazin [129]), and of the extended hot halos (~ 1 keV; Donnelly et al. [36]; Trussoni et al. [147]). Therefore for the spectral analysis of the PSPC data we used composite models allowing for the presence of both a thermal and a non–thermal (power-law) component. The free physical parameters in the spectral fits are, besides the two normalizations, the hydrogen column density N_H, the photon index Γ for the power–law spectrum, the temperature T and metallicity μ for the thermal component (optically thin plasma, Raymond & Smith [121]). As count rates are usually quite low, some parameters must be fixed in order to deduce usefully constrained fits. In all cases (except for 3C 264) we set N_H to its galactic value $N_{H,gal}$, and $\mu = 0.5$, as typical for hot galactic halos (Fabbiano [41]). Fixing the metallicity does not significantly affect our results as the parameters describing the non-thermal component depend only weakly on μ – at least if it lies within the plausible range $0.2 \leq \mu \leq 1$. To establish the statistical significance of the non thermal component, we have then checked through an F-test when its inclusion improves the fit. The results of the X-ray spectral analysis are summarized in Table 5.3.

The HRI data should allow in principle to spatially separate the unresolved central component from the coronal emission. However, the spatial resolution of the HRI is insufficient to fully resolve the cores of the galactic coronae, particularly for the more distant sources. Furthermore, problems in the aspect solution associated with the satellite wobble may lead to smearing of point-like sources (algorithms proposed to overcome this problem work only for bright sources, Morse [105]; Harris et al. [64]; Sarazin et al. [130]) compromising the spatial

[1] The minimum signal to noise ratio per energy channel is 5σ for 3C 264 and 3C 270, 4σ for 3C 31 and 3σ for 3C 465.

Table 5.2: Log of ROSAT observations for the four FR I radio galaxies

Source	Instrument	Obs. Date	t_{exp} (s)	Counts[a]	r^{extr}_{source}	$r^{extr\,(c)}_{bkg}$	Ref.[d]
3C 31	PSPC	Jul 91	29430	552 ± 38	$75''$	$125''$	(1)(2)
	HRI	Apr 94	25007	165 ± 33			(2)(3)
3C 264	PSPC	Nov 91	18745	5068 ± 85	$100''$	$175''$	(3)(4)(5)
3C 270	PSPC	Dec 91	21863	1935 ± 65	$150''$	$250''$	(6)
	HRI	Jun 95	18477	584 ± 51			
3C 465	PSPC	Jun 91	9866				
	PSPC	Dec 92	10522	252 ± 21[b]	$35''$	$75''$	(7)
	HRI	Jan 95	29063				
	HRI	Jun 95	33392	304 ± 29[b]			(3)(8)

[a] Background subtracted; the errors are at 1σ

[b] Merging the data of the two observations

[c] External radius, the inner radius $\equiv r^{extr}_{source}$

[d] References: (1) Trussoni et al. ([147]); (2) Komossa & Böhringer ([81]); (3) Hardcastle & Worrall ([62]); (4) Edge & Röttering ([38]); (5)Tananbaum et al. ([143]); (6) Worral & Birkinshaw ([160]); (7) Schindler & Prieto (citeschin); (8) Sakelliou & Merrifield ([128])

analysis. We therefore preferred to use the HRI observations just to check their consistency with the count rates predicted by the PSPC spectral decomposition.

No statistically significant variability has been found in the light curves of the observations, and in the targets observed with PSPC and HRI the count rates are consistent in both instruments.

5.1.1 Summary of the X-ray data

Non–thermal emission is detected in 3 out of the 4 targets with pointed X–ray observations: in 3C 264 it is the dominant source, while in 3C 270 and 3C 31 the inclusion of a non–thermal component significantly improves the fit. Only an upper limit can be set for the power-law emission from the nucleus of 3C 465. The photon fluxes predicted by the spectral decomposition agree with those observed in the HRI images.

Table 5.3: Fits of PSPC data with a thermal + power-law spectrum. Errors are at 1σ. Upper and lower limits are at 2σ confidence level. Quantities without errors are fixed. Metallicity is always set to $\mu = 0.5$ solar.

Source	N_H $\times 10^{20}$ cm^{-2}	T keV	Γ	χ^2 (d.o.f.)	$L_{[0.1-2.4\,\mathrm{keV}],\mathrm{th}}$ $\times 10^{41}$ erg s^{-1}	$L_{[0.1-2.4\,\mathrm{keV}],\mathrm{pl}}$ $\times 10^{41}$ erg s^{-1}
3C 31	5.23	$0.75^{+0.17}_{-0.20}$	2.3	0.30 (15)	$0.65^{+0.17}_{-0.16}$	$1.30^{+0.54}_{-0.58}$
	5.23	$0.59^{+0.17}_{-0.20}$	1.7	0.30 (15)	$0.70^{+0.20}_{-0.22}$	$1.00^{+0.38}_{-0.23}$
3C 264	$2.6^{+0.4}_{-0.2}$	1	$2.46^{+0.06}_{-0.06}$	0.88 (81)	$1.00^{+1.17}_{-1.00}$	$47.1^{+0.9}_{-1.3}$
3C 270	1.63	$0.81^{+0.09}_{-0.13}$	$1.71^{+0.21}_{-0.18}$	0.70 (33)	$0.49^{+0.08}_{-0.06}$	$0.54^{+0.1}_{-0.1}$
3C 465	5.22	$1.16^{+0.20}_{-0.15}$	2.3	1.10 (17)	$3.20^{+0.27}_{-0.76}$ ($\gtrsim 2.2$)	0 ($\lesssim 1.3$)
	5.22	$1.16^{+0.14}_{-0.18}$	1.7	1.09 (17)	$3.07^{+0.36}_{-0.49}$ ($\gtrsim 1.2$)	0 ($\lesssim 2.1$)

Worral & Birkinshaw ([160]) and Worral ([159]) found a correlation between the luminosities of FR I radio galaxies in the radio and soft X-ray bands, recently confirmed by Canosa et al. ([21]) and Hardcastle and Worrall ([62]) who analyzed the PSPC and HRI brightness profiles of a large sample of objects. This trend appears to hold also at harder X-ray energies for brighter radio galaxies (Trussoni et al. [148]). The non-thermal luminosity of the three detected sources we found is consistent with this correlation. Conversely, the upper limit for 3C 465 is ≈ 4 times lower than expected.

5.2 The HST/NICMOS observations

HST/NICMOS observations are available in the public archive for 3C 264, 3C 270 and NGC 7052. For the first two objects we analyzed images taken with the F110W, F160W and F205W wide band filters (approximatively corresponding to the H, J and K bands, respectively), while for NGC 7052 only F160W images exist.

The targets were observed using NICMOS Camera 2 (0.″075/pixel). The field of view of this 256 × 256 pixels camera is 19.″4 × 19.″4. All observations were carried out with a MULTIACCUM sequence (MacK-

Table 5.4: Log of NICMOS observations

Source	Obs. Date	Filter	t_{exp} (s)	Flux[a]
3C 264	May 98	F110W	112	6.7
		F160W	112	4.3
		F205W	112	2.6
3C 270	Apr 98	F110W	192	0.69
		F160W	192	1.2
		F205W	192	1.6
NGC 7052	Aug 98	F160W	160	0.06

[a]Fluxes in units of 10^{-17} erg s^{-1} cm^{-2} $Å^{-1}$

enty et al. [94]), i.e. the detector is read out non-destructively several times during each integration to facilitate removal of cosmic rays and saturated pixels. The data were re-calibrated using the pipeline software CALNICA v3.0 (Bushouse et al. [20]) and the best reference files in the Hubble Data Archive to produce flux calibrated images. Bad pixels were removed interpolating from values of neighboring pixels. A log of the observations is given in Table 5.4.

The final images are presented in Fig. 5.1. While in NGC 7052 the extended dusty disc seen in the optical images is clearly visible, we do not find evidence for circum–nuclear structures in 3C 264 and 3C 270. This is somewhat expected at this longer wavelengths where dust absorption is less efficient, confirming that these discs are associated with dust with small optical depth (e.g. Jaffe et al. [74]). On the other hand, similarly to what found in the optical band, in all targets it is detected a central IR source, whose emission can be now easily isolated from that of the host galaxy. We performed aperture photometry to measure their nuclear fluxes in the different bands (reported in Table 5.4). Photometric errors are dominated by the accuracy of the NICMOS internal flux calibration, which is within 5%, except in the case of NGC 7052 where the relative error is ~ 30 %.

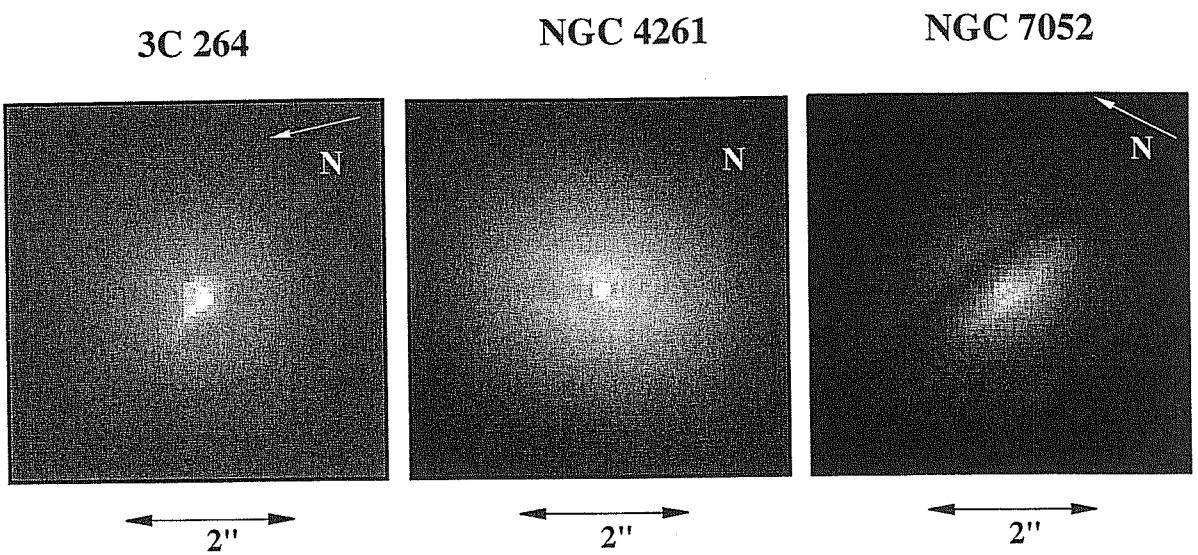

Figure 5.1: HST/NICMOS F160W images of 3 FR I radio galaxies. Note the presence of the central nuclear sources and of the dusty disc in NGC 7052. The arrows indicate the direction of the radio jet.

5.3 The role of absorption in FR I nuclei

As absorption could have significantly affected our measurements in the optical and X–ray bands, and thus in principle alter the inferred SED properties, in this section we carefully examine its possible role.

Photoelectric absorption can be very effective on soft X-rays, and thus measures in this band provide a powerful tool to estimate the (equivalent) column density in neutral hydrogen $N_{\rm H}$. In 3C 264 the X-ray emission is dominated by a power–law component over the whole ROSAT energy range and its spectrum is sufficiently well determined that we could directly measure a column density which – as already mentioned – is fully consistent with the Galactic one: no significant

local absorption is present in this source. This is somewhat expected as 3C 264 is likely to be seen at a small angle from the jet axis (see Table 5.1) and thus along an unobscured line of sight (within the nuclear region). Conversely, in 3C 31, 3C 270 and 3C 465, the observed X-ray flux is dominated by extended thermal emission which is unaffected by nuclear absorption. The detection in 3C 31 and 3C 270 of non–thermal emission above 1 keV only sets an upper limit of $N_{\rm H} \lesssim 10^{23}$ cm^{-2}. This column density corresponds to an attenuation of a factor 100 in the intensity at 2 keV. Note that these results are in agreement with the conclusions of Chapter 2, namely that optically thick material (torii) affects the nuclear emission at most in a minority of FR I. Clearly only X-ray observations at higher spatial resolution, increasing the fraction of nuclear vs extended component, can provide more stringent and valuable estimates of N_H in these cases.

Obviously optical images do not directly lead to estimates of absorption. However, the tight linear correlation which exists between the optical (R band) and radio fluxes/luminosities of FR I cores (Chapter 2) can set interesting upper limits on the nuclear extinction. In fact, even if the entire dispersion of this correlation (0.4 orders of magnitude) was due unically to foreground dust absorption varying from source to source, the extinction could not exceed $\sim$ 2 magnitudes. This limit translates into a gas column density of $N_{\rm H} \lesssim 5 \times 10^{21}$cm^{-2} (assuming a standard gas-to-dust ratio and the extinction curve by Cardelli, Clayton & Mathis [27]), and thus the flux at 1 keV could be depressed at most by a factor of 4 (photoelectric absorption values tabulated by Morrison & McCammon [109]).

Given these upper limits on the exctintion, what would be its effect on the SED properties (and more specifically on the broad band spectral indeces)? As the fluxes in the V band and at 1 keV can be underestimated by a factor $\lesssim$ 10 and $\lesssim$ 4 respectively, the corresponding (maximum) changes in the spectral indeces are limited to $\Delta\alpha_{\rm RO} \lesssim -0.20$, $\Delta\alpha_{\rm RX} \lesssim -0.08$ and $\Delta\alpha_{\rm OX} \lesssim 0.15$. Such uncertainties

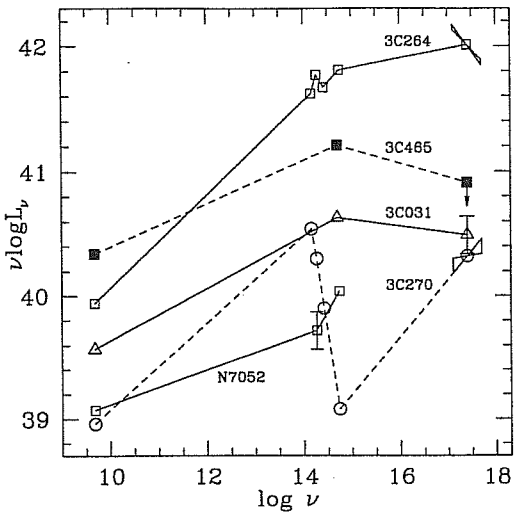

Figure 5.2: Spectral energy distribution of FR I nuclei. Errors are smaller than the symbol size, except when marked.

do not affect significantly our findings and conclusions.

5.4 Spectral Energy Distributions of FR I nuclei

Combining the available data in different energy bands, it is possible to build a SED for the FR I nuclei, isolating for the first time this emission from that of the host galaxy (see Fig. 5.2 and Table 5.5). Besides the IR and X–ray data presented in the previous sections, we used HST optical fluxes from Chapter 2 and CC99, and radio data taken from the literature. In the following we describe the individual SED – always referring to a νL_ν representation – and characterize them through the broad band spectral indices, $\alpha_{\rm RO}$, $\alpha_{\rm RX}$ and $\alpha_{\rm OX}$ (the potential effects produced by the presence of local absorption are discussed in the previous Section).

• **3C 31.** The average radio-to-optical spectral index is $\alpha_{\rm RO} = 0.79$ while the optical-to-X–ray one is $\alpha_{\rm OX} = 1.03$. These spectral indices imply the presence of a peak in the energy distribution. A better energy coverage or the determination of the optical (or X–ray) spectral slope

Table 5.5: FR I nuclear luminosities[a] and spectral indeces

Name	L_R	L_{IR}	L_O	L_X	α_{RO}	α_{RX}	α_{OX}
3C 31	39.57	—	40.63	40.49	0.79 ± 0.03	0.88 ± 0.05	1.05 ± 0.12
3C 264	39.94	41.77	41.81	42.01	0.63 ± 0.02	0.73 ± 0.02	0.93 ± 0.05
3C 270	38.96	40.30	39.08	40.32	0.98 ± 0.04	0.82 ± 0.04	0.54 ± 0.09
3C 465	40.34	—	41.21	<40.91	0.83 ± 0.02	> 0.92	> 1.11
NGC 7052	39.07	39.72	40.04	–	0.81 ± 0.06	—	—

[a] Luminosities, log (νL_ν), in erg s^{-1} measured at 5 GHz, 1.6 μm, 0.5 μm and 1 keV.

are necessary in order to better constraint its location.

• **3C 264**. Its SED is the better determined in our sample as there are data at radio, infrared and optical frequencies, the X–ray spectrum is also well defined and the absorption is constrained to a negligible value. The energy distribution rises from the radio toward higher frequencies (with an average index $\alpha_{RO} = 0.63$) and it is still rising in the IR/optical band. At 1 keV the intensity is 20% larger than in the optical (in νL_ν) but the X–ray spectrum is rather steep (α_X= 1.45) indicating that the SED has already reached its peak, which must be thus located in the interval $10^{15} - 10^{16.5}$ Hz.

• **3C 270**. This SED is characterized by the sharp decline in the IR/optical range described by a spectral index $\alpha \sim 3.5$. Clearly dust absorption can play a significant role in producing this rapid decline. However its spectrum in the X–ray band, as also measured by ASCA, indicates that the minimum observed at optical energies is real, although possibly enhanced by the presence of dust. Moreover, its representative point is not located significantly below the radio-optical correlation described by Chapter 2, arguing against an obscuration larger than average.

• **3C 465**. After rising from the radio to the optical ($\alpha_{RO} = 0.83$), the SED of 3C 465 is already falling at higher energies as the X–ray upper limit lies below the optical point. This indicates that also in this

case a peak in the emission is reached below the X–ray band, although the poorly determined SED does not allow us to better constrain its location.

• **NGC 7052**. The average radio-to-optical spectral index is $\alpha_{RO} = 0.80$. Contrarely to what seen in 3C 270, the nuclear source in NGC 7052 is (marginally) fainter in the infrared than in the optical band. This indicates that, although the extended disk is seen at the highest inclination ($\sim 70°$) and has a very large optical depth, the nuclear emission is not significantly affected by dust obscuration. The upper limit derived from the RASS requires a steepening of the SED slope at higher energies.

Summarizing, the nuclear SED of the selected FR I present a wide variety of behaviors. However three common features can be recognized: i) it always rises from the radio to the infrared/optical; ii) no SED can be described as a single power law; iii) for all of the sources with pointed X–ray data the presence of a peak in the emission can be localized at energies lower than soft X–rays.

5.5 Discussion

5.5.1 Comparison of the SED of FR I and BL Lacs

Let us now compare the SED of FR I with those of BL Lacs. Despite of the poor spectral coverage of the FR I SED (somewhat reminiscent of the SED coverage of BL Lac objects in the 80s), it is possible to recognize a qualitative similarity with the SED of blazars, and in particular the likely presence of one broad peak (see Fig. 5.2). In fact, as discussed in Section 5.4, the spectra appear to raise from the radio to the IR/optical band, and in all cases - except for NGC 7052 - the X–ray information (flux and/or spectrum) suggest that a peak in the SED occurs at lower energies.

In the specific case of 3C 270 the flat X–ray spectrum is plausibly due to the dominance of a rising Compton component in this band.

And interestingly its extremely steep IR-optical spectrum seems to indicate the presence of a minimum, fully consistent with the indications derived from the X–ray spectral shape. Agreement between the hints inferred from the IR/optical and X–ray spectra is also found in the SED of 3C 264 in which the X–rays can be interpreted as the steep high energy cut-off of the synchrotron component.

Clearly, the paucity of spectral information limits any detailed analysis and in particular does not allow us to determine the location of the energy peak precisely enough to identify the 'type' of blazar putatively hosted in the radio galaxies, except possibly for 3C 270 and 3C 264, which resemble an LBL and HBL, respectively.

Nevertheless, it is possible to profitably use the available data to compare the broad band spectral indices with those of BL Lacs, as shown in Fig. 5.3 where complete samples of BL Lacs (and FSRQ) are considered. Three out of the four radio galaxies (3C 31, 3C 264 and 3C 465) lie in the area occupied by FSRQ and LBL. Particularly puzzling is the case of 3C 264. In fact this source is observed at a small angle with respect to the jet axis, re-enforcing the view that its nucleus should be rather similar to that of a BL Lac. Furthermore its SED suggests that the putative synchrotron peak is located between the optical and X–ray bands, analogously to HBL, in contrast with its position in the spectral index planes. The fourth source, 3C 270, is located on its own in the upper left corner of the diagrams.

However, as discussed in detail by Chapter 4 relativistic beaming can have strong effects on the position of the source in the $\alpha_{\rm ro}$–$\alpha_{\rm ox}$ plane. Due to the shift in energy caused by beaming, these quantitatively depend on the shape of the SED if there are changes in the spectral slope (even in the simplest case in which the degree of beaming does not depend on energy). The transformation law for broad band spectral indices, derived in Appendix A and reported here for clarity, is

$$\alpha_{\rm BLLac} - \alpha_{\rm FR\ I} = (\alpha_1 - \alpha_2)\frac{\log(\delta_{\rm BLLac}/\delta_{\rm FR\ I})}{\log(\nu_2/\nu_1)},$$

where α_1, α_2 are the radio, optical or X-ray spectral indices and $\delta_{\rm BLLac}$, $\delta_{\rm FR\ I}$ are the relativistic beaming factors.

For 3C 264 and 3C 270, for which α in both the optical and X-ray bands are measured, we can determine "beaming tracks", i.e. the changes of the broad band spectral indices for increasing Doppler boosting (Fig. 5.3), adopting $\alpha_r = 0$. For 3C 264, since the SED slope in the X–ray is steeper than in the IR/optical and radio bands, blue-shifting the SED has the effect of reducing all spectral indices. Its representative point thus moves toward the origin in both the $\alpha_{\rm ox}$–$\alpha_{\rm ro}$ and $\alpha_{\rm ox}$–$\alpha_{\rm rx}$ planes and the beaming track crosses the region in which HBL are located. Similarly, the track of 3C 270 intercepts the region typical of LBL. [2] For both objects, the inconsistency between SED shape and the values of the spectral indices might be thus resolved, once the effects of beaming are properly taken into account.

We note, however, that the beaming factor required in the case of 3C 264 is $\delta_{\rm BLLac}/\delta_{\rm FR\ I} \sim 10 - 100$ (the beaming correction for 3C 270 is heavily dependent on possible effects of dust extinction and thus is not quantitatively reliable). As the nuclear luminosity increases as $\delta^{p+\alpha}$ (with $p = 2 - 3$), when seen pole-on 3C 264 would be 3 - 6 orders of magnitude brighter in the optical band (where $\alpha \sim 1$ and for $p = 2$). This is only marginally consistent with the estimates of the ratio between its luminosity and that of BL Lacs of similar extended (isotropic) power, which are only $\sim 10^2 - 10^3$ times brighter (CC99). Furthermore, the radio luminosity of BL Lacs appears to be univocally connected with their SED (Fossati et al. [48]). As the nuclear radio luminosity of 3C 264 is $\nu L_\nu \sim 10^{39.9}$ erg s^{-1}, if seen pole-on this would increase by $\sim 10^2 - 10^4$ (again for $p = 2$) reaching values which are typical of LBL and higher than those seen in HBL (Fossati et al. [48]). Indeed, in Chapter 4 we have found a similar problem when comparing

[2] As dust absorption can cause an enhancement of the minimum in the IR/optical region of the SED of 3C 270, we also estimated its 'beaming track' allowing for the presence of extinction. This turns out to be similar to the case of no absorption.

the luminosities of complete samples of FR I and BL Lacs: FR I appear to be overluminous with respect to what is expected by debeaming the BL Lacs emission, modeled with a single emitting component.

Summarizing, the SED of FR I are qualitatively similar to those of BL Lac objects, supporting the identification of these sources as their mis-oriented counterparts, but their intensity does not seem to be compatible with the simplest model in which we are observing a single beamed emitting component in both classes of objects. As discussed in Chapter 4, this discrepancy can be ascribed to a velocity structure within the relativistic jet and that in FR I the emission is dominated by components/regions moving slower than those seen in BL Lacs.

5.5.2 X-ray emission and radio-galaxy orientation

Following the method developed by CC99, we compare the luminosity of FR I nuclei with that of BL Lac objects in the X-ray band. In order to restrict the comparison to objects which potentially belong to the same region of the luminosity function of the FR I/BL Lacs population, we identify BL Lacs whose isotropic properties are similar to those of our radio-galaxies. More specifically, we consider objects whose extended radio luminosity (data taken from Kollgaard et al. [79]) differs by less than a factor of two from each of our FR I. [3] We thus selected between 6 and 10 'relatives' for each FR I. Their X–ray fluxes (1 keV rest frame energy, corrected for absorption) and spectral indices in the ROSAT band are taken from Lamer et al. ([84]) and Urry et al. ([151]). The X-ray nuclear emission of FR I is fainter than that of BL Lacs by a factor which ranges from ~ 10 up to 3×10^4.

For a given FR I, the X-ray luminosity ratios with respect to the different 'relative' BL Lacs present a very large dispersion, of $2 - 3$

[3] With respect to CC99, we dropped the further requirement of similar host galaxy magnitude since this does not appear to correlate with the nuclear properties neither in BL Lacs nor in FR I. This less restrictive choice enables us to increase the number of BL Lac counterparts for each FR I.

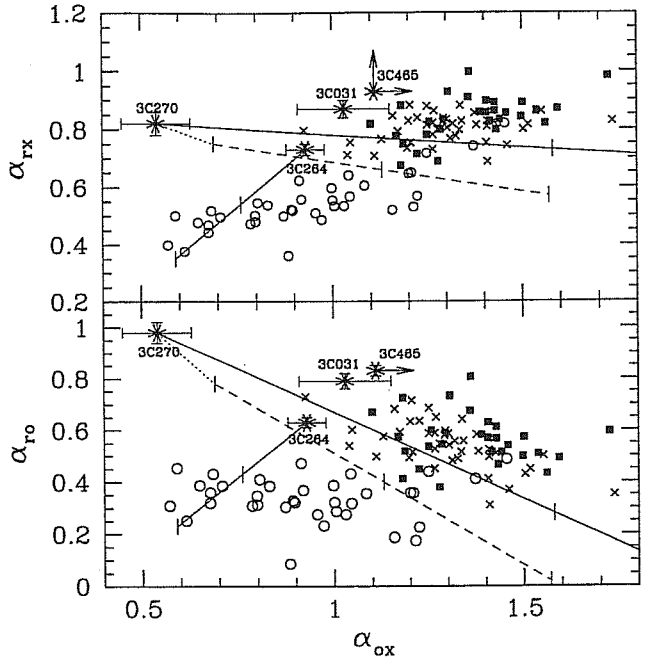

Figure 5.3: Broad band spectral indices of the FR I nuclei (large stars) compared to those of blazars (circles are XBL, crosses ad squares are RBL and FSRQ, respectively), as from Fossati et al. ([48]). Continuous lines represent the variations of spectral index due to the shift in energy of the Doppler boosting. Ticks on the lines correspond to a increase of δ by 10 and 100. The dashed line follows the beaming track of 3C 270 after a correction for absorption corresponding to $A_R = 2$.

orders of magnitude, and therefore, contrarily to what is found in the optical band (CC99) we cannot draw any conclusion on whether a trend with orientation is present.

5.6 Conclusions

We used ROSAT and HST observations to isolate the emission originating from the nuclei of 5 FR I sources with the aim of studying their Spectral Energy Distributions. For the ROSAT PSPC observations,

in order to disentangle the nuclear non-thermal emission from that of the host galaxy halo, we performed fits allowing for the presence of both a thermal and a power–law component: in the case of 3C 264 the emission is dominated by a power law spectrum; in 3C 31 and 3C 270 the inclusion of the non–thermal component improves the fit, while this is not required in 3C 465. A nuclear source is clearly seen in the HST/NICMOS infrared images, available for 3 objects.

Combining the measurements in the X-ray and IR band with optical nuclear luminosities derived from HST/WFPC2 images and radio data taken from the literature, we have been able to build for the first time the SED of FR I nuclei.

These indicate the presence of a peak between the IR and the soft X–ray bands, and the X–ray slopes are consistent with the broad band indications. For the two best constrained SED, it is also possible to tentatively classify the FR I nuclei similarly to what is done for BL Lacs, in High and Low Energy Peaked sources. This turns out to agree with that derived from the comparison of the broad band spectral indices once the changes in the SED due to the beaming are properly taken into account. However, the intensity of the nucleus of 3C 264 does not appear to be compatible with the simplest model in which we are observing a single beamed emitting component in both FR I and BL Lacs. The SED of FR I are thus qualitatively (but not quantitatively) similar to those of BL Lacs.

The proposed approach of comparing the SED of the parent and beamed population appears to be promising. Better data and energy coverage are clearly required, particularly in the X–ray band, as the spectral shape at these energies is essential in giving clues on the frequency range where most of the synchrotron emission is released and thus in 'classifying' FR I sources similarly to what is done for BL Lacs. Both the AXAF and XMM missions will soon provide us with X–ray spectra for large, and especially complete, samples of FR I. However, there is one radio galaxy for which a sufficiently large set of photomet-

ric data is already available to build a well sampled SED: the closest radio galaxy Centaurus A. This object will be discussed in details in the next chapter.

Chapter 6

The BL Lac heart of Centaurus A

Modeling of the SED is a fundamental tool for obtaining information on the physical conditions of the emitting region, as it is usually done for blazars (e.g. Ghisellini et al. [49]). Unfortunately, as it has been pointed out in the previous chapter, nuclear SED of radio-galaxies are in general not sufficiently well described to follow directly the same approach.

Centaurus A is the closest radio galaxy ($d = 3.5$ Mpc (Hui et al. [72]) and it is the only radio galaxy for which a large set of photometric data are available, from the radio to the gamma ray band. In this chapter we collect such data from the literature and we build the overall nuclear SED, which appears to be remarkably similar to those of blazars (Sect. 6.1). In Sect. 6.2 we briefly describe the synchrotron self-Compton scenario (SSC) and in Sect. 6.3 we apply such model to the SED of Centaurus A, and discuss the obtained physical parameters. In Sect. 6.4 we analyze the problem of the absorption in this source, and in Sect. 6.5 we summarize our findings.

6.1 Building the nuclear SED

In order to build the overall nuclear SED of Centaurus A, we collected from the literature the nuclear fluxes spanning the widest range of frequencies, from the radio to the gamma-ray band (see Table 6.1).

Starting from the highest energies, we consider the gamma-ray data taken in 1991 by OSSE, COMPTEL and EGRET instruments on board CGRO, which are the only published simultaneous data in such bands (Steinle et al. [136]). The source was observed for two weeks, and appeared to be in an intermediate emission state. This high energy emission shows interesting similarities with gamma-ray blazars, and it has been interpreted as due to inverse Compton scattering of softer photons. The *X–ray* data reported in the SED refer to the *Beppo*SAX MECS+PDS 1998 observation (Grandi et al. [58]), and the RXTE ones are from Rothschild et al. ([127]). The near-IR nuclear component is clearly seen in the HST/NICMOS images and its optical counterpart has been identified in the I and V bands (Marconi et al. [97]). A power law has been fitted to the mid-IR continuum emission in the ISO spectrum published by Mirabel et al. ([104]). From the same paper we also derived the sub-mm SCUBA measurements, while JCMT (James Clerk Maxwell Telescope) data are from Hawarden et al. [65]. The radio band is covered by VLA observations (Burns et al. [19]). These data produce the observed SED shown in Fig. 6.1 in a $\log(\nu L(\nu)) - \log \nu$ representation.

The SED appears to be surprisingly similar to that of blazars. Indeed, it is composed by two broad peaks, the lower-energy one reaching its maximum in the far-IR, between 10^{12} and 10^{13} Hz, while a well defined maximum is present at about 0.1 MeV. It is worth noting that about the same amount of energy is emitted in the two peaks, the high energy one being possibly the dominant spectral component of the nuclear emission. In the frame of the AGN unification scheme, this is (qualitatively) what expected in a misaligned BL Lac object, in which

the low energy peak is attributed to synchrotron emission and the high energy one being adduced to inverse Compton scattering of softer photons. Although absorption from the dust lane plays an important role, the double-peaked shape of the SED of Centaurus A is well determined regardless of the amount of extinction. In particular, the low energy emission peak is defined by the flat slope in the sub-mm region and by the steep ISO spectrum, and absorption could heavily affect the optical and near–IR bands, leaving instead essentially unchanged the mid and far–IR regions of the spectrum. As this is indeed a crucial point in the modeling of the nuclear SED we will discuss it more thoroughly in the following.

However, as the prominent kpc scale dust lane of Centaurus A certainly causes significant extinction[1], we de-reddened the observed data points using $A_V \sim 8$ and adopting the reddening law of Cardelli et al. ([27]). The corrected SED is presented in Fig. 2. The main effect of this procedure is to substantially reduce the depth of the SED minimum at $\nu \sim 10^{15}$ Hz.

In the frame of the unification schemes it is qualitatively expected to observe a misaligned-blazar SED, and the double-peaked shape of the SED observed in Centaurus A is therefore a clue that its nuclear emission might be interpreted as due to non-thermal synchrotron and inverse Compton emission. We will explore this possibility in the next section, modeling the observed SED in order to obtain information on the physical parameters of the source.

6.2 The synchrotron self-Compton scenario

As already pointed out in chapter 1, in blazars the low and high energy peaks are thought to be produced through the synchrotron and inverse Compton processes, respectively. For the lowest luminosity objects

[1]Marconi et al. ([97]) found color excesses as high as E(B-V) ~ 2.5 in the circumnuclear regions and this can be considered as a lower limit to the nuclear absorption

Table 6.1: References for the nuclear fluxes of Centaurus A

Instrument	Reference
VLA	Burns et al. 1998
JCMT	Hawarden et al. 1993
SCUBA	Mirabel et al. 1999
ISOCAM	Mirabel et al. 1999
HST/NICMOS	Marconi et al. 2000
HST/WFPC2	Marconi et al. 2000
*Beppo*SAX	Grandi et al. 1999
RXTE	Rothschild et al. 1999
CGRO	Steinle et al. 1998

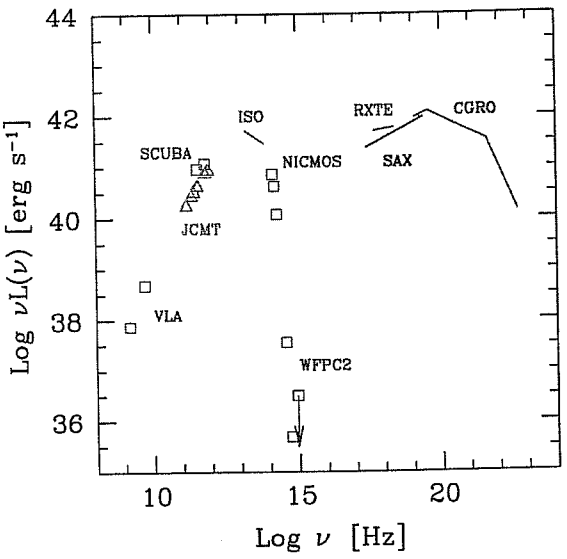

Figure 6.1: The observed spectral energy distribution of the nucleus of Centaurus A (see text).

(i.e. BL Lacs) the contribution of the external photon field is probably small, and the SED is well fitted by the synchrotron self-Compton model (Ghisellini et al. [49]).

According to the unified models, the beamed counterpart of Centaurus A should appear as a faint BL Lac, as its total radio power is $\log L_{408} = 31.5$ erg s^{-1}, which is in the same range of luminosity of the weakest BL Lacs. Furthermore, the absence of strong broad emission lines in its spectrum, indicates the lack of substantial external photons to be Compton-scattered towards high energies. All these things appear to suggest that the emission observed can be interpreted as synchrotron and SSC radiation from the *BL Lac heart* of Centaurus A.

6.2.1 The model

The simplest geometrical representation of the source is a spherical homogeneous region, embedded in a tangled magnetic field. Relativistic electrons (distributed in energy as a power-law of index p, between γ_{min} and γ_{max}, γ being the Lorentz factor), are continuously injected at a rate $Q(\gamma)$ [cm^{-3} s^{-1}] $\propto \gamma^{-p}$ and they loose their energy radiatively. The free parameters of the model are: the size of the source R, the magnetic field B, the injected luminosity L_{inj}, the relativistic beaming factor δ, γ_{min}, γ_{max} and the slope p. The resulting electron distribution is, at the equilibrium, a broken power-law. on the model and the method used for obtaining the equilibrium solution, see Ghisellini et al. [49] and Chiaberge et al. [30].

When the Klein-Nishina decline of the cross section for Compton scattering and pair production effects can be neglected, the physical parameters of the source are well constrained once that the position and the intensity of the peaks of the SED are known. Indeed, as a first step, we can analytically evaluate the physical parameters of the source knowing the frequencies and luminosities of the synchrotron and Compton peaks, together with an estimate of the variability time scale. The electron distribution energy break γ_b, the magnetic field B and the

beaming factor δ can be obtained with the simple expressions relating them to the observed quantities (e.g. Ghisellini, Maraschi & Dondi [50]). In the case of Centaurus A, one can identify the position of the high energy peak $\nu_c \sim 3 \times 10^{19}$ Hz, while the low energy one is at $\nu_s \sim 10^{13}$ Hz. Adopting such values, we can derive the value of γ_b and the product $B \times \delta$:

$$\gamma_b = \left(\frac{3}{4}\frac{\nu_c}{\nu_s}\right)^{1/2} = 1.5 \times 10^3$$

$$B\delta = \frac{\nu_s}{3.7 \times 10^6 \nu_c} = 0.9\mathrm{G}$$

The values of B and δ can be determined using the peak luminosities (in units of 10^{45} erg s^{-1}) and the variability timescale[2] $t_d \sim 1$ (in days) as additional constraints:

$$\delta = 1.67 \times 10^4 \left(\frac{\nu_c}{\nu_s^2 t_d}\right)^{1/2} \left(\frac{L_{C,45}^2}{L_{s,45}}\right)^{1/4} \sim 1.6$$

where $t_d = 1$, $L_{s,45} \sim L_{C,45} = 10^{-3}$ are used, and

$$B = 2.14 \times 10^{-11} \frac{\nu_s^3 t_d^{1/2}}{\nu_c^{3/2}} \left(\frac{L_{C,45}}{L_{s,45}^2}\right)^{1/4} \sim 0.7\mathrm{G}$$

A more refined model, extensively described in Chiaberge & Ghisellini ([30]), leads to a more precise solution for the electron distribution at the equilibrium, taking also into account both the Klein-Nishina effects and the possible escape of the electrons from the source, occurring in a timescale t_{esc}. This can be achieved by numerically obtaining the stationary solutions of the continuity equation, which governs the temporal evolution of the electron distribution:

$$\frac{\partial N(\gamma,t)}{\partial t} = \frac{\partial}{\partial \gamma}\left[\dot{\gamma}(\gamma,t) N(\gamma,t)\right] + Q(\gamma,t) - \frac{N(\gamma,t)}{t_{esc}} = 0$$

[2]The minimum variability time scale of ~ 1 day is determined from the OSSE observations (Kinzer et al. [78]), although shorter time scales variations have been observed.

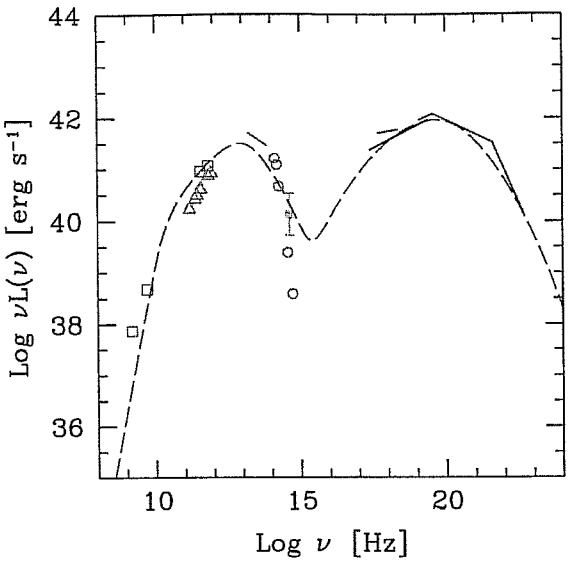

Figure 6.2: The nuclear SED of Centaurus A. The empty circles represent the optical and near-IR luminosities de-reddened with $A_V = 8$. The dashed line is the fit with the SSC model described in the text. The filled circle with the large error bar represents the optical luminosity predicted using the radio-optical correlation found for FR I in chapter 2.

where $\dot{\gamma} = \dot{\gamma}_S + \dot{\gamma}_C$ is the total (synchrotron + self–Compton) cooling rate. The fit to the SED of Centaurus A obtained with this method is represented as the dashed line in Fig. 6.2, and the corresponding model parameters are listed in Table 6.2.

6.3 The physical parameters of Centaurus A nucleus

In Table 6.2 we have reported the physical parameters used to fit the SED of Centaurus A. All of them are typical of blazars except for the beaming factor, which is lower. A lower δ is qualitatively expected in the frame of the unified models, however, from VLBI information (jet-counterjet ratio) it has been found that the jet is observed at an angle between 50° and 80° (Tingay et al. [146]). Therefore, if we assume $\Gamma \sim 15 - 20$ as typical bulk Lorentz factors for a BL Lac, a much lower δ is expected at such large angles of view. In fact, for the above range

Table 6.2: Model parameters

	Centaurus A	Low Luminosity BL Lacs
R	1.2×10^{16} cm	10^{16} cm
B	0.5 G	0.44 G
δ	1.2	15 (fixed "a priori")
L_{inj}	2.7×10^{42} erg s^{-1}	2.6×10^{41} erg s^{-1}
p	3.0	3.0
γ_{min}	2×10^3	2.5×10^4
γ_{max}	1×10^4	1.0×10^6

R is the size of the source; B is the magnetic field; L_{inj} is the injected power (in particles of energy equal to $\gamma m_e c^2$); the injection function is of the kind $Q(\gamma) \propto \gamma^{-p}$, starting from γ_{min} and with an exponential cutoff at γ_{max}; δ is the beaming factor. For comparison, we have reported the parameters obtained from the fit (same emission model) to the average SED of blazars with observed luminosity at 5 GHz $\log L_r = 41.5$ (from Ghisellini et al. [49]).

of viewing angles, such velocities imply a δ factor between 0.18 and 0.06. In the frame of the unification models, aligned and misaligned objects must share the same range of (unbeamed) extended radio luminosity, which, for Centaurus A, is in the range of the faintest BL Lacs included in the *Einstein* Slew Survey ($L_{1.4} \sim 10^{29} - 10^{30}$ erg s^{-1}). If we set $\delta = 0.2$, a reasonably good fit to the SED can be still produced, but the magnetic field becomes more than 1 order of magnitude higher than the value found in low luminosity BL Lacs. Notice that luminosity depends on δ^4, therefore small changes in the beaming factors imply large changes in the observed luminosity. Therefore, the other physical parameters of the source must be changed significantly. For lower values of δ the radius of the source exceeds the limit implied by variability constraints. In addition to this, the injected luminosity L_{inj} should be $\sim$ 4 order of magnitude higher than what is found in faint BL Lacs.

Although we cannot exclude the possibility of $\delta \sim 0.2$, we note that a Lorentz factor of $\sim$ 1 is consistent with what we found in the

comparison between the optical and radio nuclear emission of complete samples of FR I and BL Lacs (chapter 4). In that case we postulated that a simple two velocity jet model (a fast *spine* with $\Gamma \sim 15 - 20$ and a slower layer with $\Gamma \sim 1.5$) could account the different observed properties of these classes of sources. Since for Centaurus A we have an indication of the viewing angle from VLBI information, given δ we can estimate the Γ factor. In the range of angles expected for this source, the equation for Γ has two possible values for $\theta < 57°$, the higher value of Γ being ~ 1.8 (at $\theta = 50°$). For $\theta = 57°$, the (unique) solution for Γ is 1.2. [3] On the other hand, if a velocity structure is not present in the jet of Centaurus A, and a lower δ is required, the other physical parameters of the source change, as noted above, and become significatively different from those usually found in BL Lacs of the same power. Therefore, the emitting region in the aligned and misaligned objects must be in any case different.

6.3.1 Centaurus A and the blazar sequence

We can further compare the physical parameters and the SED of Centaurus A with those of blazars, in the frame of the trend between the overall spectral properties and the radio luminosity found by Fossati et al. [48] and modeled by Ghisellini et al. [49]. In fact, for the beamed sources, the position of the peaks of the SED, the bolometric luminosity and the relative dominance of the Compton component versus the synchrotron one show a significant trend with the radio luminosity at 5 GHz. This is reflected in the different physical parameters obtained from the spectral fitting to the SED of objects with different luminosities. The position of the peaks in the SED is similar to Flat Spectrum Radio Quasars, the highest luminosity sources of the blazar family. The synchrotron components of BL Lacs with extended radio power similar

[3] Notice, however, that if we adopt the jet velocity inferred from VLBI information ($\beta > 0.45$, which correspond to $\Gamma = 1.12$, Tingay et al. [146]) only the highest of the two solutions is acceptable.

to Centaurus A reach their maximum at very high energies, generally in the X-ray band, therefore this shift cannot be adduced only to a different amount of beaming. Therefore, if velocity structures in the jet are indeed present, it is plausible that the physical conditions (e.g. the intensity of the magnetic field and/or the injected electron distribution) in the external layer might be different from those of the spine. From the spectral analysis of one single object it is not possible to draw any conclusion on this issue, however it appears that the injected electron distribution needed for modeling the SED of Centaurus A are narrower in energy and reach lower Lorentz factors with respect to faint BL Lacs (see Table 6.2).

6.4 The origin of the near-IR emission

As already pointed out above, although the double-peaked shape of the SED is well defined, regardless of the amount of absorption, a crucial point is to determine the nature of the source observed in the near-infrared (and optical) band, which is still debated. Two are the proposed scenarios: i) emission from the jet observed directly (Bailey et al. [5]); ii) scattered light from a central hidden source (e.g. Antonucci & Barvainis [3]). We analyze this issue in the following. Notice that the following considerations are independent of the above spectral modeling, although they also lead to a synchrotron origin for this emission.

In fact, concerning the former interpretation, we must consider that the measured optical (V) flux is $\sim 11 - 13$ mag fainter than the one predicted with the radio-optical core correlation (the filled circle in Fig. 6.2) for FR I radio galaxies chapter 2. If this is interpreted as due to absorption, it translates in a value of A_V which is consistent with the ones derived both from mid-infrared information and from the color distribution outside and inside the dust lane, close to the nucleus (Marconi et al. [97]). However, it is well known that the

estimate of the nuclear absorption from X-ray observations (Grandi et al. [58], Rothscild et al. [127]) leads to much a higher A_V ($\sim$ 50 mag, assuming galactic dust to gas ratio). If this value is adopted, the resulting K-band de-reddened luminosity (νL_ν) should be a factor $\sim$ 40 higher than the ISO ones. In this case, the optical emission should be completely absorbed.

On the other hand, the presence of a high level of IR polarization (11.1%), perpendicular to the jet direction, has been interpreted as a sign of scattered light from a hidden nucleus. We must point out, however, that other radio galaxy nuclei show the same behaviour (e.g. M 87) and these are certainly observed directly. The absence of obscuring tori in FR I appears in fact to be a characteristic of such class of sources, even if some exceptions cannot be ruled out, at present. Furthermore, in the case of scattered light from a central source, after correction for the dust lane absorption, one can evaluate the efficiency of the scattering process for the near-IR flux not to exceed largely the mid-IR one (which is assumed to be pure nuclear emission, or possibly overestimated, due to the limited spatial resolution of the observing instruments). Considering an $A_V = 15$ mag, the de-reddened K-band luminosity would then be $\nu L_\nu \sim 3 \times 10^{41}$, approximately equal to the ISO one. Therefore, unplausible high scattering efficiencies (in the IR!) should be required.

We conclude that the most likely (and also the simplest) picture for the nuclear emission of Centaurus A is that we are directly observing the inner jet radiation at all wavelengths, heavily hidden in the optical only by the presence of the dust lane. However, the origin of the large discrepancy between the amount of absorption estimated using different (X-ray and optical-IR) methods, analogously to what is found also in other classes of AGNs (e.g. Granato, Danese & Franceschini [57]), has to be further investigated.

6.5 Conclusions

We have built for the first time the overall nuclear Spectral Energy Distribution of Centaurus A, the only radio galaxy for which nuclear data from the radio to the gamma ray band are available. The SED appears to be remarkably similar to that of blazars, as in a $\nu - \nu L_\nu$ representation it is composed by two broad peaks, regardless the amount of absorption.

Although we cannot exclude that the observed emission at different wavelengths might be produced by different components, and that more complex models could reproduce the nuclear SED of Centaurus A, we have shown that a simple one zone, homogeneous SSC model is sufficient to account for the overall spectrum. In the frame of the unification models it is indeed expected to observe the misaligned blazar emission. It is possible to fit the SED with physical parameters which are similar to those usually found for low luminosity BL Lacs, except for a lower beaming factor. However, this beaming factor is not compatible with being originated by a misoriented fast ($\Gamma \sim 15-20$) blazar component. Possible solutions are either the presence of velocity structures in the jet, in analogy with what has been found in the comparison of complete samples of BL Lacs and radio galaxies (chapter 4), or a lower jet velocity ($\Gamma < 10$).

Chapter 7

Conclusions and future perspectives

The main thread of the work presented in this thesis is the investigation of the very innermost regions of radio galaxies with Hubble Space Telescope images. Thanks to the high resolution and sensitivity of the HST, nuclear components directly related to the active nucleus are detected in the great majority of a complete sample of FR I and in about half of complete samples of FR II. Our results show that the central compact cores (CCC) of FR I appear to be strongly connected with the radio core emission and they appear to radiate anisotropically. We have proposed that they are the optical counterparts of the radio cores, and that we are indeed observing optical synchrotron radiation produced in the inner regions of a relativistic jet, indicating that we have a direct view of the innermost regions of the AGN, inside $100R_S$. This can be considered the main result of the work presented here, and also rise the following interesting key issues.

- *FR I have unobscured synchrotron nuclei and low accretion rates*

The high detection rate of CCC casts serious doubts on the presence of obscuring thick tori in FR I as a whole, and therefore the lack of broad

emission lines in FR I cannot be adduced to obscuration. Given the dominance of non-thermal emission, the CCC luminosity represents a firm upper limit to any thermal component, which translates into an optical luminosity of only $\lesssim 10^{-5} - 10^{-7}$ times the Eddington one (for a $10^9 M_\odot$ black hole). This limit suggests that accretion might take place in a low efficiency radiative regime.

The picture which emerges is that the innermost structure of FR I radio galaxies differs in many crucial aspects from that of the other classes of AGN; they lack the substantial BLR, tori and thermal disc emission, which are usually associated with active nuclei. These results are qualitatively consistent with the unifying model in which FR I radio galaxies are misoriented BL Lac objects.

From our analysis there is evidence that things might change for objects of increasing luminosities. Therefore, we have extended this study to higher luminosity radio galaxies, in order to determine if either a continuity between low and high luminosity sources exists or, alternatively, they represent substantially different manifestations of the accretion process onto a supermassive black hole. Another important issue is to explore how the differences in radio morphology are related to the optical nuclear properties. In the case of nearby FR II ($z < 0.1$), we detected optical cores in half of the sample. This is in fact by itself an unexpected result, as it infer a covering fraction of any obscuring material which is less than ~ 0.5, or equivalently, an opening angle of the putative torus of $\sim 60°$. Our determination of the critical angle between obscured and unobscured sources appears therefore to be inconsistent with the division between higher redshift ($0.5 < z < 1$) 3CR quasars and radio galaxies, which has been found to be $\theta \sim 45°$ (Barthel [6]).

• *The FR I/FR II dichotomy revised*

We have then compared the nuclei of FR II and FR I, in the plane defined by the optical and radio core luminosities. Our results suggest

that there is not a single homogeneous population of low redshift FR II: unlike FR I, they show a complex behavior, which is however clearly related to their optical spectral classification. In BLRG optical nuclei are likely to be dominated by thermal (disc) emission. In agreement with the current unification scheme of radio loud AGNs, we also identify their possible obscured counter–parts. It seems that broad lines and obscuring tori are closely linked and both are present only associated to radiatively efficient accretion.

Most importantly, we also find five FR II sources, spectrally identified as narrow or weak lined objects, which harbor nuclei essentially indistinguishable from those seen in FR I. By analogy with FR I, we argue that their optical nuclear emission is produced primarily by synchrotron radiation, they are not obscured to our line of sight and therefore intrinsically lack a BLR.

The radio morphology appears to be not univocally connected with the optical properties of the innermost structure of radio galaxies. Clearly, a classification based on the optical nuclear properties, as seen in the HST images, is more likely to reflect true similarities (or differences) on the nature of the central engine (such as, e.g., the rate of radiative dissipation in the accretion disc) than the traditional dichotomy of radio morphology.

These results have also interesting bearings from the point of view of the unified models between blazars and radio galaxies. In fact, this picture argues against the idea that all FR II radio galaxies constitute the parent population of radio-loud quasars. We propose instead that galaxies with FR II morphology and an FR I-like core are possibly mis-aligned counter–parts of BL Lac objects. This can account for the observation that some radio-selected-type BL Lacs show radio morphologies more consistent with FR II than with FR I (e.g. Kollgaard et al. [80]).

- *Future perspectives for the study of FR I and FR II*

The synchrotron dominance in the nuclear emission of FR I can be further tested through polarimetric observations. We have proposed to obtain UV imaging polarimetry of a sample of FR I with the HST, in order to determine both the degree of polarization of the optical cores (and thus to definitively establish their synchrotron origin) and to search for polarized beams in the near vicinity of the nucleus. If the unifying picture is correct, polarization "cones" are expected in FR I, in circumnuclear regions where the collimated beamed emission is scattered into our line of sight.

Other intriguing aspects are both the apparent lack of broad emission lines in the FR I class as a whole and the relationship between the presence/absence of emission lines with the innermost nuclear structures among FR II. This uncertainty rises mainly from the lack of spectroscopic data on the 3CR sources which, when available, is however inadequate, in particular in order to set useful upper limits to the broad components. Again, similarly to the case of the detection of faint nuclear components, the main reason for this is the difficulty to obtain "pure" nuclear spectra of sources which are dominated by the stellar emission, in ground based observations. Therefore, spectroscopic HST observations of both FR I and FR II are needed to significatively enhance the contrast between the nuclear source and the underlying stellar component.

The most intriguing result of our study of FR II is the discovery of objects with FR I–like synchrotron dominated optical cores. As already pointed out, this is unexpected in the frame of the AGN overall picture, as narrow lined objects are believed to contain hidden quasars. This finding can be further tested through infrared observations, as in the optical band these observations are strongly affected by dust obscuration. We have requested (and obtained) observing time at the Telescopio Nazionale Galileo (La Palma, Canarias) to perform K–band imaging of all 3CR sources with $z < 0.3$. If a hidden quasar is present, a nuclear excess in the brightness profile of the galaxy should be easily

observed at such wavelengths and at the TNG resolution.

- *The FR I – BL Lac unification and clues for jet velocity structures*

The identification of optical cores of FR I radio galaxies with misoriented BL Lac emission has opened the possibility of studying this class of AGNs from a different line of sight. This is be particularly useful in understanding the jet structure and the level of the activity occurring near the central object whose emission in blazars is swamped by the highly beamed component. With the aim of exploring the viability of the unification scenario between (HBL, LBL) BL Lacs and FR I radio galaxies we have compared their nuclear emission in the radio, optical and (with much less reliability) X–ray bands. The values of the bulk Lorentz factors inferred by the direct comparison of the inner jet emission are not compatible with the higher bulk velocities requested by theoretical arguments, such as the pair production opacity and the spectral modeling of the SED of BL Lacs. As a natural consequence of this inconsistency, we also found that the simple one-zone model does not account for the observed spectral properties of FR I.

The simplest and rather plausible hypothesis to account for this observations within the unification scenario, is to assume a structure in the jet velocity field, in which a fast spine is surrounded by a slow (but still relativistic, $\Gamma \sim 2$) layer. The observed flux is dominated by the emission from either the spine or the slower layer, in the case of aligned and misaligned objects, respectively. Interestingly, the existence of velocity structures in the jet has been suggested by various authors (Komissarov [83], Laing [86], Laing et al. 1999) in order to explain some observed properties of FR I (and FR II) radio jets, but on larger scales. Also, the same indication has been found through a different approach: Capetti & Celotti [23] reveal a trend in the radio galaxy/BL Lac relative powers with the line of sight, which is consistent with a slower (less beamed) component dominating at the largest angles.

• *The SED of FR I radio galaxies* Combining the measurements in the X-ray and IR band with optical nuclear luminosities derived from HST/WFPC2 images and radio data taken from the literature, we have been able to build for the first time the SED of FR I nuclei. We have shown that the study of better sampled SED of five radio galaxies and the comparison with their beamed counterparts is compatible with the presence of a slower relativistic layer which dominates the emission observed in the misaligned object at all wavelengths. Clearly, this kind of studies is still at the very beginning, and much has to be understood on the dynamics and emitting properties of relativistic jets. Multifrequency studies of the nuclear properties of beamed sources and their parent populations and their comparison – according to unification scenarios which are well supported by other independent indications – constitute a new and powerful tool to achieve that, both for well studied individual sources as well as complete samples. Near IR observations by HST, mm data and higher resolution and sensitivity by Chandra and XMM in X–rays, and in the future GLAST, which will observe between 20 MeV and 300 GeV and will be at least 30 times more sensitive than EGRET, will further open this possibility.

• *The case of Centaurus A: a BL Lac heart in the closest radiogalaxy* The only radio galaxy for which a nearly complete coverage of the nuclear spectral energy distribution exists, from the radio to the gamma-ray band, is Centaurus A. We have shown that its overall emission can be satisfactorily explained and well reproduced by a homogeneous one-zone SSC emission model. The physical parameters obtained from modeling the SED are perfectly compatible with those obtained for blazars. This result represents a direct confirmation of the unification schemes between BL Lacs and FR I radio galaxies.

Summarizing, the picture of radio galaxies which emerges from our HST study is that the old classification based on a morphologic criterium

is not indicative of the physical structure of the nucleus as inferred by optical imaging. In particular, it appears that the low-luminosity sources (which are morphologically classified as FR I) present many differences from other AGNs, as they lack substantial Broad Line Region, radiatively efficient accretion and dusty obscuring tori. A significative fraction of FR II ($\sim$ 20%) present the same characteristics, therefore such sources should be re-classified. From the point of view of the unification schemes, Type-I sources can be unified with BL Lac objects, independently of their radio morphology, as observations of the extended radio structures of BL Lacs seem to require. HST observations have made possible to compare directly the nuclear emission of misaligned and aligned sources, and this lead to the necessity of velocity structures in the inner (sub-pc scale) relativistic jets. Our studies of the optical nuclei of radio galaxies lead to the construction of the SED of radiogalaxies, which represent a powerful tool to investigate the physical conditions of misaligned relativistic jets, and to further constrain the unification schemes. For the first time, we have built the "pure" nuclear SED of a small sample of radiogalaxies, putting together radio, HST and X-ray data. For Centaurus A, in particular, a large (and unique) spectral coverage is available, allowing us to model the SED in details. Our finding that its nuclear emission (from the radio to the gamma-ray band) can be reproduced with a simple homogeneous synchrotron self-Compton model, with physical parameters similar to those found in BL Lacs, represents a further, direct confirmation of the unification schemes.

Appendix A

Debeaming and the broad band spectral slopes

In the case of a one-component model, and under the assumption that the local spectral indices are constant, we can derive the transformation law for the change of the spectral slope due to relativistic beaming. If the flux density in the frame comoving with the emitting region is $F'_{\nu'}$, the observed one is

$$F_\nu^{\text{object}}(\nu) = \delta_{\text{object}}^{p+\alpha} F'_{\nu'}(\nu),$$

where δ_{object} is the beaming factor of the same object for different lines of sight (i.e. observed as BL Lac or as radio galaxy). Substituting these transformations in the definition of the broad-band spectral index α_{12} (where 1 and 2 refer to radio, optical or X-ray flux), one obtains

$$\alpha_{12}^{\text{BLLac}} = -\frac{\log\{\frac{F_2^{\text{FR I}}(\nu_2)(\delta_{\text{BLLac}}/\delta_{\text{FR I}})^{p+\alpha_2}}{F_1^{\text{FR I}}(\nu_1)(\delta_{\text{BLLac}}/\delta_{\text{FR I}})^{p+\alpha_1}}\}}{\log(\nu_2/\nu_1)}$$

which can be written as

$$\alpha_{12}^{\text{BLLac}} - \alpha_{12}^{\text{FR I}} = (\alpha_1 - \alpha_2)\frac{\log(\delta_{\text{BLLac}}/\delta_{\text{FR I}})}{\log(\nu_2/\nu_1)},$$

where α_1 and α_2 are the local spectral indices.

Bibliography

[1] Aloy, M. -A., Gómez, J. -L., Ibáñez, J. -M., Martí, J. -M., Müller, E. 2000, ApJ 528, L85

[2] Antonucci R. R. J. 1984, ApJ 278, 499

[3] Antonucci R. and Barvainis R. 1990, ApJ, 363, L17

[4] Antonucci R.R.J., Miller J.S., 1985, ApJ 297, 621

[5] Bailey J., Sparks W. B., Hough J. H. and Axon D. J. 1986, Nature 322, 150

[6] Barthel P.D., 1989, ApJ 336, 606

[7] Baum S. A. and Heckman T. 1989, ApJ, 336, 702

[8] Becker R. H., White R. L., Gregg M. D., Brotherton M. S., Laurent-Muehleisen S. A. and Arav N. 2000, ApJ 538, 72

[9] Bicknell G. V. 1995, ApJS, 101, 29

[10] Biretta J. A., Sparks W. B. and Macchetto F. 1999, ApJ 520, 621

[11] Biretta J.A., Burrows C.J., Holtzman J.A. et al. 1995, Wide Field and Planetary Camera 2 Instrument handbook, ed. J.A. Biretta (Baltimore:STScI)

[12] Black A. R. S., Baum S. A., Leahy J. P. et al. 1992, MNRAS 256, 186

[13] Blandford R. D., in Active Galactic Nuclei, Blandford R. D., Netzer, H., Woltjer, L., Courvoisier, T. and Mayor, M. 1990, Berlin ; New York : Springer-Verlag, 1990

[14] Blandford R. D., Begelman M. C., 1999, MNRAS 303, L1

[15] Blandford R. D. and Rees M. J. 1978, Pittsburgh Conference on BL Lac Objects, Pittsburgh, Pa., April 24-26, 1978, Proceedings. (A79-30026 11-90) Pittsburgh, Pa., University of Pittsburgh, 1978, p. 328-341; Discussion, p. 341-347. NATO-supported research, 328

[16] Bolton J.G., Stanley G.J., Slee O.B., 1949, Nature 164, 101

[17] Bower G. A., Green R. F., Danks A. et al. 1998, ApJL 492, L111

[18] Braatz J. A., Wilson A. S., Henkel C. 1996, ApJS 106, 51

[19] Burns J. O., Feigelson E. D., & Schreier E. J. 1983, ApJ, 273, 128

[20] Bushouse H., Skinner C.J., MacKenty J.W, 1997, NICMOS Instrument Science Report, 97-28 (Baltimore STScI)

[21] Canosa C.M., Worrall D.M., Hardcastle M.J., Birinshaw M., 1999, MNRAS, 310, 30

[22] Capetti A., Axon D. J., Macchetto F. D., Marconi A. and Winge C. 1999, ApJ, 516, 187

[23] Capetti A., Celotti A., 1999, MNRAS 304, 434

[24] Capetti A., Axon D. J., Macchetto F., Sparks W. B. and Boksenberg A. 1996, ApJ 466, 169

[25] Capetti A., Macchetto F., Axon D. J., Sparks W. B. and Boksenberg A. 1995, ApJ 452, L87

[26] Capetti A., Fanti R., Parma P. 1995, A&A 300, 643

[27] Cardelli, J.A., Clayton, G.C., Mathis, J.S. 1988, ApJ, 329, L33

[28] Celotti A., Fabian A. C., Rees M. J. 1998, MNRAS 293, 239

[29] Chen X., Abramowicz M.A., Lasota J.-P. 1997 ApJ, 476, 61

[30] Chiaberge M., Ghisellini G. 1999, MNRAS, 306, 551

[31] Colina L., De Juan L., 1995, ApJ, 448, 548

[32] Dermer C. D. and Schlickeiser R. 1993, ApJ 416, 458

[33] De Koff S., Baum S., Sparks W.B. et al. 1995, BAAS 187, 1202

[34] De Koff S., Baum S. A., Sparks W. B. et al. 1996, ApJS 107, 621

[35] Djorgovski S., Mazzarella J. and Thompson D. E. A. 1991, BAAS 23, 893

[36] Donnelly H.L., Faber S.M., O'Connell R.M., 1990, ApJ 354, 52

[37] Edelson R.A., Malkan M.A. 1986, ApJ 308, 59

[38] Edge A.C., Rottgering H., 1995, MNRAS, 277, 1580

[39] Elvis M., Plummer D., Schachter J., Fabbiano G. 1992, ApJS, 80, 257

[40] Eracleous M., Halpern J. P. 1994, ApJS 90, 1

[41] Fabbiano G., Miller L., Trinchieri G., Lomgair M., Elvis M., 1984, ApJ 277, 115

[42] Fabian A. C., Rees M. J. 1995, MNRAS 277, L55

[43] Fanaroff B. L., Riley J. M. 1974, MNRAS 167, 31

[44] Fanti R. et al. 1990, A&A, 231, 333

[45] Feinstein C., Macchetto F. D., Martel A. Sparks W. B. and McCarthy P. J. 1999, ApJ 526, 623

[46] Ferrarese L., Ford H., Jaffe, W., 1996, ApJ 470, 444

[47] Ford H. C., Harms R. J., Tsvetanov Z. I. et al. 1994, ApJL 435, L27

[48] Fossati, G., Maraschi, L., Celotti, A., Comastri, A., Ghisellini, G., 1998, MNRAS, 299, 433

[49] Ghisellini G., Celotti A., Fossati G., Maraschi L., Comastri A. 1998, MNRAS, 301, 451

[50] Ghisellini, G., Maraschi, L. and Dondi, L. 1996, A&AS, 120, 503

[51] Ghisellini G. and Madau P. 1996, MNRAS 280, 67

[52] Ghisellini G., Maraschi L. 1989, ApJ 340, 181

[53] Giommi P., Padovani P. 1994, MNRAS 268, L51

[54] Giovannini, G., Taylor, G. B., Arbizzani, E. et al. 1999, ApJ 522, 101

[55] Giovannini G., Cotton W. D., Feretti L., Lara L., Venturi T. 1998, ApJ 493, 632

[56] Giovannini G., Feretti L., Gregorini L., Parma P. 1988, A&A 199, 73

[57] Granato G. L., Danese L. and Franceschini A. 1997, ApJ 486, 147

[58] Grandi P., Urry C. M., Maraschi L., et al., in Advances in Space Research, proceedings of 32nd COSPAR Symposium (1998), astro-ph/9901266

[59] Gonzales-Serrano I., Carballo R., Perez-Fournon I. 1993, AJ 105, 1710

[60] Govoni F., Falomo R., Fasano G. and Scarpa R. 2000, A&A, 353, 507

[61] Gower J. F. R., Scott P. F., Wills D. 1967, Mem R. Astron. Soc. 71, 49

[62] Hardcastle, M. J., Worrall, D. M. 1999, MNRAS, 309, 969

[63] Harms R. J., Ford H. C., Tsvetanov Z. I. et al. 1994, ApJL 435, L35

[64] Harris D.E., Silverman J.D., Hasinger G., Lehman I., 1998, A&AS 133, 431

[65] Hawarden T. G., Sandell G., Matthews H. E., Friberg P., Watt G. D. and Smith P. A. 1993, MNRAS 260, 844

[66] Henkel C., Wang Y. P., Falcke H., Wilson A. S., Braatz J. A. 1998, A&A 335, 463

[67] Hes R., Barthel P. D. and Fosbury R. A. E. 1993, Nature 362, 326

[68] Hill G. J., Goodrich R. W. and Depoy D. L. 1996, ApJ 462, 163

[69] Ho L.C. 1999, ApJ 516, 672

[70] Impey C., Gregorini L., 1993, AJ, 105, 853

[71] Iwasawa, K. et al. 1996, MNRAS 282, 1038

[72] Hui X., Ford H. C., Ciardullo R., Jacoby G.H. 1993, ApJ 414, 463

[73] Jackson N. and Rawlings S. 1997, MNRAS, 286, 241

[74] Jaffe W., Ford H. C., Ferrarese L., Van den Bosh F., Ó Connell R.W. 1993, Nature 364, 213

[75] Jaffe W, Ford H., Ferrarese L., Van den Bosh F., Ó Connell R.W. 1996, ApJ 460, 214

[76] Junor W., Biretta J. A. 1995, AJ 109, 506

[77] Kellermann K. I., Sramek R., Schmidt M., Shaffer D. B. and Green R. 1989, AJ 98, 1195

[78] Kinzer R. L. et al. 1995, ApJ 449, 105

[79] Kollgaard R. I., Palma C., Laurent-Muehleisen S. A., Feigelson E. D. 1996, ApJ 465, 115

[80] Kollgaard R. I., Wardle J. F. C., Roberts D. H., Gabuzda D. C. 1992, AJ 104, 1687

[81] Komossa S., Böhringer H., 1999, A&A 344, 755

[82] Kühr H., Witzel A., Pauliny-Toth I. I. K., Nauber U. 1981, A&AS 45, 367

[83] Komissarov S. S. 1990, Soviet Astronomy Letters, 16, 284

[84] Lamer G., Brunner H., Staubert R., 1996, A&A, 311, 384

[85] Laing R. A., Parma P., de Ruiter H. R., Fanti R. 1999, MNRAS, 306, 513

[86] Laing R. A., 1993, in Burgarella D., Livio M., O'Dea C.P., eds Space Telescope Sci. Inst. Symp. 6: Astrophysical Jets. Cambridge University press, Cambridge, p. 95

[87] Laing R. A., Riley J. M., Longair M.S. 1983, MNRAS 204, 151

[88] Lauer T. R., Ajhar E. A., Byun Y.-I. et al. 1995, AJ 110, 2622

[89] Leahy J. P., Black A. R. S., Dennett-Thorpe J. 1997, MNRAS 291, 20

[90] Leahy J. P., Perley R. A. 1991, AJ 102, 537

[91] Lehnert M. D., van Breugel W. J. M., Heckman T. M. and Miley G. K. 1999, ApJS, 124, 11

[92] Macchetto F., Albrecht R., Barbieri C. et al. 1991, ApJ 373, L55

[93] Macchetto F., Marconi A., Axon D. J., Capetti A. et al. 1997, ApJ 489, 579

[94] MacKenty J.W., et al., 1997, NICMOS Instrument Handbook, Version 2.0 (Baltimore STScI)

[95] Macomb D. J., Akerlof C. W., Aller H. D., et al. 1996, ApJl, 459, L111

[96] Maraschi L., Ghisellini G., Celotti A. 1992, ApJ 397, L5

[97] Marconi A., Schreier E. J., Koekemoer A., Capetti A., Axon D., Macchetto D. and Caon N. 2000, ApJ 528, 276

[98] Martel A. R., Baum S. A., Sparks W. B. et al. 1999, ApJS 122, 81

[99] Mastichiadis A., Kirk J. G. 1997, A&A, 320, 19

[100] Miyoshi M., Moran J., Herrnstein J., Greenhill L. et al. 1995, Nat 373, 127,

[101] McCarthy P. J., et al. 1997, ApJS 112, 415

[102] McCarthy P. J. 1993, ArA&A, 31, 639

[103] McLure R. J., Kukula M. J., Dunlop J. S., Baum S. A., O'Dea C. P. and Hughes D. H. 1999, MNRAS 308, 377

[104] Mirabel I. F. et al. A&A 341, 667

[105] Morse J.A., 1994, PASP 106, 675

[106] Morganti R., Killeen N. E. B., Tadhunter C. N. 1993, MNRAS 263, 1023

[107] Morganti R., Ulrich M.H., Tadhunter C.N. 1992, MNRAS 254, 546

[108] Morganti R., Robinson A., Fosbury R. A. E., di Serego Alighieri S., Tadhunter C. N. and Malin D. F. 1991, MNRAS 249, 91

[109] Morrison R., McCammon D., 1983, ApJ, 270, 119

[110] Narayan R., Yi I. 1995, ApJ 444, 231

[111] Owen F. N., Ledlow M. J., Keel W. C. 1996, AJ 111, 53

[112] Owen F. N. and White R. A. 1991, MNRAS, 249, 164

[113] Owen F. N., Hardee P. E., Cornwell T. J. 1989, ApJ 340, 698

[114] Padovani P. and Giommi P., 1995, ApJ, 444, 567

[115] Padovani, P. 1992, A&A, 256, 399

[116] Parma P., De Ruiter H. R., Fanti C., Fanti R., Morganti R. 1987, A&A 181, 244

[117] Parma P., Murgia M., Morganti R. et al. 1999, A&A 344, 7

[118] Perley R. A., Dreher J. W. and Cowan J. J. 1984, ApJ, 285, L35

[119] Perlman E. S., Stocke J. T., Schachter J. F., et al. 1996, ApJS, 104, 251

[120] Perez E. , Mediavilla E., Penston M. V., Tadhunter C., Moles M. 1988, MNRAS 230, 353

[121] Raymond J.C., Smith B.W., 1977, ApJS 35, 419

[122] Rawlings S. and Saunders R. 1991, Nature 349, 138

[123] Rees M. J., Phinney E. S., Begelman M. C., Blandford R., 1982, Nat 295, 17

[124] Rees M. J., Nature 229, 312

[125] Reynolds C. S., Iwasawa K., Crawford C. S., Fabian A. C. 1998, MNRAS 299, 410

[126] Riley J. M. Pooley G. G. 1975, Mem. R. Astron. Soc. 80, 105

[127] Rothschild R. E., et al. 1999, ApJ, 510, 651

[128] Sakelliou I., Merrifield M.R., 1998, MNRAS 304, 434

[129] Sarazin C.L., 1986, Rev. Mod. Phys. 58, 1

[130] Sarazin C.L., Koekemoer A.M., Baum S.A., O'Dea C.P., Owen F.N., Wise M.W., 1999, ApJ 510, 90

[131] Schindler S., Prieto M.A., 1997, A&A 327, 37

[132] Sikora M., Begelman M. C., Rees M. J. 1994, ApJ 421, 153

[133] Simpson C., Ward M., Clements D. L., & Rawlings S. 1996, MNRAS 281, 509

[134] Sparks W. B., Biretta J. A., Macchetto F. 1994, ApJS 90, 909

[135] Sparks W. B., Golombek D. , Baum S. A. et al. 1995, ApJL 450, L55

[136] Steinle H. et al., A&A 330, 97

[137] Spinrad H., Djorgovski S., Marr J., Aguilar L. 1985, PASP 97, 932

[138] Stickel M., Fried J. W., Kühr H., Padovani P., Urry C. M. 1991, ApJ 374, 431

[139] Strom R. G. , Willis A. G., Wilson A.S. 1978, A&A 68, 367

[140] Swain, M. R., Bridle, A. H. Baum, S. A. 1998, ApJl, 507, L29

[141] Szuszkiewicz E., Malkan M. A., Abramowicz M. A. 1996, ApJ 458, 474

[142] Tadhunter C. N., Morganti R., Robinson A., Dickson R., Villar-Martin M. and Fosbury R. A. E. 1998, MNRAS, 298, 1035

[143] Tananbaum H., Tucker W., Prestwich A., Remillard R., 1997, ApJ 476, 83

[144] Tavecchio F., Maraschi L., Ghisellini G. 1998, ApJ 509, 608

[145] Taylor G. B., Vermeulen R. C., Readhead A. C. S. et al. 1996, ApJS 107, 37

[146] Tingay S. J. et al., 1998, AJ 115, 960

[147] Trussoni E., Massaglia S., Ferrari R., Fanti R., Feretti L., Parma P., Brinkmann W., 1997, A&A 327, 27

[148] Trussoni E., Vagnetti F., Massaglia S., Feretti L., Parma P., Morganti R., Fanti R. Padovani P., 1999, A&A 348, 437

[149] Tsvetanov Z. I., Hartig G. F., Ford H. C. et al. 1998, ApJ 493, L83

[150] Urry C. M., Scarpa R., O'Dowd M., Falomo R., Pesce J. E. and Treves A. 2000, ApJ 532, 816

[151] Urry, C.M., et al., 1996, ApJ, 463, 424

[152] Urry C. M., Padovani P. 1995, PASP 107, 803

[153] Urry C. M., Padovani P., Stickel M. 1991, ApJ 382, 501

[154] Van der Marel R. P., Van den Bosch F. C. 1998, AJ 116, 2220

[155] Vermeulen R. C., Cohen M. H. 1994, ApJ 430, 467

[156] Wagner S. J. et al. 1995, A&A 298, 688

[157] Willott C. J., Rawlings S., Blundell K. M. and Lacy M. 2000, MNRAS 316, 449

[158] Wilson A. S., Braatz J. A., Heckman T. M., Krolik J. H. and Miley G. K. 1993, ApJ, 419, L61

[159] Worral D.M., 1997, in Relativistic Jets in AGN's, M. Ostrowski, M. Sikora, G. Madjeski, M. Begelman eds., Astron. Obs. of the Jagiellonian Univ., Krakow, p. 20

[160] Worrall D.M., Birkinshaw M., 1994, ApJ, 427, 134

[161] Zimmermann H.U., Becker W., Belloni T., Döbereiner S., Izzo C., Kahabka P., Schwentker O., 1995, EXSAS User's GUide, ed. 5, MPE Rep. n 257

[162] Zirbel E. L. 1997, ApJ 476, 489

[163] Zirbel E. L. 1996, ApJ 473, 713

[164] Zirbel E. L., Baum S. A. 1995, ApJ 448, 521

[165] Zirbel E. L., Baum S. A. 1998, ApJS 114, 177

[166] Zirbel E. L., Baum S. A., O'Dea C. P. 1995, ApJ 451, 88